Magnetism
on the timescale of the exchange interaction:
explanations and predictions

Johan Mentink

Printed by Ipskamp Drukkers, Enschede, The Netherlands
ISBN: 978-94-6191-386-9

Illustrated with references
Cover design by J.A. Rauwerdink, Red horse shoe magnet from `www.istockphoto.com`
An electronic version of this thesis can be found at `www.johanmentink.com`

Magnetism on the timescale of the exchange interaction:

explanations and predictions

Proefschrift

ter verkrijging van de graad van doctor
aan de Radboud Universiteit Nijmegen
op gezag van de rector magnificus prof. mr. S. C. J. J. Kortmann,
volgens besluit van het college van decanen
in het openbaar te verdedigen op donderdag 4 oktober 2012
om 10.30 uur precies

door

Johan Hendrik Mentink

geboren op 8 juli 1979
te Winterswijk

Promotoren:	Prof. dr. Th. Rasing Prof. dr. M.I. Katsnelson
Copromotoren:	Dr. A. V. Kimel Dr. A. Kirilyuk

Manuscriptcommissie:

Prof. dr. ir. G.C. Groeneboom	
Prof. dr. U. Nowak	Universität Konstanz
Prof. dr. M. Eckstein	Max-Planck Department for Structural Dynamics at the University of Hamburg

The work described in this thesis has received funding from the Nederlandse Organisatie voor Wetenschappelijk Onderzoek (NWO), the European Union's Seventh Framework Programme (EU-FP7) [grants NMP3-SL-2008-214469 (Ultramagnetron) and 214810 (FANTOMAS), and NMP-2011-SMALL-5-281043 (FEMTOSPIN)], the National Academy of Sciences of Ukraine (NASU) [grant 228-11], the Science and Technology Center in Ukraine (STCU) [grant 5210], the Swedish Research Council (VR), the Knut and Alice Wallenberg foundation (KAW) and the European Research Council [grants 257280 (Femtomagnetism) and 247062 (ASD)].

Voorwoord

Promoveren doe je niet alleen. Het is ongelofelijk wie ik allemaal tegenkwam onderweg: van collega's en studenten, buitenlandse contacten en vrienden, tot promotoren en familie... Ik wil jullie allemaal heel graag bedanken, maar dit lijkt bijna moeilijker dan het schrijven van het proefschrift zelf! Laat ik allereerst *iedereen* bedanken voor de prachtige tijd die ik heb gehad. En mocht ik toch nog iemand zijn vergeten, bij deze ook diegene heel hartelijk bedankt!

De sfeer in Nijmegen was altijd erg stimulerend voor mij. Hiervoor wil ik allereerst mijn kamergenoten bedanken: Addis (co-young father!), Alex, Diana, Dima M, Ilie, Ilya, Kadir (taxi's in Istanbul...), Matteo, Thomas (gefeliciteerd met je aanstaand vaderschap!). Er waren dagelijks de gezamenlijke lunches en koffiepauzes, maandelijks de voetbaltrainingen, jaarlijks de Sinterklaasvieringen, Glühwien parties en "day out", *ad hoc* diners in de stad en overwinningen met de IMM sportdag. En natuurlijk de vele, vele wetenschappelijke discussies. Dit zou allemaal heel erg anders zijn geweest zonder de fantastische collega's van de SSI groep: Addis, Alex, Benny, Boldizsar, Chris, Davide, Dennis, Diana, Dima A., Dima M., Fred, Ilie, Ilya, Jan V., Jan K., Jeroen, Jing, Johan dJ., Jonas, Joris, Jos, Kadir, Koen, Lars, Laura, Loic, Mathieu, Matteo, Magnus, Raja G., Rajasekhar, Roman, Ruslan, Sam, Sasha, Steven, Sergey, Shoken, Siebe, Tahoora, Victoria, Wei-ta Wu, Weizhe en Yusuke. Allemaal heel erg bedankt! Net zoveel dank voor de collega's en studenten van de TCM groep, ook hier voelde ik me altijd thuis. Speciaal noem ik de discussies met Astrid en Hartmut. De laatste tijd komen vooral Frank en Andrea op mijn pad: ik hoop dat we nog veel zullen samenwerken! Ook de SPM groep mag hier niet ontbreken: heel erg bedankt Bas, Duncan, Fresia, Jelena, Joost, Joris, Lucian, Hans, Michiel, Minko, Monique en Serhiy!

Bas, Frederik, Remko. Ik heb echt heel veel plezier beleefd aan het begeleiden van jullie Bachelorprojecten en jullie hebben bovendien allemaal hele mooie resultaten behaald. Siebe, hetzelfde geldt zeker ook voor jouw Masterproject. Je gedrevenheid was enorm en ik ben er ook heel trots op dat ik je heb weten te motiveren voor de mooie samenwerking met Jülich. Natuurlijk zal ik ook jouw binnenkomst met Lars niet snel vergeten, net als het vele voetbalplezier met jullie en de rondleiding in de toren van de Moscow State University.

Various great international scientist came on my way during my PhD. This was really fantastic and I hope we can continue working together in future as well!

Many thanks Olle Eriksson, the first visit was to your group in Uppsala. Your hospitality, our great discussions and your help with the paper were fantastic for me. I really enjoyed working with you and your group and I hope that we will do also in future. Johan H., thanks a lot for introducing me into UppASD, our scientific work together, the impressive concert and afterwarde the special Swedish wine. Many thanks also for Anders, Andrea, Diana and Lars B., Igor, Karel, Marco, and Peter O. My time in Uppsala was great with your presence, which has furthermore a very nice atmosphere owing to the presence of many young fathers!

Many thanks Michael Tretyakov. The project with you was really fantastic and illustrates how fruitful multidisciplinary science can be. It is still surprising for me that we never physically met each other, all the creative work was efficiently done using only Skype and email! Nonetheless, this did not hinder you to send me very nice gifts for the birth of Naomi, many thanks again!

Many thanks Boris Ivanov, it has always been a pleasure to work with you and I became quickly impressed by your scientific independence. Our discussions, mainly over Skype, were always very insightful and to the point. Dima A., I really enjoyed our work in the summer of 2011.

Many thanks Martin Eckstein, what started as inspiring discussions during the Volga-river conference, continued this year with a very successful application for a Rubicon grant to become postdoc in your group in Hamburg. Martin, I really look forward to work with you! Many thanks also for all the people that supported me with applying for the Rubicon grant and especially NWO for the funding.

I also want to thank the manuscript committee for their time and interest: Prof. Uli Nowak, prof. Martin Eckstein and prof. Gerrit Groeneboom, thank you very much!

Met veel trots wil ik mijn paranimfen Alex en Cor bedanken. Alex, there is probably no other colleague with whom I discussed so intensively and lengthy as with you. While less frequently, our discussions continued with you being in Stanford and I am therefore truly happy that you will come over for my defense. Cor, de vriendschap van Isabelle en jou met Ina en mij die in Eindhoven begon, heeft zich nadien alleen maar versterkt. Ik waardeer dit enorm en ben daarom ook heel blij dat je mijn paranimf wilt zijn.

Heel veel mensen zijn in bredere zin bij mijn promotie betrokken geweest. Lieve vrienden, ooms, tantes, neven en nichten. Jullie bijdrage aan de totstandkoming van dit proefschrift is groter dan jullie mogelijk in de gaten hebben. Ik ben heel erg blij dat jullie er allemaal zijn. Bedankt Koninklijke Harmonie Oosterbeek: voor de prachtige projecten en de muziek die we hebben gemaakt. Dankjewel Hélène te Hennepe, het loopbaantraject bij jou heeft me veel meer gebracht dan alleen mijn keuze voor de wetenschap. Heel veel dank ook voor Jacqueline, voor veel meer dan alleen de laatste stelling.

Dankjewel Marilou. Het is ongelofelijk wat je allemaal voor mij hebt gedaan. Ik waardeer enorm je organisatorische kwaliteiten, je zorgzaamheid en trots voor alle promovendi, en je muzikaliteit. Je krijgt (bijna) alles geregeld en samen met Marie-Louise en daarvoor Riki ben je cruciaal voor het reilen en zeilen van de groep.

Dankjewel Alexey. Het meest voor je eerlijke kritiek waarmee je mijn onderzoek weer wakker schudde nadat ik wel heel veel onderwijstaken en studenten op me had genomen. Je leerde me ook heel veel over het schrijven van onderzoeksvoorstellen en persberichten en ook het grootste deel van de titel van dit proefschrift komt van jou. Zonder jouw aansturing had mijn promotie er zeker heel anders uitgezien en was nooit de samenwerking met Boris Ivanov ontstaan. Ook waardeer ik erg je initiatieven buiten de wetenschap. Alles met ambitie natuurlijk: met voetbal zegevierden we niet alleen in Nijmegen, maar ook op de vele conferenties tot in Moskou toe.

Dankjewel Andrei. Ik waardeer je toegankelijkheid en scherpzinnigheid en je brede kennis en begrip. Jouw deur staat altijd open voor vragen en het testen van ideeën. En je gaf me de kans om opgaven te ontwikkelen voor jouw vak nanomagnetisme, waar ik enorm van heb geleerd en genoten.

Dankjewel Annalisa. Je continue betrokkenheid, je stimulerende commentaar en complimenten waren, zeker aan het begin van mijn promotie, van onschatbare waarde voor mij. Ik waardeer het dat je altijd zo attent bent en ik heb ook erg veel plezier beleefd aan het assisteren van jouw vak analytische mechanica.

Dankjewel Misha, in het bijzonder voor je buitengewone wetenschappelijke kwaliteit. Voor mij was het altijd een verademing dat ik met jou op een abstract niveau kon discussieren - zonder direct de details van een methode in te hoeven. Naast een breed inzicht heb je ook nog eens een enorme feitenkennis, iets waar ik alleen van kan dromen. Zonder jouw begeleiding was ik nooit in staat geweest zo'n breed overzicht te krijgen over de theorie van magnetisme. Zonder jou was ik nooit op de fantastische Volga-river conferentie geweest en had ik nooit zo eenvoudig in contact gekomen met Michael Tretyakov, Olle Eriksson en Martin Eckstein. Ik heb ook erg veel geleerd en plezier beleefd aan het assisteren van jouw vak condensed matter theory.

Dankjewel Theo, voor eigenlijk alles. Toen ik, nog werkend bij het KNMI, jouw benaderde voor een optie B had ik niet veel meer dan een artikel uit het Nederlands Tijdschrift voor Natuurkunde van je gelezen waarin een zekere eigenwijsheid me aansprak. Ik had nooit kunnen verwachten dat je mij zou aanstellen op een

Spinoza premie als een theoretische promovendus in jouw groep waar samenwerking en discussie gemeengoed is. En waar een zekere gemoedelijkheid wordt gecombineerd met een bijzonder hoge kwaliteit en ambitie. Dankjewel dat je mij zoveel vertrouwen en ruimte hebt gegeven en zoveel internationale contacten liet opdoen. Je hebt een omgeving gecreëerd waarin ik tot bloei kon komen. Je was er altijd op de momenten dat het nodig was, steunde me bij de strijd voor eerlijke referee rapporten en je had oog voor en was betrokken bij veel meer dan alleen mijn wetenschappelijke output. Ik heb enorm geleerd van je brede wetenschappelijke blik en uitzonderlijke organisatorische kwaliteiten en van je snelle en goede kritiek op teksten en presentaties. Je zorgde voor de fantastische theoretische begeleiding door Misha en Annalisa. Je maakte flexible werktijden mogelijk voor mij als jonge vader, waardoor ik het grootste deel van dit proefschrift in sneltreinvaart heb kunnen schrijven. Ik kan me geen betere eerste promotor voorstellen. En natuurlijk wil ik hierbij ook Maria bedanken. Ina en ik waarderen enorm je warmte, hartelijkheid, oprechtheid en gastvrijheid. De jaarlijkse barbecues in jullie tuin waren altijd erg fijn.

Een bijzonder woord van dank geef ik aan mijn ouders en schoonouders. Jullie betrokkenheid, meeleven en meegenieten, tot aan de verdediging toe; maar ook jullie zorgen (houdt Johan het wel vol?), natuurlijk jullie trots en bovendien jullie vertrouwen zijn echt fantastisch! En niet te vergeten al jullie praktische hulp: het oppassen op Naomi, wekelijks en tijdens de vele conferenties in het buitenland, en de vele praktische klussen in en om huis. En natuurlijk een bijzonder woord van dank voor mijn zus en zwager, schoonzus, (stief)neefjes en stiefnichtje. Mariska en Frank: voor de verbazing en trots, relativering en Bourgondische trekken; en ook nog alle praktische hulp! Lieve Hanke, voor je meeleven en trots, je zorgzaamheid en kennis van de etiquette. Jouw bijdrage is ook echt zichtbaar in het prachtige omslagontwerp van dit proefschrift. Echt superbedankt! Superlief is je zorgzaamheid voor Ina en Naomi (jouw grootste vriendinnetje!), speciaal als ik in het buitenland ben. Bedankt ook Stan en Lynn, Lucas en Simon: het is echt super met jullie erbij! Ik geniet zo van jullie ontwikkeling en al het leuks dat we samen doen.

Bedankt mijn liefste Ina. Woorden schieten tekort om te beschrijven wat je voor mij betekent. Bij nieuwe ontdekkingen, onverwachte tegenvallers of gewoon een dag als altijd: Je bent er voor mij en houdt me met beide benen op de grond. En je bracht ter wereld ons grootste geluk tot nu toe: Naomi. Dankjewel Naomi, het is niet te beschrijven hoe gelukkig ik met je ben. Ik had nooit verwacht dat het zó leuk zou zijn om je te verzorgen, met je te spelen, je te zien opgroeien en nu steeds meer op te voeden. Je komst heeft mijn leven veel meer in balans gebracht. En ik ben zo trots en gelukkig dat je binnenkort grote zus wordt. Bedankt lief kindje op komst, nog voor je geboorte ben je al een wonder voor mij. En eerlijk is eerlijk: zonder jou was dit proefschrift denk ik niet zo snel klaar geweest.

Als afsluiting nogmaals *iedereen* heel erg bedankt!

Contents

1 Introduction **1**
- 1.1 The magic of magnetism . . . 1
- 1.2 Spin dynamics . . . 2
- 1.3 Ultrafast laser-induced spin dynamics . . . 4
  - 1.3.1 Ultrafast demagnetization . . . 4
  - 1.3.2 Three-temperature model . . . 5
  - 1.3.3 Multisublattice magnets . . . 6
- 1.4 Scope of this thesis . . . 7
- References . . . 9

2 Theoretical Concepts of Spin Dynamics **13**
- 2.1 Energy scales in spin dynamics . . . 14
- 2.2 The problem of connecting energy scales . . . 16
- 2.3 *Ab initio* spin dynamics . . . 18
  - 2.3.1 Stoner model . . . 19
  - 2.3.2 Rigid spin approximation and effective exchange interactions . 20
  - 2.3.3 Limitations of the approximations . . . 22
- 2.4 Relaxation and finite temperature effects . . . 23
- 2.5 Effective model approximations . . . 26
- 2.6 Phenomenological theory . . . 28
- 2.7 Modeling laser-induced spin dynamics in multisublattice magnets . . . 29
- References . . . 32

3 Stable and fast numerical integration of the stochastic Landau-Lifshitz equation 35
3.1 Introduction . . . 35
3.2 Numerical Methods . . . 37
3.3 Numerical methods . . . 41
3.3.1 Existing explicit and implicit numerical methods . . . 41
3.3.2 New semi-implicit numerical methods . . . 43
3.3.3 Properties of the methods . . . 44
3.4 Numerical Experiments . . . 46
3.4.1 Two interacting spins . . . 46
3.4.2 1D Heisenberg chain . . . 49
3.5 Conclusions and Outlook . . . 53
References . . . 54

4 Onsager's relations for spin dynamics 57
4.1 Microscopic derivation of Onsager's relations . . . 58
4.2 Longitudinal spin dynamics from Onsager's relations . . . 61
4.3 Nonequilibrium Free Energy . . . 63
References . . . 67

5 Ultrafast spin dynamics in multisublattice magnets 69
5.1 Introduction . . . 69
5.2 General theory . . . 70
5.3 Temperature Dominated Regime . . . 71
5.4 Exchange Dominated Regime . . . 71
5.5 Critical Regime . . . 73
5.6 Comparison with Atomistic Spin Dynamics . . . 74
5.7 Conclusions . . . 77
References . . . 77

6 Microscopic modeling of longitudinal spin dynamics in multisublattice magnets 79
6.1 Introduction . . . 79
6.2 Ultrafast Demagnetization in Multisublattice Magnets . . . 80
6.3 Exchange-driven Magnetization Reversal . . . 84
6.4 The role of orbital degrees of freedom . . . 92
6.4.1 Modeling additional spin and orbital degrees of freedom . . . 92
6.4.2 Orbit-resolved spin and orbital dynamics . . . 94
6.4.3 The role of anisotropy in exchange-driven reversal . . . 96
6.5 Conclusions . . . 98
References . . . 98

A Stochastic Numerics **101**
A.1 Weak order convergence and statistical errors 101
A.2 Ergodicity of the stochastic Landau-Lifshitz equation 103
References 104

Summary **105**

Samenvatting **109**

List of Publications **113**

Curriculum Vitae **115**

CHAPTER 1

Introduction

1.1 The magic of magnetism

Magnetism has been intriguing mankind already for several millennia. Historical studies go back to the ancient Chinese and Greek civilizations, where the mineral magnetite was found to attract iron. Interestingly, already in that time also the practical use of magnetism was realized, nowadays well-known in the form of a compass needle. The usefulness of magnetism is certainly not restricted to mankind. Also part of the living nature on earth, such as some birds and fishes, effectively use biological compass needles. While useful, further applications were only possible based on a deeper understanding of the origin of magnetism. The latter has become possible after the development of electro-magnetism and quantum mechanics. This lead us to understand that magnetism is fundamentally a phenomenon of angular momentum, which is well-known as the rotational motion seen in spinning tops and gyroscopes. The speciality of magnets is that they possess a finite amount of angular momentum in equilibrium, which stems from the intrinsic angular momentum of the electron, called *spin*. A characteristic property of angular momentum is that it has a direction, which can also be viewed as the sense of rotation. This rotation can be clockwise or counter clockwise, which can be referred to as magnetization up or down. Therefore, magnetism can be used to store information. Nowadays magnetic hard-disc drives routinely use this principle to define magnetic bits (”0” for magnetization down and ”1” for magnetization up, for example) and it has become a widely used technology,

the influence of which on the technological revolutions in our society is hard to underestimate. Seen in the broader historical perspective, it is the intimate connection between discovery and practical use which causes most of the magic of magnetism, and it is certainly illustrative for the magic of science in general.

1.2 Spin dynamics

The applications in magnetic-storage and information technology are also one of the key motivations for the study of magnetism in this thesis. For this application, one of the central figures of merit is the speed at which magnetic bits can be recorded. This immediately brings us to the fundamental question how fast angular momentum can be reversed. To address this problem, we thus need to study the dynamics of angular momentum, often simply called *spin dynamics*.

The fundamental description of all spin dynamics relies on the interaction of magnetic moments with magnetic fields. A magnetic field $\mathbf{H}$ excerts a torque $\mathbf{T} = \mathbf{m} \times \mathbf{H}$ on the magnetic moment $\mathbf{m}$ of the spins. The conservation of angular momentum dictates that for a closed system the total torque should be zero, and therefore $d\mathbf{L}/dt = \mathbf{T}$, where $\mathbf{L}$ is the angular momentum of the spin. Quantum mechanics shows that on a fundamental level there is a linear relation between the magnetic moment and angular momentum: $\mathbf{m} = -\gamma\mathbf{L}$, where γ is called the gyromagnetic ratio. For elementary electron spins we have $\gamma = -ge/(2m) > 0$, where e and m are the electron charge and mass. As a result, we have an equation of the form

$$\frac{d\mathbf{m}}{dt} = -\gamma \mathbf{m} \times \mathbf{H}. \tag{1.1}$$

Hence, the resulting dynamics is a precession of the magnetic moment around the magnetic field. The characteristic frequency of precession is given by $\omega = \gamma|\mathbf{H}|$ and scales linearly with the field.

So far we have only considered the case of an isolated spin. This result can however easily be generalized to magnetically ordered media, by assuming that the internal forces that order the microscopic moments $\mathbf{m}_i$ are so strong that the system rotates as a rigid body around the applied field, with a macroscopic magnetization per unit volume given by $\mathbf{M} = \sum_i \mathbf{m}_i/v$, v being the unit volume. Furthermore, the dynamics is usually also influenced by for example magneto-crystalline anisotropy and demagnetizing fields. In many situations such effects can, in combination with $\mathbf{H}$, be taken into account as an effective magnetic field $\mathbf{H}_{\text{eff}}$.

In equilibrium $\mathbf{M}$ is parallel with $\mathbf{H}_{\text{eff}}$ and there is no dynamics at all, as follows indeed from Eq. (1.1). However, Eq. (1.1) cannot describe the relaxation of $\mathbf{M}$ to $\mathbf{H}_{\text{eff}}$ after being brought out of equilibrium and therefore we need to invoke a damping term. Usually this relaxation proceeds slower than the precession and we can model it as a damping torque perpendicular to the precessional motion, with the precessional

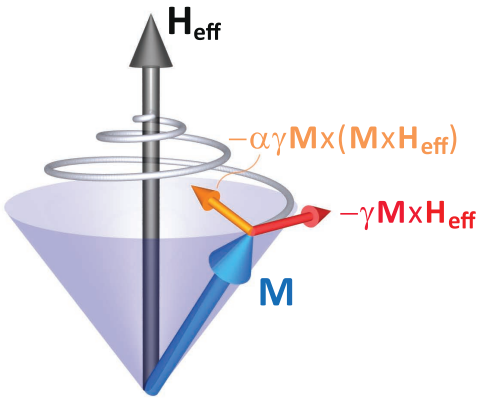

Figure 1.1: Illustration of the precessional spin dynamics described by the Landau-Lifshitz equation Eq. (1.2). The magnetization $\mathbf{M}$ precesses along the effective magnetic field $\mathbf{H}_{\text{eff}}$. A small damping torque gradually aligns the magnetization with the effective field. Figure adapted from [3].

motion itself unperturbed by the damping. This leads to the famous Landau-Lifshitz equation [1]:

$$\frac{d\mathbf{M}}{dt} = -\gamma \mathbf{M} \times \mathbf{H}_{\text{eff}} - \frac{\alpha}{M} \gamma \mathbf{M} \times (\mathbf{M} \times \mathbf{H}_{\text{eff}}) \,. \tag{1.2}$$

The dynamics governed by the Landau-Lifshitz equation is illustrated in Fig. 1.1 which shows the precession of the magnetization around the effective magnetic field. In the course of precession, the magnetization gradually aligns with the field owing to the damping term. Both the precession term and the damping term conserve the magnitude of the magnetization. The reason is that both precession and damping are perpendicular to $\mathbf{M}$, yielding $d|\mathbf{M}|^2/dt = 2\mathbf{M} \cdot d\mathbf{M}/dt = 0$. Alternatively, we could introduce the damping term in the Gilbert form $\sim \alpha \mathbf{M} \times d\mathbf{M}/dt$. Then, the mathematical structure is the same as the Landau-Lifsthiz equation with the replacement $\gamma \to \gamma/(1+\alpha^2)$ [2], which becomes relevant when modeling systems with strong damping ($\alpha \sim 1$).

To finish this section, we estimate the reversal speed that follows from the Landau-Lifsthiz equation. Using that the electron gyromagnetic ratio is $|\gamma| \approx 28\text{GHz/T}$, we find that with a realistic laboratory field and damping parameter ($H = 1\,\text{T}$, $\alpha = 0.1$), we obtain reversal times $\tau = 4\pi/(\omega\alpha) \sim 0.72\,\text{ns}$. While in principle the reversal

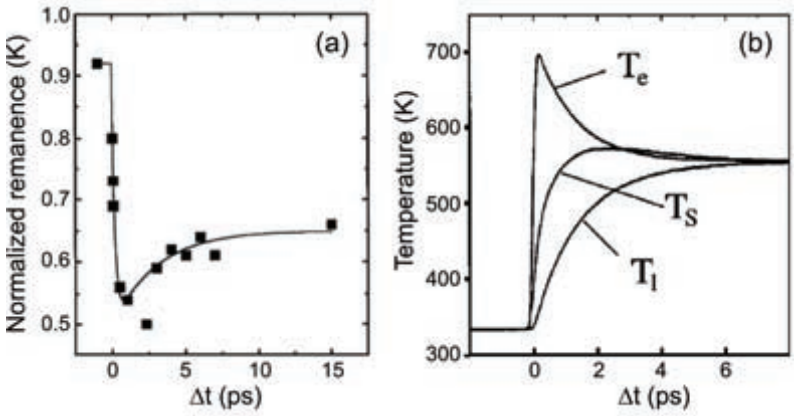

Figure 1.2: (a) Ultrafast quenching of magnetic order in ferromagnetic Ni following femtosecond laser excitation. The spin dynamics is much faster than what is expected from conventional precessional dynamics. (b) Three-temperature model used to analyze the results. Adapted from [4].

speed can be further increased by using stronger damping and/or higher fields, this is technologically extremely challenging. Therefore, industry is currently looking for novel ways to control magnetism by other means than magnetic fields.

1.3 Ultrafast laser-induced spin dynamics

1.3.1 Ultrafast demagnetization

The availability of femtosecond laser pulses has opened fundamentally different approaches to control magnetic order. Owing to their temporal resolution, femtosecond laser pulses enable to study spin dynamics at much shorter timescales than previously accessible. This was clearly illustrated by the pioneering work of Beaurepaire and coworkers in 1996 [4], who used femtosecond optical pulses to excite ferromagnetic Ni. Remarkably, they observed an ultrafast quenching of magnetization on the subpicosecond timescale, as illustrated in Fig. 1.2. These results were soon confirmed by other experiments [5, 6]. Later, it was also shown that a femtosecond laser pulse could act as an equally short magnetic field pulse [7–9], which even led to the discovery of complete reversal of magnetization by a laser pulse alone [10, 11]. These intriguing observations triggered intense experimental and theoretical efforts to understand the fundamental processes lying behind such ultrafast laser-induced dynamics [12].

In addition, we emphasize that laser excitation is very different compared to the

excitation with conventional magnetic fields. This difference becomes apparent by considering the energy-scales responsible for the long-range ordering of the microscopic magnetic moments. Macroscopic magnetic order is determined by the exchange interactions between the microscopic spins. The strength of these interactions can be estimated from the Curie temperature T_C, which is the temperature above which long-range magnetic order vanishes. For transition metals we typically have $T_C = 1000\,\mathrm{K}$ and we can estimate the precession period of the spins in the exchange field of all the other spins as $t = \hbar/(k_B T) \sim 10\,\mathrm{fs}$. Hence, the excitation with a femtosecond laser pulse occurs on a timescale comparable to that of the intrinsic dynamics of the magnetic material. Therefore, for sufficiently intense pulses and large absorption, laser pulses may bring the magnet strongly out of equilibrium, where the description of spin dynamics as an effective macroscopic rigid-body rotation might break down.

For the understanding of the large variety of laser-induced spin dynamics, it is useful to distinguish between laser-induced magnetic excitations that are dominated by heating and those that are not. When the laser-induced heating is only a small effect, the magnitude $|\mathbf{M}|$ hardly changes and can thus be considered constant. While the actual laser-excitation usually still involves the absorption of photons, the majority of experimental studies in this regime are concerned with laser-induced precessional dynamics, which can therefore conveniently be described by the Landau-Lifshitz equation Eq. (1.2). In contrast, in cases such as the results shown in Fig. 1.2, the effect of heating is crucial and the experiments display a very different type of ultrafast spin dynamics. First of all, the dynamics is much faster than can be expected from precession. Furthermore, the dynamics is *longitudinal* in character, *i.e.* it concerns changes in the absolute value $|\mathbf{M}|$, which is completely incompatible with the precessional dynamics which conserves the magnitude of the magnetization. The theoretical study of such strongly nonequilibrium and longitudinal spin dynamics is the main focus of this thesis.

1.3.2 Three-temperature model

While it may seem almost evident that heating gives rise to a change of $|\mathbf{M}|$, it is not trivial to understand why the observed longitudinal dynamics is so fast. Significant insight to this question was obtained by considering a three-temperature model [13]. Since the laser-pulse is so short, the absorption of heat proceeds with different rates over the different internal degrees of freedom of the system. Instead of assigning one temperature to the system as a whole, the nonequilbrium spin dynamics was modeled by assigning different temperatures to electronic, spin and lattice degrees of freedom,

the evolution of which is described by three coupled differential equations:

$$\begin{aligned} C_e dT_e/dt &= -G_{el}(T_e - T_l) - G_{es}(T_e - T_s) + P(t), \\ C_s dT_s/dt &= -G_{es}(T_s - T_e) - G_{sl}(T_s - T_l), \\ C_l dT_l/dt &= -G_{el}(T_l - T_e) - G_{sl}(T_l - T_s). \end{aligned} \tag{1.3}$$

Here G_{ij} describes the coupling between the ith and jth subsystem, C_i and $T_i = T_i(t)$ describe their heat capacity and temperature, respectively, and $P(t)$ describes the laser excitation. Within this model, the ultrafast laser-induced demagnetization is essentially understood as an ultrafast heating of electrons, the temperature of which rises essentially on the same timescale as the laser pulse. Due to electron-spin and spin-lattice coupling, the latter also quickly increases the temperature of the spins, as is illustrated in Figure 1.2b. Eventually, the reduction of the magnetization is described as $M(T_s(t))$, where $M = |\mathbf{M}|$.

This three-temperature model was later improved by also taking into account explicitly the angular momentum conservation in the interaction between the spin and lattice degrees of freedom [14]. This appeared to be an effective model for the ferromagnetic metals such as Ni, Fe, Co and Gd, capable of fitting experimental data over a large range of temperatures and laser fluences [15]. Further improvements were reported by using microscopic simulations based on the direct numerical time integration of a large system of interacting atomic spins coupled to a two-temperature model for the electron and lattice system [16]. These studies do not rely on the concept of spin temperature, and it was shown that, in fact, the whole concept of a spin temperature could not well be defined on the sub-picosecond timescale at which the ultrafast demagnetization takes place. This elucidates the essentially nonequilibrium character of the spin dynamics induced by femtosecond laser pulses.

1.3.3 Multisublattice magnets

While the first experiments on ultrafast demagnetization were performed using pure ferromagnetic Ni, many of the subsequent studies have been performed with magnetic materials that contain at least two magnetic elements [12]. More generally, the spin dynamics of other well-known multi-component materials like NiFe and yttrium-iron-garnet have demonstrated interesting observations such as Bose-Einstein condensation [17], magnetic vortices [18] and spin-Seebeck effects [19]. On a microscopic scale the different magnetic elements form different magnetic sublattices, such as illustrated in Fig. 1.3a, for a ferrimagnetic GdFe alloy. However, so far most experiments on these materials were analyzed using an effective macrospin approximation, where several sublattices are represented with just one macroscopic magnetization vector. This may be a good approximation only when the sublattices are in equilibrium with each other. Recent experimental advances with fs X-ray probes [20, 21], make it possible to study the spin dynamics in an element-specific way and with femtosecond time resolution.

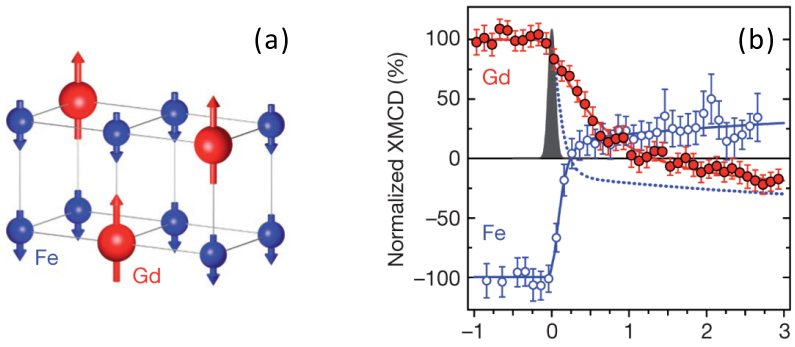

Figure 1.3: (a) Illustration of ferrimagnetic GdFe, which can be thought of as containing two magnetic sublattices. In the ground state, the Gd and Fe sublattice are oriented antiparallel. (b) Ultrafast and distinct demagnetization of Gd and Fe sublattices followed by switching between two antiferromagnetically ordered states via a transient ferromagnetic state following laser excitation as measured using fs X-ray probes. Adapted from [22].

Interestingly, the use of such probes has revealed that the different magnetic elements in ferrimagnetic GdFeCo alloys have distinct dynamics after femtosecond laser excitation [22], which more recently has also been observed in NiFe compounds [23]. These experiments thus clearly demonstrate that the sublattices are out of equilibrium. Furthermore, the measurements on GdFe alloys demonstrated full laser-induced reversal of magnetization. This is illustrated in Fig. 1.3b, as a switching between two antiferromagnetically ordered states via a transient ferromagnetic state [22]. These findings were also supported by numerical simulations. However, the actual mechanism of the reversal remains unclear. This reveals a fundamental gap in our understanding of spin dynamics, *i.e.* it is generally unknown what kind of spin dynamics can be expected when the spins in different sublattices are not in equilibrium with each other. At the same time, this problem is highly relevant for technology, which becomes evident by examining the timescale of the reversal illustrated in Fig. 1.3b. This appears to be on the ps timescale, which is roughly a 1000 times faster than state-of-the art technology. Therefore, the main goal of this thesis is the theoretical study of ultrafast longitudinal spin dynamics in multisublattice magnets.

1.4 Scope of this thesis

Among the fundamental problems in the field of ultrafast laser-induced spin dynamics mentioned above, the lack of understanding of longitudinal spin dynamics in magnets with multiple magnetic sublattices seems to be the most pressing. This not only deals with fundamental issues regarding the description of magnets out of equilibrium and

the timescale at which transfer of angular momentum takes place, but moreover potentially may have a huge impact on future magnetic data storage and information technology, owing to the ultrafast magnetization reversal observed in these magnets. Therefore, the main focus of this thesis is to develop a theoretical understanding on the ultrafast longitudinal spin dynamics in multisublattice magnets.

After this introductory chapter, Chapter 2 describes the theory of spin dynamics on a general level, addressing the fundamental concepts and approximations used for the description of spin dynamics at various levels of detail. This eventually leads to two complementary approaches we use in this thesis to address the longitudinal spin dynamics in multisublattice magnets. The first approach is a microscopic approach based on atomistic spin dynamics simulations. The second approach is a phenomenological approach based on Onsager's relations, which directly yields equations of motion for the macroscopic spin dynamics.

Chapter 3 is devoted to the development of stable and fast numerical integration routines for the atomistic spin dynamics simulations. These methods enable much faster simulations than previously possible. We argue that this is related to the intrinsic conservation properties of the new methods, which we illustrate for simple model systems.

Chapter 4 deals with a general theoretical treatment of Onsager's relations for the derivation of macroscopic equations of motion for spin dynamics. We derive the macroscopic equations of motion directly from first principles using the formalism of linear response. In addition, we generalize the existing applications of the Onsager's relations to the case of general multisublattice magnets with arbitrary exchange interactions. Furthermore, we show how the macroscopic free energy, which determines the effective magnetic fields acting on the magnetic sublattices, can be derived directly from the microscopic Heisenberg spin model.

In Chapter 5 we work out the purely phenomenological theory for the assessment of laser-induced spin dynamics in multisublattice magnets on a general level. In particular, we discuss the different roles of relaxation of relativistic origin and relaxation of exchange origin. The latter is the main new ingredient of the theory. We further classify the longitudinal dynamics in three different regimes, depending on wether the temperature is below, above or in the vicinity of the Curie temperature. We will show that the theory can explain the recently observed reversal in ferrimagnets, and we argue that the mechanism of reversal stems from the exchange relaxation, which describes the transfer of angular momentum between the magnetic sublattices. These results are further supported by atomistic spin dynamics simulations, using the methods developed in Chapter 3. Furthermore, we show that the phenomenological theory provides interesting predictions for the ultrafast demagnetization in general multisublattices, with both ferromagnetic and antiferromagnetic coupling between the sublattices, which recently have also been confirmed by experiments.

Chapter 6 deals with more microscopic modeling of the longitudinal spin dynamics in multisublattice magnets. For this we use the relation between the microscopic Heisenberg spin model and the macroscopic nonequilibrium free energy as derived in Chapter 4. This enables us to study in more detail how the spin dynamics depends on the sign and strength of the exchange interaction. We work this out for the ultrafast demagnetization in multisublattice magnets, and discuss the example of ferromagnetic NiFe alloys in particular. Furthermore, we use the microscopic model to assess the criteria under which exchange-driven magnetization reversal can take place and discuss the role of the inter-sublattice exchange interaction in particular. This eventually leads to the prediction of a novel reversal path for exchange driven magnetization reversal. This chapter is concluded by an assessment of the role of the orbital degrees of freedom, which we investigate separately for transition metals and rare-earth metals. We find that the most pronounced effect of the orbital degrees of freedom on the spin dynamics is found for rare-earth metals, owing to their strong anisotropy. This effect can be so strong that it may even reduce the possibility of exchange-driven reversal in rare-earth transition-metal alloys.

Probably one of the most striking features elucidated by our modeling in Chapters 5 and 6 is that it desribes spin dynamics that is purely driven by the exchange interaction. In other words, we are dealing with *magnetism on the timescale of the exchange interaction*. The exchange interaction is the strongest force in magnetism and can easily reach strengths one thousand times larger than typical externally applied magnetic fields ($\sim 1\,\mathrm{T}$). This provides the clue *why* the reversal observed in multisublattice magnets (Fig. 1.3) can be so much faster than conventional magnetization reversal. In addition, this thesis provides *predictions* for new spin dynamics appearing on the timescale of the exchange interaction. We conclude with a summary of the main results of this thesis and indicate future directions to further explore and exploit the power of the exchange interaction in the field of ultrafast spin dynamics.

References

[1] L. Landau and E. Lifshitz, Phyz. Z. Sowjetunion **8**, 153 (1935).

[2] T. Gilbert, IEEE Tans. Magn. **40**, 3443 (2004).

[3] K. Vahaplar, Ph.D. thesis, Radboud University Nijmegen (2011).

[4] E. Beaurepaire, J.-C. Merle, A. Daunois, and J.-Y. Bigot, Phys. Rev. Lett. **76**, 4250 (1996).

[5] J. Hohlfeld, E. Matthias, R. Knorren, and K. Bennemann, Phys. Rev. Lett. **78**, 4861 (1997).

[6] A. Scholl, L. Baumgarten, R. Jacquemin, and W. Eberhardt, Phys. Rev. Lett. **79**, 5146 (1997).

[7] A. Kimel, A. Kirilyuk, P. Usachev, R. Pisarev, A. Balbashov, and T. Rasing, Nature **435**, 655 (2005).

[8] F. Hansteen, A. Kimel, A. Kirilyuk, and T. Rasing, Phys. Rev. Lett. **95**, 047402 (2005).

[9] A. Kalashnikova, A. Kimel, R. Pisarev, V. Gridnev, A. Kirilyuk, and T. Rasing, Phys. Rev. Lett. **99**, 167205 (2007).

[10] C. Stanciu, F. Hansteen, A. Kimel, A. Kirilyuk, A. Tsukamoto, A. Itoh, and T. Rasing, Phys. Rev. Lett. **99**, 047601 (2007).

[11] K. Vahaplar, A. Kalashnikova, A. Kimel, D. Hinzke, U. Nowak, R. Chantrell, A. Tsukamoto, A. Itoh, A. Kirilyuk, and T. Rasing, Phys. Rev. Lett. **103**, 117201 (2009).

[12] A. Kirilyuk, A. Kimel, and T. Rasing, Rev. Mod. Phys. **82**, 2731 (2010).

[13] M. Agranat, S. Ashitkov, A. B. Granovskii, and G. Rukman, Zh. Eksp. Teor. Fiz **86**, 1376 (1984).

[14] B. Koopmans, J. Ruigrok, F. Longa, and W. de Jonge, Phys. Rev. Lett. **95**, 267207 (2005).

[15] B. Koopmans, G. Malinowski, F. D. Longa, D. Steiauf, M. Fähnle, T. Roth, M. Cinchetti, and M. Aeschlimann, Nature Mater. **9**, 259 (2010).

[16] N. Kazantseva, U. Nowak, R. Chantrell, J. Hohlfeld, and A. Rebei, Europhys. Lett. **81**, 27004 (2008).

[17] S. Demokritov, V. Demidov, O. Dzyapko, G. Melkov, A. Serga, and A. Hillebrands, B.and Slavin, Nature **443**, 430 (2006).

[18] B. Van Waeyenberge, A. Puzic, H. Stoll, K. Chou, T. Tyliszczak, R. Hertel, M. Fähnle, H. Brückl, K. Rott, G. Reiss, et al., Nature **444**, 461 (2006).

[19] K. Uchida, S. Takahashi, K. Harii, J. Ieda, W. Koshibae, K. Ando, S. Maekawa, and E. Saitoh, Nature **455**, 778 (2008).

[20] C. Stamm, T. Kachel, N. Pontius, R. Mitzner, T. Quast, K. Holldack, S. Khan, C. Lupulescu, E. Aziz, M. Wietstruk, et al., Nature Mater. **6**, 740 (2007).

[21] C. La-O-Vorakiat, M. Siemens, M. M. Murnane, H. C. Kapteyn, P. Grychtol, R. Adam, C. M. Schneider, J. M. Shaw, H. Nembach, and T. J. Silva, Phys. Rev. Lett. **103**, 257402 (2009).

[22] I. Radu, K. Vahaplar, C. Stamm, T. Kachel, N. Pontius, H. Dürr, T. Ostler, J. Barker, R. Evans, R. Chantrell, et al., Nature **472**, 205 (2011).

[23] S. Mathias, C. La-O-Vorakiat, P. Grychtol, P. Granitzka, E. Turgut, J. M. Shaw, R. Adam, H. T. Nembach, M. E. Siemens, S. Eich, et al., PNAS **109**, 4792 (2012).

CHAPTER 2

Theoretical Concepts of Spin Dynamics

In this chapter we review theoretical concepts for the description of spin dynamics. First, we discuss on a general level the various energy scales that are relevant for the description of solid-state magnetism and argue that it is the coexistence of all these energy scales which makes it in general very difficult to describe spin dynamics within one theoretical framework. Second, we consider the two limiting cases of a complete first-principle approach and the phenomenological Landau-Lifshitz equation. Both are in principle exact and we give the example of the spin-wave stiffness for which a rigorous connection between the energy scales can be obtained. In general we need to resort to approximations and we subsequently discuss in detail the adiabatic approximation and the rigid spin approximation, which together lead to the possibility of studying *ab initio* spin dynamics. Furthermore, we discuss how finite temperature effects may be included in this approach. Subsequently, we review various intermediate levels of description that can be used to address specific problems which is followed by an account of the pure phenomenological theory, as can be derived on the basis of the theory of irreversible thermodynamics. We conclude this chapter by discussing the approximations and concepts that we regard as most useful for the problem of laser-induced spin dynamics in magnets with multiple magnetic sublattices.

2.1 Energy scales in spin dynamics

In this section we discuss the different energy scales that are relevant for spin dynamics on a general level, as are illustrated in Fig. 2.1. We start by discussing the highest energy scales from a fundamental level and subsequently introduce the relevant energies for a macroscopic description. Finally we summarize and indicate why magnetism in general is such a challenging problem.

The description of magnetism on a fundamental level should be based on quantum mechanics. For solids we then start with the description of electrons in the crystal lattice which leads to the formation of energy bands. Their characteristic energy scale is the band width, which is in the order of 5 eV for transition metals. Only the formation of bands is not sufficient to explain magnetism. For this also the correlation between the electrons needs to be taken into account. Similar as in atoms, the repulsive Coulomb interactions between the electrons and the Pauli exclusion principle are responsible for the formation of atomic spin and orbital moments. The typical energy scale for this interaction, which we refer to as on-site or intra-atomic exchange-interaction, is for 3d metals in the order of 1 eV. The next relevant energy scale describes the interaction between spins at different sites and determines the long-range magnetic order of atomic magnetic moments. The Curie temperature, which is the characteristic temperature where this order vanishes, is in the order of 1000 K, roughly corresponding to about 100 meV.

At the same time, it is well-known that the characteristic spin dynamics that appears on the macroscopic scale, that is, at distances much larger than the lattice spacing, is usually governed by very different energy scales. These deal with the formation of magnetic domains and the motion of domain walls and are determined by the magneto-crystalline anisotropy and the dipolar interactions. Their characteristic energy scale is only in the order of 0.1-0.2 meV.

We have thus seen that spin dynamics covers energies scales over more than 4 orders of magnitude. We cannot simply neglect the small energy scales. In fact, they are crucial for technological applications, since for example without anisotropy it would be impossible to write stable magnetic domains. At the same time, these small energy scales should be connected somehow with the more fundamental interactions between the electrons and the spins. The main problem in the theory of spin dynamics can thus be defined as to obtain a description for the interconnection of these various energy scales in one theoretical framework. In other words, spin dynamics is fundamentally a multi-scale problem.

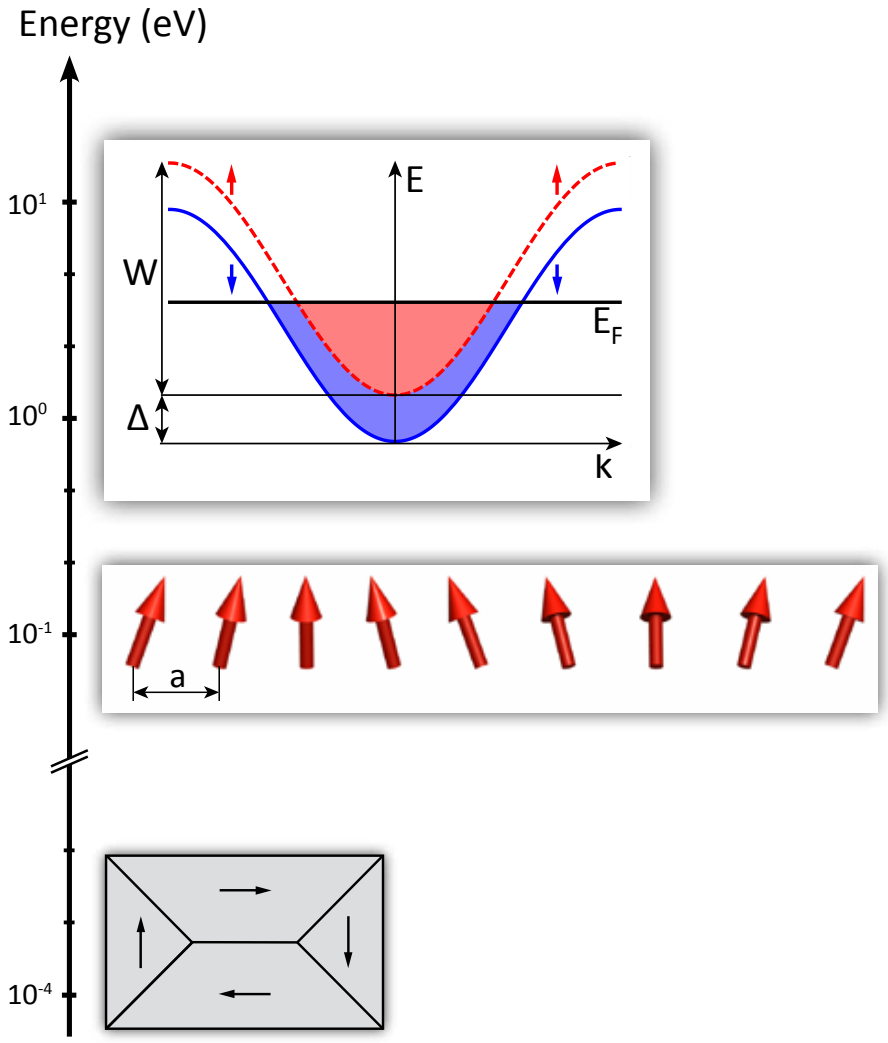

Figure 2.1: Illustration of the different energy scales of magnetism in 3d metals. The highest energy is the band width $W \sim 5\,\mathrm{eV}$. The splitting of the spin-up and spin-down bands occurs at an energy of approximately $\Delta \sim 1\,\mathrm{eV}$, yielding an imbalance of the filling of these bands up to the Fermi-energy E_F. The rotations of the on-site spin moments at adjacent sites have an energy in the order of $\hbar\omega \sim 0.1\,\mathrm{eV}$. At much lower energy, $E \sim 0.1 - 0.2\,\mathrm{meV}$ and at distances much larger than the lattice spacing a magnetic domains are formed which is illustrated by a Landau-domain pattern with arrows indicating the direction of the magnetization.

2.2 The problem of connecting energy scales

In addition to the coexistence of very different energy scales, spin dynamics also governs qualitatively very different phenomena. As we have seen in the introductory chapter, for isolated spins the dynamics is purely precessional and described by the Landau-Lifsthitz equation (1.2). When the spins are strongly coupled, the same equation can be used also for the macroscopic dynamics. On the other hand, when the coupling between the spins is not entirely rigid, also the magnitude of the total magnetization changes, giving rise to longitudinal dynamics. This may appear on the atomic scale due to changes of the length of the atomic spins, as well as on the macroscopic scale as collective transverse spin excitations, or *spin waves* as schematically illustrated in Fig. 2.2. It is clear that the energy associated with spin-waves should be related to the coupling between spins at different sites and therefore should somehow connect the microscopic description at high energy scales with the macroscopic description at low energy scales. In this section we elaborate on one specific quantity, the so called spin-wave stiffness, for which such a connection can be made rigorously.

In principle the equation that describes magnetism on a fundamental level is known. In the non-relativistic limit it is the 2-component Schrodinger-equation for the electrons in the crystal lattice. This problem can be formally solved exactly within the framework of the time-dependent density functional theory [1] for non-collinear spins, see for example [2] for a recent account. In the opposite limit, on the macroscopic scale we also have a formally exact theory. In this limit the use of the continuum approximation is certainly applicable, and the macroscopic dynamics can be described by the phenomenological Landau-Lifshitz equation. The phenomenological theory can be used, for example, to describe the exchange energy associated with nonuniform magnetization distributions $\mathbf{M}(\mathbf{r})$ with a spatial size much larger than the lattice spacing[1]. In this regime the dynamics is described by spin waves, and their characteristic energy can be written as

$$\hbar\omega(\mathbf{q}) = D_{jk} q_j q_k \tag{2.1}$$

where $\mathbf{q}$ the wavevector of the spin-wave and summation over the repeated cartesian indices j, k is assumed. The quantity $D_{jk} = \partial^2 E / \partial q_j \partial q_k$ is known as the spin-wave stiffness, with E is the total energy of the system. Note that the introduction of D_{jk} does not rely on a particular microscopic spin model, which generally involves approximations. It turns out that only for the spin-wave stiffness it is possible to obtain a rigorous mapping between the electronic description at high energy and the phenomenological description at low energy.

[1] The situation is similar to the problem of elasticity, which for many situations can be described in terms of macroscopic elastic constants if the characteristic wavelength of the deformation is long in comparison with the lattice distance and if the relative deformation is small [3, Ch. 4].

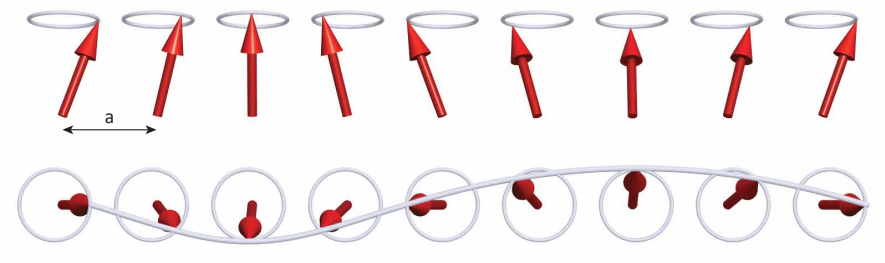

Figure 2.2: Schematic one-dimensional illustration of the collective transverse spin excitations in the form of spin waves. Top: perspective view of arrows indicating the local spins at different lattice sites separated by the lattice spacing a. The spins are rotated from the collinear ground state, yielding a reduced total magnetization. Bottom: projection of the rotated spins in the plane of the circles, illustrating the phase relationship between the rotations of the spins at different sites.

The possibility to make such a rigorous connection has been demonstrated for the first time in the 1980s by Lichtenstein, Katsnelson and coworkers. Initially it has been worked out in a series of three papers [4–6] within the framework of the local spin-density approximation. Later it was generalized also for correlated electron systems [7, 8]. The main idea is the introduction of a new small parameter, which is the rotation angle θ of the local spin density from a given magnetic configuration. This parameter can always be defined and does not rely on, for example, the smallness of the ratio of two different energy scales or the type of magnetic ordering. Indeed, on a formal level it is always possible to describe the atomic scale magnetization per atomic site by a quantum mechanical field operator for the three components of the spin density and treat the angle of rotation as a *classical* variable that can be made arbitrarily small. Consequently, the change of the energy under infinitesimal rotations can in principle always be calculated within a full-first principle formalism, taking the deviation from a given state as a small perturbation and calculate the corresponding changes in linear response. At the same time, it is clear from the outset that small deviations from the given magnetic configuration in the limit $\mathbf{q} \to 0$ describe the weak nonuniformity of the macroscopic magnetization and therefore the spin-wave stiffness. Hence, the full first-principle expression for the spin-wave stiffness should coincide with the phenomenological expression in the long wave-length limit.

Although the mapping on phenomenological parameters can always be done within linear-response, such calculations usually contain some uncontrollable errors. This can only be fully understood by considering the diagrammatic approach to many-body perturbation theory. The expressions for the linear response usually contain series of diagrams from which the so-called vertex corrections can be defined. Neglecting such vertex corrections is usually necessary for practical calculations and this is why the

accuracy of the calculation is usually not controllable. The calculation of the spin-wave stiffness is however special in this respect. It can be proven that within the local spin-density approximation [4, 6] as well as within the framework of the dynamical mean-field theory [8, 9], the vertex corrections are zero. Therefore, the calculation of the spin-wave stiffness is rigorous, *i.e.* it contains no uncontrollable errors. As a consequence, the spin-wave stiffness can be calculated rather accurately, while the calculation of other phenomenological parameters always contain some uncontrollable errors due to the neglect of (part of the) vertex corrections.

So far, the spin-wave stiffness seems to be the only rigorous connection between the different energy scales and therefore a general framework for the description of spin dynamics does not exist. As a consequence, for all practical purposes we need to resort to approximations. This will be the topic of the next sections.

2.3 Ab initio spin dynamics

A full description of spin dynamics in magnetic materials is only possible by making approximations. In this section we discuss two important approximations that enable the connection of the full electronic description with the macroscopic description and thereby in principle allow to model spin dynamics without free parameters. These two approximations are the adiabatic approximation and the rigid spin approximation. We first provide a qualitative description of *ab initio* spin dynamics. In the next two subsections, we will discuss in more detail the Stoner model and the calculation of effective exchange parameters within the rigid spin approximation that enable us to define the criterion for adiabaticity and assess their range of applicability.

Conceptually, the idea of the adiabatic approximation is that usually the rotations of the atomic-like spins, such as apparent in the collective spin-wave excitations (Fig. 2.2), are much slower than the electronic dynamics, which determine the electron density and the magnitude of the atomic spin moments. In analogy to the Born-Oppenheimer approximation, the directions of the atomic magnetic moments correspond to the slow nuclear motion while the evolution of the magnitudes of the atomic magnetic moments corresponds to the change of the electronic wave functions, which are the fast degrees of freedom. Consequently, we can study the dynamics of the orientation of the moments with their lengths fixed. The idea to use this type of adiabatic approximation has been introduced already in the 1950s, see for example [10]. The applicability of this approximation within a parameter free framework was first discussed by Antropov and coworkers in 1995 [11, 12] and is closely related with the possibility to calculate the magnetic interactions directly from the electronic structure for small deviations from a given magnetic configuration. In particular, the approach developed in [4–6] enables the calculation of the effective torques acting on the spins for any given non-collinear magnetic configuration and for any type of

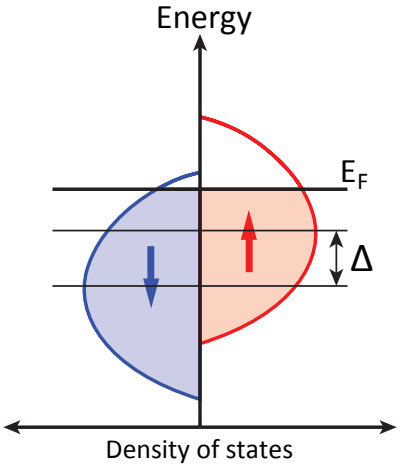

Figure 2.3: Illustration of the Stoner model for a simplified density of states. Spin up and spin down bands are shifted with respect to another by the on-site Stoner splitting Δ. This leads to an imbalance in the filling of states with spin up and down and thereby to the formation of a spin moment.

magnetic interaction. In the *ab initio* implementation of spin dynamics, the calculation starts from some given spin configuration for which the effective torques are calculated. Subsequently, the orientations of the atomic spins are advanced in time through numerical time integration and a new spin configuration is obtained, from which the whole procedure is repeated. In such an implementation, the smallness of the deviation angle θ from the non-collinear magnetic configuration is simply realized by choosing an appropriately small time step in the numerical integration.

To gain more insight in the adiabatic approximation and rigid spin approximation, below we compare in some more detail the stability of the atomic spin moment with the stability of long-range magnetic order under rigid spin rotations.

2.3.1 Stoner model

To assess the stability of the atomic spin moment we briefly consider the Stoner model, following [13]. In this model the effective Coulomb-interaction between the electrons is supplemented by an additional spin-dependent potential $V_{\pm} = \pm I\tilde{\mu}$, where $+$ and $-$ indicate spin up and down, respectively, I is the characteristic energy related to the on-site Coulomb repulsion between the electrons and $\tilde{\mu} = \mu/\mu_{\mathrm{B}}$, with μ the average magnetic moment per site in units of μ_{B}. This potential induces a uniform shift of the spin-up and spin-down bands by an amount of $\Delta = 2I\tilde{\mu}$, as is illustrated in Fig. 2.3.

The value of the spin moment should be determined self-consistently from the integration of the density of states over all occupied states:

$$\tilde{\mu} = \int^{E_{\mathrm{F}}(\tilde{\mu})} [D_0(E + I\tilde{\mu}) - D_0(E - I\tilde{\mu})]\, dE \equiv f(\tilde{\mu}), \tag{2.2}$$

where $D_0(E)$ is the nonmagnetic density of states and $E_{\mathrm{F}}(\tilde{\mu})$ is implicitly defined by the total number of electrons as determined by charge neutrality. The function $f(\tilde{\mu})$ is odd in $\tilde{\mu}$ and saturates at values $\pm\tilde{\mu}_s$ for $\tilde{\mu} \to \pm\infty$, which corresponds to the situation that all occupied states have the same spin. As is easily confirmed by considering a graphical solution of $\tilde{\mu} = f(\tilde{\mu})$, non-zero solutions always exist when $df/d\tilde{\mu}|_{\tilde{\mu}=0} > 1$. This leads to the Stoner criterion

$$2ID_0(E_{\mathrm{F}}) > 1. \tag{2.3}$$

This criterion allows for a simple physical interpretation. According to the Pauli exclusion principle only electrons with different spin can occupy the same state. However, this costs a large amount of energy owing to the Coulomb repulsion between the electrons. To minimize the interaction energy, it is favorable to fill the states only partly, and thereby form spin moments. A spin-imbalanced filling is possible for sufficiently large on-site interaction and density of states, such that many different states can be populated. The density of states scales roughly as the inverse energy of tunneling between lattice sites, hence the Stoner criterion can also be seen as a balance between kinetic and interaction energy. Only when the electrons interact strong enough, itinerant magnetism is possible. For localized systems (small tunneling and hence large density of states) the Stoner criterion is always satisfied and the magnetic moment is almost maximal, in agreement with Hund's first rule. The latter case corresponds to the situation of the 4f spins in rare-earth metals. The energy $\Delta = 2I\tilde{\mu}$, which can also be interpreted as the on-site exchange interaction, determines the energy associated with a single-electron spin-flip, which is in the order of 1 eV for transition metals.

2.3.2 Rigid spin approximation and effective exchange interactions

Next we consider the stability of the long-range magnetic order. To this end we investigate the energy required for small rotations from the collinear situation. First we show that this energy is determined by the tunneling between the sites. Subsequently we give a physical interpretation of the expressions for the effective exchange parameters.

Following [8], we assume a general multi-band Hubbard model with Hamiltonian

$$\mathcal{H} = \sum_{\lambda\lambda'\sigma} t_{\lambda\lambda'}\; c^+_{\lambda\sigma} c_{\lambda'\sigma} + \frac{1}{2} \sum_{\{\lambda_i\}\sigma\sigma'} U_{\lambda_1\lambda_2\lambda'_1\lambda'_2}\; c^+_{\lambda_1\sigma} c^+_{\lambda_2\sigma'} c_{\lambda'_2\sigma'} c_{\lambda'_1\sigma}, \tag{2.4}$$

where $\lambda = im$ denote the site numbers i and orbital quantum numbers m, whereas $\sigma = \uparrow, \downarrow$ is the spin projection and $c^\dagger$ (c) are fermionic creation (annihilation) operators. $t_{\lambda\lambda'}$ and $U_{\lambda_1\lambda_2\lambda_1'\lambda_2'}$ are single-particle tunneling and Coulomb matrix elements. To study the influence of a small rotation we consider a spiral magnetic configuration. The *rigid rotation* of the spinor-electron operators $c_\lambda = c_{im}$ at site i can be written as:

$$c_{im} \to \mathbb{U}_i(\theta, \phi_i) c_{im} \tag{2.5}$$

where

$$\mathbb{U}_i(\theta, \phi_i) = \begin{pmatrix} \cos\theta/2 & \sin\theta/2 \exp(-\mathrm{i}\phi_i) \\ -\sin\theta/2 \exp(\mathrm{i}\phi_i) & \cos\theta/2 \end{pmatrix}, \tag{2.6}$$

with polar angles $\theta_i = \theta$ and $\phi_i = \mathbf{q}\mathbf{R}_i$, $\mathbf{R}_i$ denoting the lattice vector.

Since the Coulomb interaction is taken only on-site, the rigid rotation of the spins at different sites does not influence the second term of the Hamiltonian. Hence, in the local approximation the inter-site exchange interaction associated with the non-collinearity of the spins at different sites is purely due to the single-particle tunneling terms. For the change of the Hamiltonian we then obtain:

$$\begin{aligned} \delta\mathcal{H} &= \sum_{\lambda\lambda'\sigma} t_{\lambda\lambda'} c^+_{\lambda\sigma} (\mathbb{U}_i^+ \mathbb{U}_j - \mathbb{I}) c_{\lambda'\sigma} \equiv \delta_1\mathcal{H} + \delta_2\mathcal{H} \\ \delta_1\mathcal{H} &= \sin^2\frac{\theta}{2} \sum_{\lambda\lambda'\sigma} t_{\lambda\lambda'} c^+_{\lambda\sigma} [\exp(\mathrm{i}\mathbf{q}(\mathbf{R}_i - \mathbf{R}_j)) - 1] c_{\lambda'\sigma} \\ \delta_2\mathcal{H} &= \frac{1}{2}\sin\theta \sum_{\lambda\lambda'} t_{\lambda\lambda'} c^+_{\lambda\downarrow} c_{\lambda'\uparrow} [\exp(\mathrm{i}\mathrm{q}\mathbf{R}_i) - \exp(\mathrm{i}\mathrm{q}\mathbf{R}_j)] \end{aligned}$$

The corresponding change of the energy follows from the calculation of the expectation value: $\delta E = \langle \delta\mathcal{H} \rangle$. Formal calculation can be done analytically using many-body Greens' functions. It follows that for small θ the change in the energy can be written in the form

$$\delta E = \frac{\theta^2}{4} (\tilde{J}(0) - \tilde{J}(\mathbf{q})). \tag{2.7}$$

The same result is obtained by considering small angle rotations within the Heisenberg model

$$\mathcal{H}_{\mathrm{spin}} = -{\sum_{ii'}}' \tilde{J}_{ii'} \mathbf{e}_i \mathbf{e}_{i'}, \tag{2.8}$$

where the sum symbol indicates a double sum ${\sum_{i,i'}}' = \sum_i \sum_{i' \neq i}$ and $\mathbf{e}_i$ indicate unit vectors in the direction of the atomic spin moment. Hence, $\tilde{J}(\mathbf{q})$ can be considered as the Fourier transform of effective pair-wise exchange interactions, which are given by the formula

$$\tilde{J}_{ii'} = -\mathrm{Tr}_{\omega L} \left(\Sigma_i^s G_{ii'}^\uparrow \Sigma_{i'}^s G_{i'i}^\downarrow \right). \tag{2.9}$$

Here $\Sigma_i^s = (\Sigma_i^\uparrow - \Sigma_i^\downarrow)/2$ is the spin-dependent part of the self-energy Σ_i and the trace is over orbital quantum numbers L and energies ω. Note that it is equally possible to rotate separately the spins of states with given orbital quantum numbers L, L', yielding the orbitally resolved effective exchange parameters

$$\tilde{J}_{iL,i'L'} = -\mathrm{Tr}_\omega \left(\Sigma_{iL}^s G_{iL,i'L'}^\uparrow \Sigma_{i'L'}^s G_{i'L',iL}^\downarrow \right). \tag{2.10}$$

Next we discuss the physical meaning of the effective inter-site exchange interactions. In the Stoner model discussed above Σ_i^s is simply the on-site exchange interaction: $\Sigma_i^s = I_i \tilde{\mu}_i$, which becomes independent of the site index when all atoms are equivalent. Hence, the values of the spin moments are included in $\tilde{J}_{ii'} = J_{ii'}\mu_i\mu_{i'}$ and have the dimension of energy. Further, Eq. (2.9) contains Greens' functions $G_{ii'}^\uparrow$, which represent the amplitude of a spin-up electron inserted at site i' to propagate to site i. The inter-site exchange interaction thus has the meaning of the coupling between the on-site spin moment at site i with a spin-up electron propagating from site i' to site i multiplied by the equivalent coupling in the reverse direction with opposite spin. Without the presence of on-site spin moments there is also no coupling and hence the inter-site exchange interactions should vanish, as indeed follows in the Stoner model ($\Sigma_i^s = 0$ for $\tilde{\mu} = 0$). Calculation for bcc Fe yields effective inter-site exchange interactions in the order of $\tilde{J}_{ii'} \sim 13\,\mathrm{meV}$ for the nearest neighbors [7]. The relevant energy scale is obtained by summing the contributions of all spins $\tilde{J}_0 = \tilde{J}_i^0 = \sum_{i' \neq i} \tilde{J}_{ii'}$ which gives energies of about $\tilde{J}_0 \sim 120\,\mathrm{meV}$.

2.3.3 Limitations of the approximations

In the above analysis we have discussed the energy of collective spin-wave excitations and the on-site exchange splitting Δ. The ratio between these two $J_0/\Delta \sim 0.1$ can be defined as the small parameter involved in the adiabatic approximation. The adiabatic approximation thus means simply that we can separate the longitudinal and transverse degrees of freedom of the atomic spins. For example, we can model the dynamics of the atomic spins as precessional motion in the exchange field of all other spins, with the magnetic moment of each of the spins constant. Although the adiabatic approximation, as well as the rigid spin approximation and the definition of the effective exchange interactions may seem reasonable, it is good to realize their limitations.

First of all, with regards to the definition of the effective exchange interactions, we emphasize that the mapping on the Heisenberg model itself is only valid for small-angle deviations, while the Heisenberg model assumes the same exchange parameter for all angles. The calculation of exchange interactions for large opening angles has been studied in [14], and shows that for Ni the deviation from the Heisenberg model

is quite pronounced already at 45 degrees, and the magnetic moment even vanishes at an angle of 90 degrees. Further, for Ni the adiabatic criterion itself is problematic. This becomes clear mostly when comparing the effective on-site exchange splitting ($\sim$ 300 meV [15]) with the characteristic spin-wave frequency ($\sim$ 100 meV [8]), yielding an adiabatic parameter of only $\hbar\omega/\Delta \sim 0.3$. In this connection it is also useful to mention that time-resolved photoemission experiments on Ni following femtosecond laser excitation indicate that the ultrafast demagnetization in Ni is governed by a reduction of the exchange splitting [16], signifying a strong violation of adiabaticity. While for Fe the resemblance with the Heisenberg model seems much better up to angles of about 90 degrees, it is well-known that no self-consistent magnetic solution for antiferromagnetic bcc Fe can be found. In addition, in contrast to the exchange stiffness, the derivation of the exchange interactions Eq. (2.9) is not rigorous since it explicitly assumes the neglect of the aforementioned vertex corrections. These corrections can be shown to be small in the adiabatic parameter [9].

In addition, situations exist where the anti-adiabatic approximation seems to be satisfied. With this we mean that spin waves are more difficult to excite than the single-particle Stoner excitations and consequently the Stoner criterion determines the Curie temperature, which therefore can be quite high. This type of magnetism was theoretically described for sp electrons in narrow half-metallic impurity bands [17]. Hence the magnetism is mediated by defects, is spatially very inhomogeneous with only a small fraction of the sample ferromagnetically ordered. This mechanism was proposed to be responsible for the magnetism of various carbon and boron systems and has recently been mentioned as well in connection with the defect-mediated ferromagnetism in certain dilute magnetic oxide films [18].

Finally, we refer to the limitations of the rigid spin approximation. Essentially, this neglects all gradients in the local spin density. While this approximation seems to work reasonably well in rare-earth and transition metals, for the description of 5f shells in for example actinide dioxides [19], higher order multipoles are crucial and the rigid spin approximation is certainly insufficient.

In summary, we have reviewed the *ab initio* spin dynamics and examined the main approximations. The next section discusses how to treat relaxation and finite temperature effects.

2.4 Relaxation and finite temperature effects

In the above discussion we have implicitly assumed that all calculations were performed at $T = 0$K. In addition, we did study only the interactions which are responsible for the dynamics, but did not treat the relaxation of the spins to equilibrium. These processes are closely connected and we discuss in this section how these processes can be included within the scheme of *ab initio* spin dynamics.

In the rigid spin approximation the equations of motion for the local magnetization is simply the dissipationless Landau-Lifsthitz equation. This equation conserves the length of the atomic moments as it should do to be consistent with the adiabatic approximation. As a result, the equations of motion have the form

$$d\mathbf{m}_i/dt = -\gamma \mathbf{m}_i \times \mathbf{H}_i \tag{2.11}$$

where $\mathbf{m}_i = \mu_i \mathbf{e}_i$, are the vectors along the direction of the magnetization of the atomic spin and $\mathbf{H}_i = -\partial E/\partial \mathbf{m}_i$ is the effective magnetic field due to the interactions of the atomic spin with the whole system. In the dissipationless Landau-Lifsthitz equation there is only dynamics, neither relaxation nor finite temperature effects are included.

In a similar way as for the Landau-Lifsthitz equation Eq. 1.2, we can include transverse relaxation for the atomic spins:

$$d\mathbf{m}_i/dt = -\gamma \mathbf{m}_i \times \mathbf{H}_i - \frac{\alpha}{\mu}\gamma \mathbf{m}_i \times (\mathbf{m}_i \times \mathbf{H}_i). \tag{2.12}$$

The inclusion of the transverse relaxation of the atomic spins, gives rise to two different types of relaxation on the macroscopic scale. Similar as in the macroscopic Landau-Lifshitz equation, the transverse relaxation on the atomic scale yields transverse relaxation on the macroscopic scale. In addition, the transverse relaxation of the atomic spins will give rise to longitudinal relaxation on the macroscopic scale. For example, when considering a ferromagnet initially in a disordered state, in the course of the simulation the atomic spins will become aligned and the total magnetization will eventually be larger than in the initial state. Note that the introduction of the damping term strictly speaking violates the adiabatic approximation. For example, it was shown in [20] that the damping term follows from the explicit time-dependence of the effective field $\mathbf{H}_i$ that is neglected in the adiabatic approximation.

In order to include finite temperature effects the system is coupled to a heat bath. There are two main approaches: a generalized Nose-Hoover (Bulgac-Kuznecov) thermal bath or Langevin (stochastic) dynamics [12]. The first method can only be used to simulate dynamics in equilibrium with the heat bath. For the study of laser-induced spin dynamics non-equilibrium properties will be very important and therefore we will discuss below only Langevin dynamics.

Langevin dynamics is conceptually very similar to modeling Brownian motion for a small macroscopic particle in a fluid. In line with the assumption of adiabaticity, we can take the conduction electrons as heat bath. These electrons are hopping fast between sites and thereby exert torques on the atomic spins, which change their orientation relatively slowly. Due to scattering the electron motion is not coherent and the torques can be modeled stochasticcally. In this spirit the effective fields $\mathbf{H}_i$

are supplemented by random fields $\mathbf{h}_i^{\mathrm{fl}}$. This yields an equation of the form[2]

$$d\mathbf{m}_i/dt = -\gamma \mathbf{m}_i \times (\mathbf{H}_i + \mathbf{h}_i^{\mathrm{fl}}) - \frac{\alpha}{\mu}\gamma \mathbf{m}_i \times [\mathbf{m}_i \times (\mathbf{H}_i + \mathbf{h}_i^{\mathrm{fl}})] \tag{2.13}$$

The problem of Brownian motion for classical spins was first discussed for non-interacting spins independently in [21, 22]. We customarily assume that the stochastic field is Gaussian distributed with zero mean value:

$$\langle h_{i,j}^{\mathrm{fl}}(t)\rangle = 0 \qquad \langle h_{i,j}^{\mathrm{fl}}(t) h_{i',j'}^{\mathrm{fl}}(t')\rangle = 2D\delta_{ii'}\delta_{jj'}\delta(t-t'). \tag{2.14}$$

Hence the noise is uncorrelated in time (t), space (atomic sites i) and in the cartesian components of each spin (j). D is a measure of the strength of the temperature fluctuations and the coupling of the spins to the heat bath, which is taken only in the linear approximation, and $\langle \cdots \rangle$ denotes averaging over different realizations of the stochastic field. When the system is in equilibrium with the heat bath, averaging over the different realizations of the stochastic variables should yield the Boltzmann distribution. This requirement determines the strength D of the noise terms, yielding [23]:

$$D = \frac{\alpha}{1+\alpha^2}\frac{k_{\mathrm{B}}T}{\gamma\mu}, \tag{2.15}$$

where T is the temperature of the heat bath and k_{B} is the Boltzmann constant. Eq. (2.15) is a manifestation of the fluctuation-dissipation theorem [24, §124], which relates equilibrium fluctuations to the dissipative motion of a macroscopic system. Note also that in the stochastic Landau-Lifshitz equation, the parameter α merely expresses the coupling to the heat bath, and generally differs from the transverse damping parameter that appears in the deterministic macroscopic Landau-Lifshitz equation Eq. (1.2).

When the system is not in equilibrium with the heat bath, the parameter α determines the speed at which equilibrium is achieved as can be understood in a simplified picture as follows. For non-interacting spins, or when the temperature of the heat bath is much higher than the effective field $\mathbf{H}_i$, the relaxation of the spin system to the temperature of the heat bath can be calculated analytically by setting up an equation of motion for the distribution function of the spins [21, 22]. This equation is often referred to as as Fokker-Planck equation in the regime of weak coupling to the heat bath and under the white-noise assumption. In particular, it was shown that for

[2] Formally, it is more transparent to introduce the damping term in the Gilbert form $\alpha\mathbf{m}\times d\mathbf{m}/dt$. This equation can be rewritten in the form of Eq. (2.13) with a rescaled gyromagnetic ratio $\gamma' = \gamma/(1+\alpha^2)$. In that case, the fluctuation-dissipation theorem Eq. (2.15) reads $D = \frac{\alpha}{1+\alpha^2}\frac{k_{\mathrm{B}}T}{\gamma'\mu} = \alpha\frac{k_{\mathrm{B}}T}{\gamma\mu}$. The Landau-Lifsthiz form Eq. (2.13) is chosen simply for numerical convenience. Note also that the fluctuation-dissipation theorem is usually derived in the framework of linear response, which assumes $\alpha \ll 1$ and hence the two representations practically coincide.

a system of non-interacting spins in the presence of an external field along the z axis, the averaging over an ensemble of spins coupled to a heat bath yields:

$$d\langle m_z\rangle/dt = -(\langle m_z\rangle - \langle m_z\rangle_0)/\tau, \tag{2.16}$$

for systems relatively close to equilibrium. This is a familiar result known as Bloch relaxation, where $\langle m_z\rangle_0$ is the equilibrium value of $\langle m_z\rangle$ in the presence of the external field. The characteristic timescale was derived to be

$$\tau = \mu/(2\alpha\gamma k_{\mathrm{B}}T). \tag{2.17}$$

Note that the relaxation of the system to equilibrium as described by Eq. (2.16) governs longitudinal dynamics, despite the fact that the magnitude μ of the atomic moment is constant. This illustrates that the equilibration of the spins in this approach is determined by the equilibration of the transverse degrees of freedom. It is the averaging over the whole ensemble that yields the longitudinal relaxation. Therefore, the longitudinal relaxation time scales with the transverse relaxation parameter α of the atomic spins. Furthermore, we see that $\tau \sim \mu/\gamma = \sigma$, which can be understood as follows. The time it takes to reach equilibrium is limited by how fast angular momentum can be transferred. Since this transfer is determined by the value of α, spins with small μ (σ) relax faster. Finally, we observe the scaling with temperature. When the temperature is high, temperature fluctuations are strong and the system becomes disordered more easily. This might lead to very fast longitudinal relaxation when $T \gg T_{\mathrm{C}}$ which is also the dominant relaxation in the high-temperature limit.

With this we complete our discussion of transverse and longitudinal relaxation and the influence of finite temperature effects within the framework of the *ab initio* spin dynamics. The next section deals with further approximate treatments that make actual calculations computationally more tractable.

2.5 Effective model approximations

So far we did not pay much attention to the more practical and computational issues. First of all, it should be noted that even within the *ab initio* framework, for the calculation of the dynamics one needs to solve the Landau-Lifsthiz equation for all atomic spins simultaneously. Generally this can only be done numerically. Hence, in practice we always should resort to computer simulations to study the spin dynamics, where the orientations of the atomic spins changes from time step to time step according to the torques experienced by the exchange fields. While this can in principle be done, accurate calculations of the full electronic structure for every new spin configuration is usually much too time consuming. Moreover, such calculations are not always really necessary and it is often useful to study first the spin dynamics using simplified model descriptions to understand better what is really required from the more fundamental

description. Hence it can be useful to parameterize part of the problem and in this section we discuss three different levels of descriptions.

The first parametrization is the mapping of the full electronic structure on a tight-binding model. This can be useful when it is expected that the actual band structure is only weakly dependent on the configuration of the spins. Even when this is the case, generally the torques derived from the model electronic structure can deviate significantly from the Heisenberg model. In particular the tight-binding approximation allows a computationally more feasible way of studying essentially non-Heisenbergian effects, which are generally expected to be relevant at high temperatures.

Instead of parameterizing the electronic structure, a more drastic approximation is to directly parameterize the spin Hamiltonian by the Heisenberg model (Eq. (2.8) and run the spin dynamics simulation with fixed exchange parameters defined by Eq. (2.9). This is known in the literature as *atomistic spin dynamics* and is currently a widely used approach [25, 26]. One could also think of intermediate levels of parametrization, such as recalculating the effective exchange parameters not every time step but only at, say, every 10th time step during the simulation. In general, the atomistic spin dynamics can be seen as a first attempt to model purely the dynamic effects that arise from the transverse dynamics of the atomic spins. This is very useful, for example, for the study of critical dynamics [27], thermally activated dynamics [28] and spin-glasses [29].

While the mapping on the Heisenberg model reduces the computational efforts significantly, it is still a numerically challenging task (see also Ch. 3). Therefore, for the modeling of macroscopic dynamics, such as domain-wall motion, it is useful to further reduce the number of degrees of freedom. Instead of solving the equation of motion for every atomic spin, it is also possible to directly write equations of motion for the collective variables or gross variables, which are statistical averages over the atomic spins. Such an approach has been worked out in recent years [30] for the modeling of spin dynamics in the presence of atomic-scale inhomogeneities. This approach takes into account explicitly the local dynamics of the short-length scale excitations induced by the inhomogeneities and thereby provides a unified description of all relevant length scales, allowing a smooth, seamless coupling.

The latter method has so far been worked out only for dynamics at $T = 0$ K. However, by coupling the system to a heat bath and using similar statistical methods, it is also possible to derive an equation for the macroscopic dynamics at finite temperature. The resulting equation for the distribution function of the atomic spins is also known as the Fokker-Planck equation. By using the mean-field approximation and by taking into account only first order deviations from the equilibrium distribution function, an effective macroscopic equation of motion can be derived as was shown by Garanin [31] for ferromagnets with one sublattice. This equation bears the name of Landau-Lifshitz-Bloch equation. It interpolates between the macroscopic Landau-Lifshitz equation below the Curie temperature to the Bloch equation above the Curie

temperature. For example, this approach has been proven to be very useful for the study of magnetization reversal in the vicinity of the Curie temperature [32].

In summary, there are various effective model descriptions that can be very useful for specific purposes. Obviously, there is still one further approximation possible, which is the spin dynamics in the continuum approximation. This regime will be discussed in the next section.

2.6 Phenomenological theory

So far, we have been discussing effective model descriptions based on parametrizations. The situation is different for the macroscopic description, which is based on the continuum approximation. Instead of specific model assumptions, here the essential assumption is only the existence of a macroscopic magnetization density that varies very weakly over the distance of the lattice spacing. Such an approximation can always be made and is independent on the validity of a specific microscopic model. The most celebrated equation of this type is the Landau-Lifshitz equation that has been derived already in 1935 [33], and even today forms the basis for numerous micromagnetic simulations. Here we introduce the phenomenological theory on the basis of the theory of irreversible thermodynamics and discuss how it can also be used as the basis for a microscopic theory.

In the 1980s, it was realized that a general phenomenological equation for spin dynamics can be obtained by applying the theory of irreversible thermodynamics, as described by Onsager's reciprocal relations [34–38], to the study of macroscopic spin dynamics. Onsager's relations themselves were first introduced in the 1930s for the description of transport processes and chemical reactions [39]. The relations are symmetry relations for the phenomenological parameters that appear in linearized macroscopic equations of motion. These macroscopic equations assume the general form $J_j = \Lambda_{jk} X_k$, where J_j are generalized fluxes and X_k are generalized forces. The products $J_j X_j$ describe the entropy production during the irreversible proces. From the invariance of the microscopic equations of motion under reversal of time, the symmetry relation $\Lambda_{jk} = \Lambda_{kj}$ is derived. For example, J_j can be the current and the heat flow, while X_k describe the voltage and temperature gradients. In this case Λ_{jj} are electrical and heat conductance, while the off-diagonal components describe the thermo-electric effects.

For the application to spin dynamics, the generalized flux $J_j = dM_j/dt$ is the rate of change of the magnetization and the effective magnetic field $H_k = -\delta F/\delta M_k$ can be taken as the generalized force. Here F denotes the free energy and M_k the cartesian components of the magnetization. Taking into account that in the presence of magnetic order we should also reverse the total magnetization when time is reversed, the symmetry relations read $\Lambda_{jk}(\mathbf{M}) = \Lambda_{kj}(-\mathbf{M})$, and from this it is possible to derive both the usual Landau-Lifshitz precession and damping (see also Sec. 4.1).

In addition, new types of relaxation processes are obtained, in particular exchange relaxation and the longitudinal relaxation of the magnitude of the magnetization, such as Bloch relaxation. The introduction of these additional relaxation terms was originally motivated by the discrepancies found in the quantitative analysis of domain wall mobility and ferromagnetic resonance line widths [36], as well as for the study of the magnetic response to sudden changes in the temperature [35]. Later, it has been used also for the study of the relaxation of magnetic solitons [40].

As has been mentioned already in Sec. 2.2, it is also possible to study spin waves using a phenomenological theory, provided that the wavelength of the excitations is much longer than the lattice spacing. It is also possible to use the dispersion relations obtained this way as definition of an energy spectrum of effective quasi-particles. Such quasi-particles should have the symmetry of bosons, since they correspond to collective degrees of freedom. Using this as a postulate, it is possible to construct a quantum theory of spin waves without the assumption of a specific microscopic spin model [3, 41] and valid at sufficiently low temperatures. Within this approach, it is possible to study thermodynamical properties as well as the relaxation of the spin system to thermodynamical equilibrium [41]. It is interesting to note that this microscopic treatment yields similar longitudinal relaxation processes as the ones obtained from the application of Onsager's relations; however, these processes are absent in the macroscopic Landau-Lifshitz equation. In addition, within the spin-wave regime, this phenomenological treatment can also be used as the basis for studying the dynamics of spin waves together with electrons and phonons and their mutual interactions.

With the discussion of the phenomenological theory we have completed our review of the theoretical concepts of spin dynamics. In the final section of the chapter we will discuss which of these concepts are at present most relevant for the study of laser-induced spin dynamics.

2.7 Modeling laser-induced spin dynamics in multisublattice magnets

In the preceding sections we have discussed the theory of spin dynamics on a general level. In the last section of this chapter we focus on to the specific problem of laser-induced spin dynamics, with an emphasis of modeling the dynamics that appears in magnets with multiple magnetic sublattices. We start by outlining why this problem is in general very difficult and can therefore only be modeled using appropriate approximations. In particular, we emphasize that laser-induced spin dynamics is dominantly longitudinal dynamics. Subsequently, we propose two complementary attempts to be used to gain understanding of longitudinal spin dynamics. The first approach is atomistic spin modeling. The second approach is to model longitudinal dynamics on a phenomenological basis, as is possible by considering the relaxation

processes derived in the framework of Onsager's relations.

As we have seen in the preceding sections of this chapter, modeling spin dynamics in general is very difficult and relies on approximations that often cannot be fully justified and/or controlled. Moreover, in addition to this already very complicated problem, the study of laser-induced spin dynamics should also take into account the light-matter interaction. The latter inevitably requires the study of the dynamics of the electrons in response to the electric field of light $\mathbf{E}$, which in the optical regime dominates over the direct coupling of the magnetic field of the laser pulse with the spins. While such an approach is in principle feasible within the framework of the time-dependent spin-density functional theory, it certainly goes beyond the adiabatic approximation which forms the basis of the *ab initio* spin dynamics. At the same time, many experiments are done with metals, in which the response to the electric field is dominated by the heating ($\propto |\mathbf{E}|^2$), and we should study spin dynamics at finite temperature. Hence it is clear that the theory of laser-induced spin dynamics is in general very difficult and for all practical purposes we should use appropriate approximations.

Therefore, it is very useful to take some experimental facts as a guide to decide what to study first. As has been mentioned in Sec. 6.2, probably the most striking feature that follows from experiments is that there is spin dynamics below the picosecond timescale. This is generally much faster than the conventional precessional dynamics as described by the macroscopic Landau-Lifshitz equation and from that you can conclude that it is longitudinal spin dynamics. This makes it relevant to gain understanding in the longitudinal dynamics as such, without a full account of the actual light-matter interaction that causes this dynamics.

Still we need to partly account for the laser pulse, otherwise there is no longitudinal dynamics at all. To simplify the actual process of laser excitation, we take into account that the fastest longitudinal dynamics is seen in metals. For such systems the heat capacity of the electrons in metals is rather small compared to the heat capacity of the spins and the lattice. Therefore, the excited electrons are expected to equilibrate quickly internally and thereby easily reach temperatures significantly above the Curie temperature, while the energy transfer to the spins (and lattice) will be much slower. This analysis forms the basis for the three-temperature model which was used already for the analysis of the first experimental studies of femtosecond laser-induced spin dynamics (see [42] and Sec. 1.3.2). Within the three temperature model, the study of laser-induced spin dynamics is essentially the study of the response of the magnetic system to a rapidly changing electron temperature. We will use the same approach in this thesis. However, rather than modeling the spin system in internal equilibrium, in this thesis we extend on the analysis by modeling the actual nonequilibrium dynamics of the spins, which does not rely on the concept of a spin temperature.

We emphasize that the above arguments implicitly assume the possibility to distinguish between the dynamics of the electrons and the spins. We have seen in Sec. 2.3,

that such an approach is indeed possible by distinguishing between the dynamics of the orientation of the atomic spins, which is considered to be slow compared to the fast electron dynamics, which determines the magnitude of the atomic spins. While in principle both a change in the length of the atomic spins and the excitation of spin waves give rise to longitudinal spin dynamics, the spin waves are easier to excite in metals and therefore expected to dominate. Hence, along with modeling the laser pulse as heat pulse, the modeling in the adiabatic approximation seems most relevant.

Further, by modeling the laser pulse as a heat pulse, it is clear that we need to study spin dynamics at finite temperature. On a microscopic level, such an approach is indeed possible using Langevin dynamics as has been introduced in Sec. 2.4. The first study of femtosecond laser-induced longitudinal dynamics using Langevin dynamics has been reported by Chantrell and coworkers [43], within the framework of the atomistic spin dynamics. Moreover, the same group where the first that could successfully simulate the highly counter-intuitive dynamics that where experimentally observed in a ferrimagnet [44], which further led them to the discovery of purely thermally driven magnetization reversal in such magnets [45]. Hence, this approach is quite successful and flexible, although it is computationally relatively costly. To reduce computational demands, one could also use the Landau-Lifshitz-Bloch model. This has been done recently [46, 47] for ferromagnets with one sublattice. Generalization of the Landau-Lifshitz-Bloch equation for ferromagnets to, for example, ferrimagnets is in principle possible but requires essentially a new solution of the Fokker-Planck equation. Therefore, the approach is less flexible than the atomistic spin dynamics method, since the latter can be used for any given spin model and for any type of Heisenberg exchange without further approximations.

As has been mentioned already in Sec. 2.6, a complementary approach to study longitudinal dynamics is possible on a phenomenological basis by using Onsager's relations. This approach has the advantage that it does not rely on specific model assumptions. So far this method has not been applied to laser-induced spin dynamics, but nevertheless it offers clear advantages. For example, a phenomenological theory generally yields a mathematically compact formalism which allows for a simplified qualitative analysis. This is very useful to assess on a general level which types of dynamics can be expected, before going into a more detailed description and assessment of the microscopic mechanisms. In addition, the phenomenological theory is rather flexible with regards to the introduction of additional magnetic sublattices. In particular, the theory has already been worked out for antiferromagnets. Hence, there seems no fundamental bottleneck to also work out the phenomenological theory for general multisublattice magnets with arbitrary exchange couplings between the sublattices.

In summary, at present the most promising approaches to the study of longitudinal spin dynamics in multisublattice magnets are the atomistic spin dynamics method and the phenomenological theory based on Onsager's relations. While the atomistic spin

dynamics method has proven to be already quite successful, it is still computationally rather expensive. In Chapter 3 we address this issue by the development of stable and fast numerical integration methods. The phenomenological theory needs to be generalized to arbitrary multisublattice magnets and has so far not been applied to laser-induced spin dynamics. We will present the derivation and generalization of the phenomenological theory in Chapter 4, and work this out and apply the theory in the Chapters 5 and 6.

References

[1] E. Runge and E. Gross, Phys. Rev. Lett. **52**, 997 (1984).

[2] S. Sharma, J. Dewhurst, C. Ambrosch-Draxl, S. Kurth, N. Helbig, S. Pittalis, S. Shallcross, L. Nordström, and E. Gross, Phys. Rev. Lett. **98**, 196405 (2007).

[3] C. Kittel, *Quantum Theory of Solids* (Wiley, New York, 1963).

[4] A. Liechtenstein, M. Katsnelson, and V. Gubanov, J. Phys. F: Met. Phys. **14**, L125 (1984).

[5] A. Lichtenstein, M. Katsnelson, and V. Gubanov, Solid State Commun **54**, 327 (1985).

[6] A. Liechtenstein, M. Katsnelson, V. Antropov, and V. Gubanov, J. Magn. Magn. Mater. **67**, 65 (1987).

[7] M. Katsnelson and A. Lichtenstein, Phys. Rev. B **61**, 8906 (2000).

[8] M. Katsnelson and A. Lichtenstein, Eur. Phys. J. B **30**, 9 (2002).

[9] M. Katsnelson and A. Lichtenstein, J. Phys.: Condens. Matter **16**, 7439 (2004).

[10] V. Korenman, J. Murray, and R. Prange, Phys. Rev. B **16**, 4032 (1977).

[11] V. Antropov, M. Katsnelson, M. van Schilfgaarde, and B. Harmon, Phys. Rev. Lett. **75**, 729 (1995).

[12] V. Antropov, M. Katsnelson, B. Harmon, M. van Schilfgaarde, and D. Kusnezov, Phys. Rev. B **54**, 1019 (1996).

[13] R. Zeller, in *Lecture Notes of the 40th IFF Spring School Juelich* (2009).

[14] S. Turzhevskii, A. Lichtenstein, and M. Katsnelson, Sov. Phys. Solid State **32**, 1138 (1990).

[15] J. Kubler, *Theory of Itinerant Electron Magnetism* (Oxford Science Publications, Oxford, 2009).

[16] H.-S. Rhie, H. Dürr, and W. Eberhardt, Phys. Rev. Lett. **90**, 247201 (2003).

[17] D. Edwards and M. Katsnelson, J. Phys.: Condens. Matter **18**, 7209 (2006).

[18] J. Coey and S. Chambers, MRS Bulletin **33**, 1053 (2008).

[19] P. Santini, S. Carretta, G. Amoretti, R. Caciuffo, N. Magnani, and G. Lander, Rev. Mod. Phys. **81**, 807 (2009).

[20] V. Antropov, J. Appl. Phys. **97**, 10A704 (2005).

[21] W. Brown, Phys. Rev. **130**, 1677 (1963).

[22] R. Kubo and N. Hashitsume, Prog. Theor. Phys. Suppl. **46**, 210 (1970).

[23] J. García-Palacios and F. Lázaro, Phys. Rev. B **58**, 14937 (1998).

[24] L. Landau and E. Lifshitz, *Course of Theoretical Volume 5: Statistical Physics I* (Pergamon Press Ltd., Oxford, 1980), 3rd ed.

[25] O. Mryasov, U. Nowak, K. Guslienko, and R. Chantrell, Europhys. Lett. **69**, 805 (2005).

[26] B. Skubic, J. Hellsvik, L. Nordström, and O. Eriksson, J. Phys.: Condens. Matter **20**, 315203 (2008).

[27] D. Landau, Phys A **205**, 41 (1994).

[28] U. Nowak, O. Mryasov, R. Wieser, K. Guslienko, and R. Chantrell, Phys. Rev. B **72**, 172410 (2005).

[29] B. Skubic, O. Peil, J. Hellsvik, P. Nordblad, L. Nordström, and O. Eriksson, Phys. Rev. B **79**, 024411 (2009).

[30] V. Dobrovitski, M. Katsnelson, and B. Harmon, Phys. Rev. Lett. **90**, 067201 (2003).

[31] D. Garanin, Phys. Rev. B **55**, 3050 (1997).

[32] N. Kazantseva, D. Hinzke, R. Chantrell, and U. Nowak, Europhys. Lett. **86**, 27006 (2009).

[33] L. Landau and E. Lifshitz, Phyz. Z. Sowjetunion **8**, 153 (1935).

[34] T. Iwata, J. Magn. Magn. Mater. **31-34**, 1013 (1983).

[35] T. Iwata, J. Magn. Magn. Mater. **59**, 215 (1986).

[36] V. Baryakhtar, Zh. Eksp. Teor. Fiz **87**, 1501 (1984).

[37] V. Baryakhtar, Fiz. Nizk. Temp. **11**, 1198 (1985).

[38] V. Baryakhtar, Zh. Eksp. Teor. Fiz. **94**, 196 (1988).

[39] L. Onsager, Phys. Rev. **37**, 405 (1931).

[40] V. Baryakhtar, B. Ivanov, A. Sukstanskii, and E. Melikhov, Phys. Rev. B **56**, 619 (1997).

[41] A. Akhiezer, V. Baryakthar, and S. Peletminskii, *Spin Waves* (North-Holland Publishing Company, Amsterdam, 1968).

[42] E. Beaurepaire, J.-C. Merle, A. Daunois, and J.-Y. Bigot, Phys. Rev. Lett. **76**, 4250 (1996).

[43] N. Kazantseva, U. Nowak, R. Chantrell, J. Hohlfeld, and A. Rebei, Europhys. Lett. **81**, 27004 (2008).

[44] I. Radu, K. Vahaplar, C. Stamm, T. Kachel, N. Pontius, H. Dürr, T. Ostler, J. Barker, R. Evans, R. Chantrell, et al., Nature **472**, 205 (2011).

[45] T. Ostler, J. Barker, R. Evans, R. Chantrell, U. Atxitia, O. Chubykalo-Fesenko, S. El Moussaoui, L. Le Guyader, E. Mengotti, L. Heyderman, et al., Nat. Commun. **3**, 666 (2012).

[46] U. Atxitia, O. Chubykalo-Fesenko, N. Kazantseva, D. Hinzke, U. Nowak, and R. Chantrell, Appl. Phys. Lett. **91**, 232507 (2007).

[47] U. Atxitia and O. Chubykalo-Fesenko, Phys. Rev. B **84**, 144414 (2011).

CHAPTER 3

Stable and fast numerical integration of the stochastic Landau-Lifshitz equation[1]

3.1 Introduction

Dynamics of magnetic materials have been theoretically studied for many years starting from the seminal work by Landau and Lifshitz [1] (see, e.g., the monographs [2–4]). The current interest in this area is rapidly growing due to new important fields of applications such as spintronics [5] and ultrafast laser-induced spin dynamics [6–9]. In many situations, such as in the ultrafast laser-induced demagnetization [10], it is crucial to model the dynamics of the spins far out of equilibrium, where the conventional macrospin approximation breaks down. Furthermore, for the modeling of amorphous alloys and the interaction of domain walls with pinning centers [11], there are atomic-scale inhomogeneities which require multi-scale simulations bridging macroscopic and microscopic lengths [12]. In [13, 14] a method of *ab initio* spin dynamics was suggested relating the first-principle electronic structure calculations with the Landau-Lifshitz-type dynamics of classical spins within the framework of the rigid-spin approximation. Thus, Atomistic Spin Dynamics (ASD) simulations are important from many points of view. To do calculations at finite temperatures and out of equilibrium, the commonly used approach is the Langevin (stochastic) dynamics [14]. This approach with first-principle magnetic interaction parameters has recently

[1] Adapted from: J. Mentink, M. Tretyakov, A. Fasolino, M. Katsnelson and T. Rasing, *J. Phys.: Condens. Matter* **22**, 176001 (2010).

been implemented [15] and applied for simulating dilute magnetic semiconductors [16] and spin glasses [17]. Langevin spin dynamics is also used as a phenomenological simulation tool, not connected with first-principle theory. An implementation of this type was reported in [18] and applied to laser-induced magnetization dynamics [19].

The heart of Langevin spin dynamics simulations is the integration of the stochastic Landau-Lifshitz (SLL) equation for each atomic spin (see also Eq. 2.13). This equation is non-linear and analytical solutions for interacting systems exist for two spins only. In systems of interest for applications the number n of spins is typically of order 10^6 and the integration should be done numerically. Due to the interactions, one has to solve a system of $3n$ coupled non-linear equations. To compute quantities in equilibrium, this very large system should be simulated over long time intervals, usually from 10 fs to 1 ns. This is a challenging computational task.

Thus, ASD requires effective numerical integrators for the SLL equation. Due to the large system size and long simulation time, such numerical methods should be, on the one hand, sufficiently stable and on the other hand very fast. The latter rules out the use of fully implicit integrators such as the implicit midpoint (IMP) scheme (for its application for Langevin spin dynamics, see e.g., [20]). Despite its superior stability properties which allows large step sizes, typically 10 fs, IMP is slow in practice since the implicitness requires solution of $3n$ non-linear coupled equations at every time step. Langevin spin dynamics simulations have often been based on the Heun method [15, 18], which has the advantage of being fast in terms of the number of operations per time step. However, this method has poor stability properties requiring a relatively small step size, typically ranging from 0.01 fs to 1 fs, depending on the implementation. We also note that since the accuracy of the first-principle magnetic interaction parameters is limited to 10%, the accuracy of numerical methods is, to some extent, less important here than their stability (in the sense of the ability to use larger step sizes for long time simulations). Hence, both the standard implicit and explicit numerical integrators are not optimal for ASD and it is desirable to develop a numerical method that is both stable and fast. Also, ASD simulations are often used to study systems with different interactions and/or different symmetries. Therefore, in addition we should require numerical integrators for ASD to be universal in their implementation. Such a method is proposed in this chapter.

As is known from the deterministic ([21–23] and the references therein) and stochastic [24–26] numerical approaches, to numerically integrate dynamical systems over long time intervals with relatively large step sizes, it is advisable to preserve geometrical properties of the continuous dynamics. Therefore, one should construct and use geometrical integrators for ASD. In the case of the deterministic Landau-Lifshitz (LL) equation, there are geometric integrators [22, 23, 27, 28] that are both stable and fast. Usually, these schemes are semi-implicit, which means that these methods, unlike IMP, require only the solution of 3 linear coupled equations for each spin individually. However, the implementation of these methods depends on symme-

try and interactions in a system under consideration, which makes it difficult to use them for models with arbitrary lattice structures. Further, semi-implicit methods for the deterministic LL equation are also considered in the review [29]. Being based on IMP, they have the potential to combine stability and low computational costs like the geometric integrators but with the advantage of a universal implementation. In this chapter we use the idea of semi-implicitness to derive new numerical methods for Langevin spin dynamics simulations, which are both stable and fast and allow universal implementation. In particular, we show that, due to the enhanced stability, our semi-implicit integrator (named SIB) allows time steps by a factor of $10 \div 10^3$ larger than the standard Heun method.

This chapter is organized as follows. In Sec. 3.2, we formulate the problem in mathematical terms, introduce the necessary notation and examine the conservation properties of the SLL equation. In Sec. 3.3, we propose two new semi-implicit methods (semi-implicit A (SIA) and semi-implicit B (SIB)) and recall the Heun scheme and IMP. Both SIA and SIB intrinsically preserve the length of individual spins while SIB (like IMP) also possesses other conservation properties in the deterministic case. The later is apparently the reason for the superiority of SIB which is the numerical method of our choice for ASD. In Sec. 3.4, we present some results of numerical experiments. We first test the considered numerical methods in the deterministic case without damping, using a simple system of two interacting spins. Then the 1D Heisenberg chain is used as a test system for the stochastic case. In the last section, we draw conclusions and recommendations for future work. Two appendices are included to provide some auxiliary knowledge of stochastic numerics and about ergodicity of the SLL equation.

3.2 Numerical Methods

In this section we formulate the problem in mathematical terms and introduce the necessary notation. In addition, we discuss why we use the Stratonovich interpretation for the stochastic LL equation. Finally, we examine the properties of the solution of the equations under study.

The (deterministic) Landau-Lifshitz equation in dimensionless variables can be written in the form:

$$\frac{dX^i}{dt} = -X^i \times B^i(\mathbf{X}) - \alpha X^i \times [X^i \times B^i(\mathbf{X})] \,, \quad i = 1, \ldots, n, \tag{3.1}$$

where n is the number of spins, $X^i = (X^i_x, X^i_y, X^i_z)^\top$ are three-dimensional column-vectors representing unit spin vectors[2] and $\mathbf{X} = ({X^1}^\top, \ldots, {X^n}^\top)^\top$ is a $3n$-dimensional

[2] In the chapter, we follow the standard notation of the theory of stochastic differential equations and use capital letters to denote solutions of differential equations while we use small letters for the initial data and for corresponding "dummy" variables.

column-vector formed by the X^i; B^i is the effective field acting on spin i; $\alpha \geq 0$ is the damping parameter. In Eq. (3.1) the time is normalized by the precession frequency $\omega_{\hat{B}} = \gamma \hat{B}$, where $\hat{B}$ is some reference magnetic field strength, and the effective field $B = ({B^1}^\top, \ldots, {B^n}^\top)^\top$ is also normalized by $\hat{B}$ and is given by

$$B(\mathbf{x}) = -\nabla H(\mathbf{x}), \tag{3.2}$$

where H is the Hamiltonian of the problem. Then

$$B^i(\mathbf{x}) = -\nabla_i H(\mathbf{x}),$$

where ∇_i is the gradient with respect to the Cartesian components of the effective magnetic field acting on spin i.

For atomistic spin dynamics, the most important contributions to the Hamiltonian are the Heisenberg exchange for the interaction between the spins H_{ex}, the Zeeman energy for the interaction with an external field H_{ext}, and the uniaxial anisotropy H_{ani} defining a preferential direction of the spins. Therefore we consider here the following Hamiltonian for our problem:

$$H = H_{\text{ex}} + H_{\text{ext}} + H_{\text{ani}}, \tag{3.3}$$

where

$$H_{\text{ex}}(\mathbf{x}) = -\sum_{i \neq j} J_{ij} x^i x^j, \qquad H_{\text{ext}}(\mathbf{x}) = -B_0 \sum_i x^i, \qquad H_{\text{ani}}(\mathbf{x}) = K \sum_i (x^i e_K)^2.$$

Here J_{ij} are the exchange parameters, B_0 is the uniform external field, K is the strength of the anisotropy, and e_K is a unit vector that defines the anisotropy axis. Note that with these contributions to the Hamiltonian the effective fields B^i are linear in x. In realistic materials usually $|J_{ij}| \gg |B_0| \gg |K|$. For the exchange parameters themselves, typically $J_{i(i+1)} \gg J_{i(i+j)}$, $j > 1$, i.e., all spins interact with each other but the nearest-neighbor interactions dominate. Since all the spins interact, Eq. (3.1) involves simultaneous solution of a $3n$ system of non-linear equations. Due to the interactions between the spins, each effective field B^i is time-dependent and Eq. (3.1) has in general no analytical solution. As a result, efficient numerical methods are required to study spin systems. In turn, the time-dependence of the effective field is usually considered as the main source of instability in the numerical integration.

In order to perform spin dynamics at finite temperature, fluctuations are included according to the Brownian motion approach for spins by adding fluctuating torques to Eq. (3.1) [30, 31]. The stochastic Landau-Lifshitz (SLL) equation is then given by

$$\frac{dX^i}{dt} = -X^i \times (B^i(\mathbf{X}) + b^i) - \alpha X^i \times [X^i \times (B^i(\mathbf{X}) + b^i)], \qquad i = 1, \ldots, n, \tag{3.4}$$

where the fluctuating magnetic fields b^i are uncorrelated Gaussian white noises interpreted in the sense of Stratonovich and

$$\left\langle b_l^i(t)\right\rangle = 0, \quad \left\langle b_l^i(t)b_k^j(0)\right\rangle = 2D\delta_{ij}\delta_{lk}\delta(t)\ , \quad i = 1,\ldots,n, \tag{3.5}$$

with $\langle\cdot\rangle$ denoting ensemble averages and $l,k = x,y,z$ labeling the Cartesian coordinates while D is the strength of the fluctuations. According to the fluctuation dissipation theorem, we choose

$$D = \frac{\alpha}{(1+\alpha^2)}\frac{k_bT}{\hat{X}\hat{B}}\ , \tag{3.6}$$

where $\hat{X}$ is the (non-normalized) magnetization of each spin.

Note that Eq. (3.4) is a differential equation with multiplicative noise which requires from us to specify in which sense we interpret the stochastic equation [32]. As said above, we use here the Stratonovich interpretation following [30]. This choice can be motivated as follows. First of all, the Stratonovich interpretation (contrary to any other one and, in particular, to the Ito interpretation) leads to preservation of the individual spin length (see Eq. (3.10) below) by Eq. (3.4), which is very important to model spin systems (see also a similar discussion in [20]). Further, it is natural to model a perturbation of the Landau-Lifshitz dynamics by Gaussian noise with a finite bandwidth spectrum (i.e., by a colored noise [32]), possibly with a very short correlation time. The white noise $b(t)$ in Eq. (3.4) has zero correlation radius (see Eq. (3.5)) and a spectrum with infinite bandwidth. This noise is a convenient idealization which can be viewed as an approximation of the colored noise with short correlation time. Indeed, if we consider a sequence of solutions $X_n(t)$ of the equations $\dot{X}_n^i = -X_n^i \times (B^i(\mathbf{X}_n) + b_n^i) - \alpha X_n^i \times [X_n^i \times (B^i(\mathbf{X}_n) + b_n^i)]$, where $b_n(t)$ is a sequence of Gaussian processes which correlation functions that go to the δ-function as $n \to \infty$, then $\mathbf{X}_n$ tends to the solution $\mathbf{X}$ of Eq. (3.4) if it is interpreted in the Stratonovich sense [33, Chapter 2], [34, Chapter 5]). We also note in passing that one can model a Gaussian colored noise by the Ornstein-Uhlenbeck process [32] which can be substituted in Eq. (3.4) instead of the white noise $b(t)$. It could be of interest to study the influence of the correlation radius on the stochastic Landau-Lifshitz dynamics. We do not pursue such questions in this chapter but remark that effective numerical methods for differential equations with colored noise are available in [25, 35] which can be adapted to the SLL equation with colored noise.

Since we will exploit some results from stochastic numerics [25] which in turn follows the standard theory of stochastic differential equations, it is convenient to re-write the SLL equation Eq. (3.4) in differential form [32]:

$$\begin{aligned} dX^i &= X^i \times a_i(\mathbf{X})dt + X^i \times \sigma(X^i) \circ dW^i(t), \\ X^i(0) &= x_0^i, \qquad |x_0^i| = 1,\ i = 1,\ldots,n, \end{aligned} \tag{3.7}$$

where $W^i(t) = (W_x^i(t), W_y^i(t), W_z^i(t))^\top$, $i = 1, \ldots, n$; $W_x^i(t)$, $W_y^i(t)$, $W_z^i(t)$, $i = 1, \ldots, n$, are independent standard Wiener processes; $a_i(\mathbf{x})$, $\mathbf{x} \in \mathbb{R}^{3n}$, are three-dimensional column-vectors defined by

$$a_i(\mathbf{x}) = -B^i(\mathbf{x}) - \alpha x^i \times B^i(\mathbf{x}) \; ; \tag{3.8}$$

and $\sigma(x)$, $x \in \mathbb{R}^3$, is a 3×3-matrix such that

$$\sigma(x)y = -\sqrt{2D}y - \alpha\sqrt{2D}x \times y \tag{3.9}$$

for any $y \in \mathbb{R}^3$. Note that the symbol '$\circ$' in Eq. (3.7) means that the corresponding stochastic integral is interpreted in the Stratonovich sense [32]. We recall [33] (see also [32, 34]) that the Stratonovich stochastic integral can be defined as the mean-square limit of the middle Riemann sums, which, in particular, makes it evident why the midpoint scheme (see Eq. (3.15) below) satisfies the Stratonovich calculus.

Let us consider some properties of the solution to (Eqns. 3.7)-(3.9). First, the length of each individual spin is a constant of motion, i.e.,

$$|X^i(t)| = 1, \;\; i = 1, \ldots, n, \quad t \geq 0. \tag{3.10}$$

Indeed, we have

$$d\frac{1}{2}|X^i|^2 = X^i dX^i = X^i \left[X^i \times a_i(\mathbf{X})\right] dt + X^i \left[X^i \times \sigma(X^i) \circ dW_i(t)\right] = 0.$$

Other general conservation laws of (Eqna. 3.7)-(3.9) and also of (Eq. 3.1) do not exist. However when we restrict ourselves to realistic systems, we have the damping coefficient $\alpha \ll 1$. This means that, in practice, solutions of (Eqns. 3.7)-(3.9) are, in a sense, close to the deterministic solutions of (Eq. 3.1) with $\alpha = 0$. Hence the precessional motion can usually be considered as dominant. In turn, the largest contribution to the precessional motion is due to the exchange interaction. Therefore, it is relevant to examine the conservation laws for $\alpha = 0$. Since the Hamiltonian has no explicit time-dependence, energy is conserved for this case. Further, when only Heisenberg exchange is included we have for the total spin:

$$\sum_i \frac{dX^i}{dt} = \sum_{i \neq j} J_{ij} \, X^i \times X^j = \sum_{i > j} J_{ij} \left(X^i \times X^j + X^j \times X^i\right) = 0 \tag{3.11}$$

since $J_{ij} = J_{ji}$. We recall that the orientation of individual spins is time dependent, which makes the effective field acting on each spin time dependent due to the exchange interaction. However, at the same time, the symmetry of the exchange interaction ensures that the total spin is time-independent. Therefore the conservation of total

spin is an important property for stable numerical integration of the exchange interaction. By the same arguments, when an external field is added, the total spin will precess in the external field:

$$\sum_i \frac{dX^i}{dt} = B_0 \times \sum_i X^i. \tag{3.12}$$

For this case, the length of the total spin is a constant of motion, as well as the component of the total spin along B_0. Hence the energy is also conserved but the transversal components of the total spin with respect to B_0 oscillate in time. When anisotropy is included, there are no conservation properties associated with the total spin. Finally, ergodicity of the solution to Eqns. (3.7)-(3.9) is a relevant property. This is discussed in Appendix A.

3.3 Numerical methods

In this section we consider numerical integrators for the stochastic Landau-Lifshitz equation Eqns. (3.7)-(3.9). We first recall two existing numerical methods, one of which is explicit (the projected Heun scheme) and the other implicit (the midpoint scheme). Both are unsatisfactory since either they violate conservation laws (HeunP) or they are computationally very expensive (IMP). Therefore, in the main part of this section we present the two newly developed numerical methods (SIA and SIB). These methods are called semi-implicit and aim at combining the advantages of the existing explicit and implicit schemes.

As it is known from the deterministic ([21–23] and the references therein) and stochastic ([24–26]) numerical approaches, to achieve accuracy in long-time simulations (e.g., for computing ergodic limits) it is advisable to preserve the structural properties of the continuous dynamics by the approximating discrete ones. Then it is important to consider not only orders of convergence but also structural properties of numerical integrators for the SSL equation. Both convergence and structural properties of the schemes presented are discussed in Sec. 3.3.3.

Throughout we use (for simplicity) a uniform discretization of a time interval $[0, t_\star]$ with step size $h = t_\star/N$. The value at the initial step is $X_0^i = x_0^i$, $i = 1, \ldots, n$, and X_k^i, $i = 1, \ldots, n$, denotes the approximate solution $X^i(t_k)$, $i = 1, \ldots, n$, to the SLL equation at time t_k, $k = 1, \ldots, N$.

3.3.1 Existing explicit and implicit numerical methods

"Heun + projection (HeunP)".

The Heun method can be seen as a predictor-corrector method. Its prediction step, which we denote by $\mathcal{X}_k$, is the Euler approximation. The standard Heun method

should be adjusted by an additional projection step which is needed to ensure that the length of each individual spin remains constant. For the SLL equation Eqns. (3.7)-(3.9), the HeunP method reads

$$\begin{aligned} \mathcal{X}_k^i &= X_k^i + hX_k^i \times a_i(\mathbf{X}_k) + h^{1/2} X_k^i \times \sigma(X_k^i)\xi_{k+1}^i, \\ {X^*}_{k+1}^i &= X_k^i + h\left[X_k^i \times a_i(\mathbf{X}_k) + \mathcal{X}_k^i \times a_i(\mathcal{X}_k)\right]/2 \\ &\quad + h^{1/2}\left[X_k^i \times \sigma(X_k^i)\xi_{k+1}^i + \mathcal{X}_k^i \times \sigma(\mathcal{X}_k^i)\xi_{k+1}^i\right]/2, \\ X_{k+1}^i &= {X^*}_{k+1}^i / |{X^*}_{k+1}^i|, \end{aligned} \tag{3.13}$$

where $\mathcal{X}_k = ({\mathcal{X}_k^1}^\top, \ldots, {\mathcal{X}_k^n}^\top)^\top$; $\xi_{k+1}^i = \left(\xi_{k+1}^{i,1}, \xi_{k+1}^{i,2}, \xi_{k+1}^{i,3}\right)^\top$; $\xi_k^{i,j}$, $j = 1,2,3$, $i = 1,\ldots,n$, $k = 1,\ldots,N$, are independent identically distributed (i.i.d.) random variables which can be distributed, e.g., as

$$P(\xi_k^{i,j} = \pm 1) = 1/2 \tag{3.14}$$

or $\xi_l^{i,j} \sim \mathcal{N}(0,1)$. This indicates that the $\xi_l^{i,j}$, are i.i.d. Gaussian random variables with zero mean and unit variance. In Eq. (3.13) we explicitly added $i = 1,\ldots,n$ to emphasize that first $\mathcal{X}_k$ has to be calculated for all spins, before $\mathbf{X}_{k+1}$ is computed. We come back to this point in the numerical experiments (Sec. 3.4).

"Implicit Midpoint (IMP)".

Contrary to the HeunP method, IMP (see, e.g. [25, p. 45])) is implicit. For the SLL equation Eqns. (3.7)-(3.9), IMP reads:

$$\begin{aligned} X_{k+1}^i &= X_k^i + h\frac{X_k^i + X_{k+1}^i}{2} \times a_i\left(\frac{\mathbf{X}_k + \mathbf{X}_{k+1}}{2}\right) \\ &\quad + h^{1/2}\frac{X_k^i + X_{k+1}^i}{2} \times \sigma\left(\frac{X_k^i + X_{k+1}^i}{2}\right)\xi_{k+1}^i, \end{aligned} \tag{3.15}$$

$$\tag{3.16}$$

where $\xi_{k+1}^i = \left(\xi_{k+1}^{i,1}, \xi_{k+1}^{i,2}, \xi_{k+1}^{i,3}\right)^\top$; $\xi_k^{i,j}$, $j = 1,2,3$, $i = 1,\ldots,n$, $k = 1,\ldots,N$, are i.i.d. random variables which can be distributed according to, e.g., Eq. (3.14). Alternatively, we can choose $\xi_k^{i,j}$ being distributed as the ξ_h defined below (see [24, 25]). Let $\zeta \sim \mathcal{N}(0,1)$ be a Gaussian random variable with zero mean and unit variance. We define

$$\xi_h = \begin{cases} \zeta, \ |\zeta| \le A_h, \\ A_h, \ \zeta > A_h, \\ -A_h, \ \zeta < -A_h, \end{cases} \tag{3.17}$$

where $A_h = \sqrt{2|\ln h|}$. We note that if one takes $\xi_k^{i,j} \sim \mathcal{N}(0,1)$, IMP can, in general, diverge (see a counter-example in [24, 25]).

3.3.2 New semi-implicit numerical methods

Here we propose two new semi-implicit integration schemes, simply called semi-implicit A (SIA) and semi-implict B (SIB). In the spirit of the review [29], they are called semi-implicit since they require only to solve n or, $2n$ in the case of the SIB scheme, linear 3×3 systems at each time-step, which can be done analytically. The starting point for derivation of the semi-implicit methods is the IMP scheme. To reduce the degree of implicitness, we replace $\mathbf{X}_{k+1}$ in the argument of a_i and σ in IMP by a predictor $\mathcal{X}_k$. As a consequence, resolving the implicitness at each time step is simplified (in comparison to IMP) to solving a linear 3×3 system per spin that is independent of the interactions between the spins. The difference between SIA and SIB is the choice for $\mathcal{X}_k$. Both semi-implicit methods have effectively the same computational cost as explicit schemes.

"Semi-implicit scheme A (SIA)".

Similar to the HeunP method, for the SIA scheme we take the Euler approximation for the predictor $\mathcal{X}_k$. The SIA method for the SLL equation reads

$$\begin{aligned} \mathcal{X}_k^i &= X_k^i + hX_k^i \times a_i(\mathbf{X}_k) + h^{1/2} X_k^i \times \sigma(X_k^i)\xi_{k+1}^i, \\ X_{k+1}^i &= X_k^i + h\frac{X_k^i + X_{k+1}^i}{2} \times a_i\left(\frac{\mathbf{X}_k + \mathcal{X}_k}{2}\right) \\ &\quad + h^{1/2}\frac{X_k^i + X_{k+1}^i}{2} \times \sigma\left(\frac{X_k^i + \mathcal{X}_k^i}{2}\right)\xi_{k+1}^i, \end{aligned} \tag{3.18}$$

where $\xi_{k+1}^i = \left(\xi_{k+1}^{i,1}, \xi_{k+1}^{i,2}, \xi_{k+1}^{i,3}\right)^\top$; $\xi_l^{i,j}$ are i.i.d. random variables as in IMP Eq. (3.15) (the same two possibilities).

"Semi-implicit scheme B (SIB)".

SIA can be viewed as a second iteration for the implicit equation due to IMP. As zero approximation of $\mathbf{X}_{k+1}$, we took $\mathbf{X}_k$ and then the second iteration was constructed so that the length of individual spins is preserved. One can see that the first iteration (or in other words the prediction step) of SIA does not preserve the spin length. We are therefore proposing the SIB method which keeps the spin-length conserving IMP structure at both iterations and, according to our numerical tests (see Sec. 3.4), this modification is crucial for the performance of the semi-implicit schemes.

The SIB method for the SLL equation reads

$$\begin{aligned} \mathcal{X}_k^i &= X_k^i + h\frac{X_k^i + \mathcal{X}_k^i}{2} \times a_i(\mathbf{X}_k) + h^{1/2}\frac{X_k^i + \mathcal{X}_k^i}{2} \times \sigma(X_k^i)\xi_{k+1}^i, \\ X_{k+1}^i &= X_k^i + h\frac{X_k^i + X_{k+1}^i}{2} \times a_i\left(\frac{\mathbf{X}_k + \mathcal{X}_k}{2}\right) \\ &\quad + h^{1/2}\frac{X_k^i + X_{k+1}^i}{2} \times \sigma\left(\frac{X_k^i + \mathcal{X}_k^i}{2}\right)\xi_{k+1}^i, \end{aligned} \tag{3.19}$$

where $\xi_{k+1}^i = \left(\xi_{k+1}^{i,1}, \xi_{k+1}^{i,2}, \xi_{k+1}^{i,3}\right)^\top$; $\xi_l^{i,j}$ are i.i.d. random variables as in IMP Eq. (3.15) (the same two possibilities).

Remark 1 *One can continue the process and make several iterations for the implicit equation due to IMP, e.g., in our tests about* 10 *iterations were sufficient to resolve the implicitness up to the machine accuracy. However, in practice the use of several iterations would be too computationally expensive while SIB already demonstrates stability and accuracy comparable with IMP.*

3.3.3 Properties of the methods

We start by examining convergence of the methods presented in this section and then discuss some conservation properties. For completeness, in Appendix B we recall some generic facts about stochastic numerics [25].

All four methods considered in this section are of weak order one for both choices of the distributions of $\xi_k^{i,j}$ (discrete and continuous). If $\xi_l^{i,j} \sim \mathcal{N}(0,1)$, then HeunP is also of mean-square order 1/2. IMP, SIA, and SIB are of mean-square order 1/2 if $\xi_k^{i,j}$ have the cut-off Gaussian distribution Eq. (3.17). These convergence properties are proved using the standard results [25, Chapters 1 and 2]. In the deterministic case (i.e., $D = 0$) all four methods are of order two.

Note that in this chapter we limit ourselves to methods of weak order 1 and of mean-square order 1/2. The system Eqns. (3.7)-(3.9) has noncommutative noise (see the definition in, e.g. [25, p. 28]). Then mean-square methods of orders higher than 1/2 require simulation of multiple Ito integrals which is computationally expensive. It is possible to construct higher order weak methods for Eqns. (3.7)-(3.9) but, due to the multiplicative, noncommutative nature of the noise, they would be too complicated and they are not considered here. We also note that the problem with multiplicative noise can be circumvented by rewriting the SLL equation in spherical coordinates, for which the system is Hamiltonian and the noise becomes additive, but then numerical difficulties arise when the polar angle is close to 0 or π.

When α is small, the SLL equation (3.7)-(3.9) is a system with small multiplicative noise. In this case the weak-sense errors of all the methods considered in this section

are of order $O(h^2 + \alpha^2 h)$ [36],[25, Chapter 3]. The smallness of noise can be further exploited to construct high accuracy but low order efficient methods following the recipe from [25, 36].

We now discuss *conservation properties* of the schemes. The HeunP method Eq. (3.13) has only one conservation property – norm-preservation which is due to the projection step. Heun without the projection step would conserve the total spin but then violates norm-preservation. Omitting the projection step also gives very poor results for the interaction with an external magnetic field. In practice the projection step can be exploited for error control. Energy is not conserved by HeunP when $\alpha = 0$. HeunP has the advantage of being very flexible, its implementation is independent of the symmetry of the system and types of interactions used. The method is also fast since integration can be done for each spin separately.

Due to the structure of IMP, the difference $X^i_{k+1} - X^i_k$ is always perpendicular to $X^i_k + X^i_{k+1}$. Therefore $(X^i_k + X^i_{k+1})(X^i_{k+1} - X^i_k) = 0$ and hence $|X^i_{k+1}|^2 = |X^i_k|^2$, i.e., the length of each spin is exactly preserved by IMP without any need of projection. In the deterministic case with $\alpha = 0$ and under only the Heisenberg exchange, IMP conserves the total spin. The proof follows directly from Eq. (3.11) with replacing dX^i/dt by $X^i_{k+1} - X^i_k$ and X^i by $(X^i_k + X^i_{k+1})/2$. The total energy conservation for the case of $\alpha = 0$ can be proven similarly. Preservation of all the main structural properties of the SLL equation by IMP comes at a cost. Since all spins are coupled, a system of $3n$ non-linear algebraic equations has to be solved at each time step. This is a major limitation for application of IMP to atomistic spin dynamics, where the number of spins is typically of order $n = 10^6$. Some further remarks on conservation properties of both HeunP and IMP in the deterministic case are given in [22].

The SIA method is very close to the HeunP method. However, unlike the HeunP method SIA preserves the constraint $|X^i(t)| = 1$ exactly, without the need of projection. This follows directly from the observation that the norm conservation of each spin is independent of the point at which a_i and σ are evaluated. Let us now look at SIA in the deterministic case with $\alpha = 0$. Regarding total spin, the relevant symmetry property is:

$$\frac{X^i_k + X^i_{k+1}}{2} \times \frac{X^j_k + \mathcal{X}^j_k}{2} + \frac{X^j_k + X^j_{k+1}}{2} \times \frac{X^i_k + \mathcal{X}^i_k}{2} \neq 0 \ ,$$

which is violated since the Euler approximation for $\mathcal{X}^i_k$ depends only on the orientation of the spins at the current time step ($\mathbf{X}_k$), but not on $\mathcal{X}^i_k$, whereas X^i_{k+1} is also determined by the value X^i_{k+1} itself. Owing to this difference, for $\alpha = 0$ the total spin cannot be preserved by SIA. Also, the energy is not a conserved quantity by SIA and the scheme introduces numerical damping. Hence SIA has the same conservation properties as HeunP, and it is of interest to investigate whether the built-in norm conservation is sufficient to improve stability properties.

Unlike SIA, SIB has the norm-conserving midpoint structure for both X^i_k and $\mathcal{X}^i_k$.

In the case of a two-spin deterministic system with $\alpha = 0$ we proved analytically that both energy and total spin are conserved quantities of SIB. Hence for this system SIB has the same conservation properties as IMP. At the same time, implementation-wise very little additional computational efforts are required by SIB compared to HeunP and SIA. Hence it is of interest to compare the performance of SIB with SIA, in particular to investigate the influence of preservation of norm-conservation and preservation of deterministic conservation laws on the stability properties of the methods. As our numerical experiments (see the next section) suggest, SIB outperforms SIA while SIA is only slightly better than HeunP. This observation implies, in particular, that the built-in norm conservation alone is not sufficient for obtaining superior numerical integrators for ASD and preservation of other structural properties of the SLL equation should guide one in constructing effective numerical methods.

3.4 Numerical Experiments

In this section, we compare performance of the integrators introduced in the previous section using two model problems. In Sec. 3.4.1, we present some results of the experiments in the deterministic case without damping (*i.e.* $\alpha = 0$), to illustrate the conservation properties of the numerical methods. In Sec. 3.4.2, we consider the stochastic case using the 1D Heisenberg chain as a test system. We show that the methods that preserve the deterministic integration laws give rise to a more stable integration for the stochastic spin dynamics.

3.4.1 Two interacting spins

In order to illustrate the conservation properties of the numerical schemes related to the deterministic precessional motion, we choose the simple case of two interacting spins with equal length $|X^1| = |X^2| = 1$. As a result of the exchange interaction, the spins rotate around a common axis, where the precession frequency is given by $\omega_J = 2J\cos\theta/2$ with the angle θ between the spins and the Heisenberg exchange parameter J.

First, we emphasize the relevance of simultaneously updating the effective field. Due to the interaction, the effective field acting on each spin is determined by the other spin. Therefore, when using a predictor-corrector method like HeunP, it is highly relevant to simultaneously update the effective fields after the prediction step before calculating the correction step. Hence, the correction step is computed taking into account that $a_i(\mathcal{X}_k)$ depends on $\mathcal{X}_k^{j\neq i}$ and not on $\mathcal{X}_k^i$ alone. Therefore, at each time step the effective field must be computed twice. By its design, a predictor-corrector method must be implemented in this way, otherwise it will, as a rule, become a scheme of lower order. Fig. 3.1 shows the computed trajectory with and without

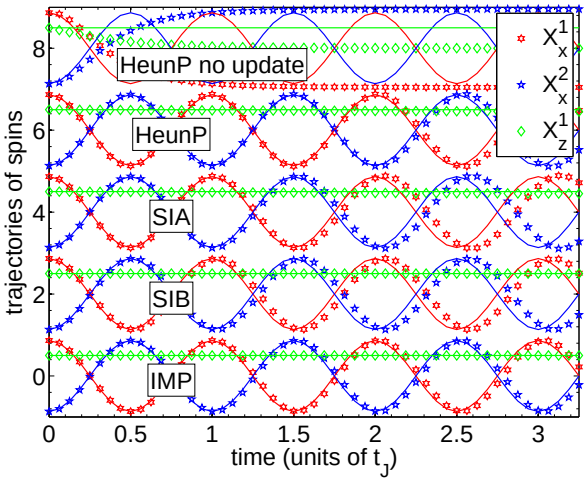

Figure 3.1: Comparison of the explicit HeunP, implicit IMP and semi-implicit methods SIA and SIB for the deterministic case $\alpha = 0$. The trajectory of 2 interacting spins is shown by plotting the x components of the 2 spins and 1 z-component. Solid lines indicate the analytical solution. The upper panel shows that without simultaneous update of the effective field the integration is very unstable. IMP demonstrates the best performance. All methods introduce errors in the precession period $t_J = 2\pi/J$ corresponding to initial condition. For the purpose of illustration, a large step size $h = 1/16$ is used.

simultaneous update for the HeunP method. To achieve a comparable accuracy without simultaneous update of the effective field, the step size should be decreased by a factor of $10^2 \div 10^3$.

In the four lowest panels of Fig. 3.1 we compare the considered integrators implemented with simultaneous update of the effective fields. For illustration purposes, a large step size is used ($h = 1/16$). For small times, all methods show reasonable agreement with the analytical solution, but IMP clearly has the best performance for this system. However, even IMP, which preserves the conservation laws instrinsically, introduces errors in the precession frequency. Since these errors do not effect the conservation properties of the methods, we do not consider them in detail.

Next, we compare the conservation properties of the considered methods for the 2-spin system. To this end, Fig. 3.2 shows the error in the total spin as a function of integration time. Both SIB and IMP exactly conserve the total spin, whereas HeunP and SIA have numerical dissipation. For clarity, only the z-component of the total spin is plotted. The errors in the x and y-components of the total spin are much smaller since the numerical errors in the x, y motion of the individual spins cancel each other due to the symmetry.

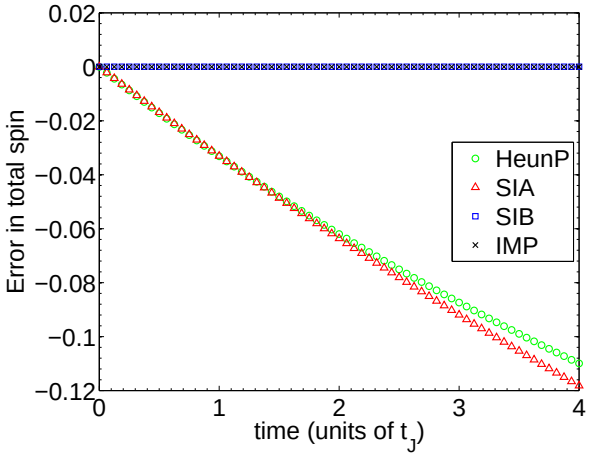

Figure 3.2: Conservation of total spin for HeunP, IMP, SIA, and SIB. Shown is the error in the total spin for the same system as in Fig. 3.1. Both IMP and SIB preserve the total spin up to machine precision, whereas SIA and HeunP introduce a numerical damping. Here $t_J = 2\pi/J$ is the precession period.

Despite the fact that SIA conserves the norm of each spin exactly, the numerical damping is slightly larger than for HeunP. Both their errors are strongly dependent on the initial condition. When the spins are almost parallel, HeunP has a larger numerical error than SIA since the projection step transforms a larger amount of transverse motion to longitudinal motion. In the case of Fig. 3.2 an initial condition with $\theta_0 = 120°$ is used, which is closer to anti-parallel motion and, therefore, HeunP has a smaller error than SIA.

For this simple 2-spin system, the energy and total spin are directly related: $(X_k^1 + X_k^2)^2 = (X_k^1)^2 + (X_k^2)^2 + 2X_k^1 X_k^2 = 2 + E_k/J$. Hence both SIB and IMP conserve energy, whereas both HeunP and SIA dissipate energy. For larger systems with only nearest neighbor interactions, SIB conserves total spin and energy like IMP as well, while obviously SIB requires much lower computational efforts than IMP. The conservation properties of SIB can be proven analytically but this is beyond the scope of the present chapter.

In conclusion, the results of the numerical experiments with 2 interacting spins and $\alpha = 0$ show that both HeunP and SIA introduce numerical errors in the conserved quantities whereas SIB and IMP preserve the total spin and energy of the test system.

3.4.2 1D Heisenberg chain

In this section we compare the semi-implicit integration schemes with the explicit and implicit methods in the stochastic case. The simplest model of classical interacting spins is the 1D Heisenberg chain with nearest-neighbor interactions. For this system, an analytical expression for the mean energy per spin is available [37, 38]:

$$\overline{H}_{\text{analytic}} \equiv \frac{\langle H_{\text{ex}} \rangle}{2nJ} = \left(1 - \frac{1}{n}\right)\left(\frac{k_b T}{2J} - \coth\left(\frac{2J}{k_b T}\right)\right). \tag{3.20}$$

This expression gives us a convenient way to check how accurately the temperature of the system is reproduced in simulations using the numerical methods from Sec. 3.3. Note that $\overline{H} \to -1 + 1/n$ as the temperature $T \to 0$ since we have normalized the energy with the number of spins n and the interaction energy of 2 spins $2JX^1X^2$ tends to $2J$ when the temperature goes to zero.

The comparison of the HeunP method with the semi-implicit schemes for the temperature is shown in Fig. 3.3 for step size $h = 1/32$, damping $\alpha = 0.1$, exchange parameter $J = 1$, spin length $|X^i| = 1$, and number of spins $n = 100$. The random variables used in the numerical schemes are simulated according to the cut-off Gaussian distribution Eq. (3.17). At a time step k the sample average $\hat{H}_k$ for the energy H per spin is computed as

$$\hat{H}_k = \frac{1}{M}\sum_{m=1}^{M} \frac{H_{\text{ex}}(\mathbf{X}_k^{(m)})}{2nJ}\ , \tag{3.21}$$

where $\mathbf{X}_k^{(m)}$ are independent realizations of $\mathbf{X}_k$ obtained by a numerical scheme (see also Appendix B). The corresponding standard deviation σ_{H_k} is also computed. In the experiment an ensemble of $M = 20$ independent trajectories was used. The values plotted in Fig. 3.3, with the 95% confidence intervals determined by the standard deviation, were obtained after equilibrating the system for a time $t_a = 1024\, t_J$, long enough for the system to be sufficiently close to equilibrium. Here $t_J = 2\pi/(2J)$ is the reference precession period for (almost) parallel spins. We find that both HeunP and the semi-implicit schemes show reasonable agreement with the analytical results, indicating that they obey the Stratonovich interpretation rule as expected.

The next question is which method is more accurate. Fig. 3.3 shows that SIB is consistent with the analytical solution at all data points. To the contrary, HeunP and SIA show slight discrepancies. To investigate this more accurately, we study the numerical error by varying the step size. For illustration, we used the lowest temperature $k_b T/(2J) = 0.1$. The results are shown in Fig. 3.4.

It is found that SIB outperforms both SIA and HeunP, and SIB remains stable down to only 4 steps per precession period. At such a large step size, SIA and HeunP are unstable though SIA performs slightly better than HeunP. Note that in physical

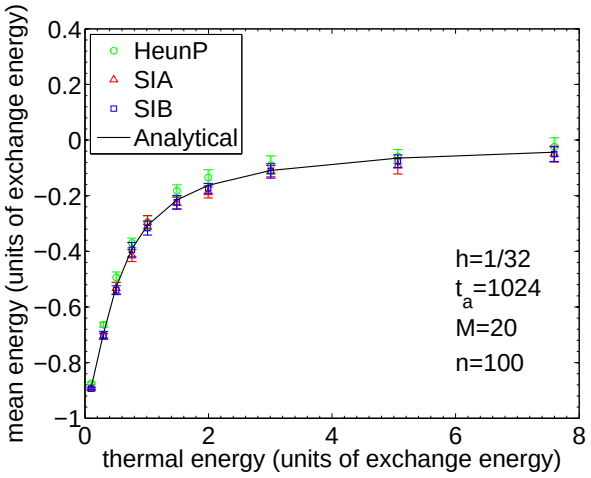

Figure 3.3: Temperature check of of the semi-implicit methods SIA and SIB compared with the explicit HeunP method. Shown is the mean energy per spin of the 1D Heisenberg chain, as function of temperature, computed with the parameter values shown at the bottom. All the schemes demonstrate reasonable agreement with the analytical result (3.20).

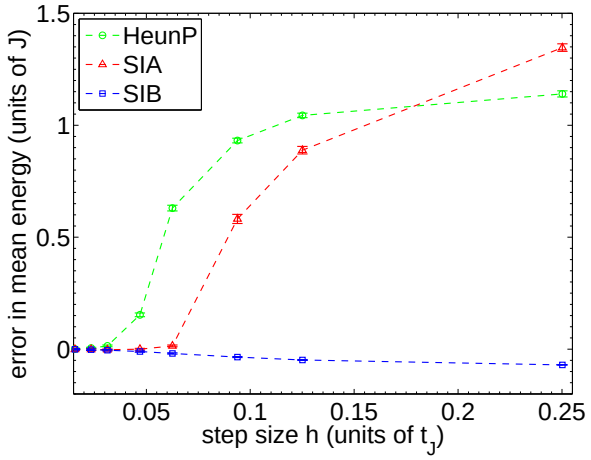

Figure 3.4: Stability of the semi-implicit methods SIA and SIB comared with the explicit HeunP method. Shown is the error in the mean energy as a function of the step size h for the lowest temperature considered in Fig. 3.3, $k_bT/(2J) = 0.1$. It is found that SIB remains stable up to 4 steps per precession period $t_J = 2\pi/(2J)$, while SIA and HeunP become unstable and produce unreliable results.

units, with the exchange energy $J\hat{X}^2 = 1$ mRy, $\hat{X} = 1\mu_B$, 4 steps per precession period corresponds to a step size of about 20 fs. Hence, for SIB the step size is only limited by the precession period of the spins, and there is no need to decrease the step size to preserve the conservation laws accurately enough. This should be compared with the step size of 10 as which was reported in [15], resulting in an enormous improvement of a factor $2 \cdot 10^3$ in the allowed step size. However, the mentioned implementation of ASD in [15] is based on HeunP without the simultaneous update of the effective field. As follows from Fig. 3.1 and Fig. 3.4, when the effective field is properly updated, HeunP also allows a larger step size. However, the increase is limited to about 2 fs for the system studied here. Compared to HeunP, SIA has only slightly better stability properties, which we attribute to the intrinsic norm conservation. The superior stability properties of SIB can apparently be explained by its built-in deterministic conservation properties. For the system studied here, SIB allows step sizes by about a factor of 10 larger than HeunP and by about a factor of 5 larger than SIA.

Let us now compare the performance of the semi-implicit methods with the full implicit IMP. The 1D Heisenberg chain is not convenient for this purpose, unless we choose a very small number of spins. In addition, for this comparison stability is not the major issue since we already know that the step size of SIB is limited only by the precession period. Therefore, we are more interested in the intrinsic properties of the integrators that are independent of the system under study. Hence the relevant property here is the convergence of the semi-implicit and IMP schemes. To reduce computational costs of the experiment, we again use a system with only 2 spins.

To experimentally observe the order of convergence, a small statistical error is needed. To this end, a combination of ensemble and time averaging was used. As before, for an ensemble with M trajectories, we let the system equilibrate for a time $t_a = 2048\, t_J$. Subsequently, the equilibrated sample mean $\hat{H}_k$ (see Eq. (3.21)) is calculated for a time $t_b = 6144\, t_J$. The calculated values of $\hat{H}_k$ are then divided in $P = 8$ subsets of length $L = t_b/P = 768\, t_J$ and in each subset the time mean $\check{H}_p$ is computed. Eventually, the total mean $\check{H}$ is the average of the time means over the P subsets and its statistical error Δ is estimated by two standard deviations of $\check{H}_p$ divided by $\sqrt{P}$, which gives half of the length of the 95% confidence intervals for $\check{H}$. The results are presented in Fig. 3.5.

Note that for this small system no instabilities appear in SIA, and this method shows the first weak-order convergence as expected. Surprisingly, SIB demonstrates a second-order convergence, which might be related to the fact that the energy is a conserved quantity for $\alpha = 0$. This means that for the energy only numerical errors from the damping term show up, hence the convergence for the energy in the stochastic case might be better than the convergence for a general quantity. The small error for SIA at the one but smallest time step in Fig. 3.5 is caused by the change in sign of the error. The error values are given in Table 3.1. Here also the data for HeunP are

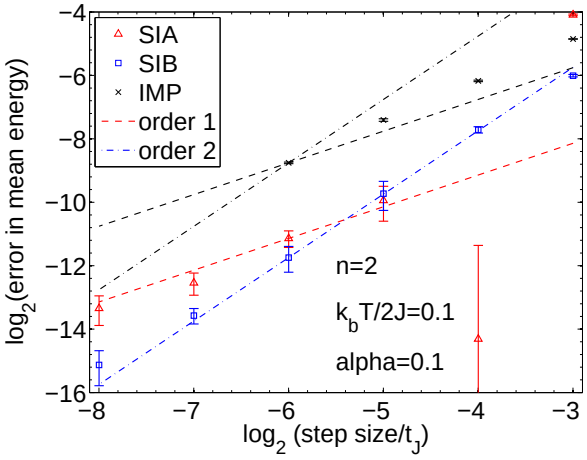

Figure 3.5: Comparison of the semi-implicit methods SIA and SIB with the full implicit IMP. Shown is the weak-order convergence of SIA, SIB and IMP schemes for the mean energy per spin. Both axes are logaritmic with base 2. For small enough step size, the slope gives the order of convergence. Surprisingly, both SIA and SIB are more accurate than IMP. Moreover, SIB shows a higher order convergence than IMP. Here $t_J = 2\pi/(2J)$ indicates the reference precession period.

provided. HeunP is not shown in Fig. 3.5 since it appears to be in the asymptotic regime only for the smallest time steps. We note that there is a sign change of the HeunP error, which is the reason for its small error at $h = 1.564 \times 10^{-2}$. IMP is very costly for a large ensemble, therefore the two smallest step sizes were not computed.

In general, the performance of SIB in the experiments has been better than SIA. Interestingly, despite the excellent stability of IMP, the accuracy of IMP in the stochastic case lags behind SIB and SIA. This is a good example of a situation when a method with better stability not necessarily has a better accuracy. It was also observed in the deterministic case with damping that SIB sometimes shows better accuracy than IMP. This implies that in the case of damped motion the numerical integration error of IMP can be larger than for SIB, as it is observed in the stochastic case. These results show that at least for the systems considered here, SIB has the same stability properties as IMP, but at considerable lower computational costs.

In conclusion, we find that in the stochastic case the semi-implicit method B, with built-in deterministic conservation laws is more stable and has smaller numerical errors than both the SIA and the HeunP method. Surprisingly, in the stochastic case SIB is even better than IMP in terms of accuracy and convergence. SIA performs only slightly better than HeunP in the stochastic case, and from this we find that norm-conservation is not the most important criterion for stable numerical integration of the

Table 3.1: The values of error in the mean energy $\epsilon = \check{H} - \overline{H}_{\mathrm{analytic}}$ and the corresponding statistical error Δ for the considered schemes. In each consecutive row the step size is smaller by a factor 2.

		HeunP		SIA		SIB		IMP	
h	M	ϵ	Δ	ϵ	Δ	ϵ	Δ	ϵ	Δ
1.251e-1	2^4	4.23e-1	1.1e-3	5.87e-2	1.1e-3	-1.55e-2	4.1e-4	-3.46e-2	1.3e-4
6.255e-2	2^5	2.71e-2	6.0e-4	-4.92e-5	3.3e-4	-4.76e-3	3.3e-4	-1.38e-2	2.3e-4
3.128e-2	2^7	1.84e-3	4.5e-4	-1.02e-3	3.7e-4	-1.18e-3	3.6e-4	-5.77e-3	1.4e-4
1.564e-2	2^{12}	-9.74e-6	8.1e-5	-4.43e-4	7.9e-5	-2.92e-4	5.9e-5	-2.31e-3	4.0e-5
7.819e-3	2^{16}	-9.55e-5	3.9e-5	-1.68e-4	4.0e-5	-8.20e-5	1.4e-5		
3.909e-3	2^{17}	-8.24e-5	3.0e-5	-9.62e-5	3.0e-5	-2.79e-5	1.1e-5		

SLL equation. Hence, SIB combines the advantages of both HeunP and IMP, being both fast and stable as well as universal. For systems with only nearest neighbor interactions, SIB allows step sizes by a factor of 10 larger than the popular HeunP scheme, and a factor of $2 \cdot 10^3$ larger than the HeunP method without simultaneous update of the effective field. Since in practice nearest-neighbor interactions dominate, SIB is expected to be also advantageous for systems with more than nearest-neighbor interactions.

3.5 Conclusions and Outlook

In this chapter we introduced two new semi-implicit integrators (SIA and SIB) for stochastic Atomistic Spin Dynamics (ASD) simulations. These schemes combine the advantages of the standard explicit projected Heun method (HeunP) and the fully implicit midpoint method (IMP). The semi-implicit methods are fast as explicit schemes since they require only the solution of 3 linear coupled equations for each spin individually and therefore they are effectively explicit. For stability, the most important conservation law is apparently the preservation of the total spin for the case without damping. Like IMP, SIB preserves this conservation law for the dominant interactions in the system and the stability properties of SIB are comparable with IMP. SIA, which has norm-conservation built-in but not the deterministic conservation laws, shows only slightly better stability than HeunP in the stochastic case. Therefore, we recommend the use of SIB for ASD simulations.

Owing to the enhanced stability, larger step sizes can be used with SIB. From our numerical experiments we can conclude that the step size can be increased by a factor of about 10 compared to the explicit HeunP. For SIB, the step size is only limited by the precession frequency of the individual atomic spins in the exchange field, which allows for step sizes of about one fourth of the precession period which can be as large as 20 fs. This value of the step size has to be compared with the 10 as that was reported for a standard implementation of ASD simulations [15], which is based on the HeunP

method without the simultaneous update of the effective field. Hence, the factor $2 \cdot 10^3$ improvement can be attributed to a proper update of the effective field and built-in conservation of the total spin for SIB. Interestingly, numerical experiments indicate that SIB can also be more accurate than IMP in the stochastic case. Further checks for the stochastic case, including larger systems, more complicated interactions, and correlations are therefore very interesting.

Future work should also study the conservation properties of SIB in more detail in order to give a further explanation of its excellent behavior. It would also be of interest to obtain a method obeying conservation laws for systems with more complicated interactions (*e.g.* next-nearest neighbor, anisotropy). In addition, one might exploit the fact that the damping motion and the precessional motion are always perpendicular, which potentially can be used to design an integrator that exactly dissipates energy like in continuous dynamics. Our method can also be of value for micromagnetic simulations and we expect that similar techniques can be exploited for other physical systems, where interactions between particles are governed by a global conservation law, e.g., systems based on diffusion equations such as the Schrödinger equation.

References

[1] L. Landau and E. Lifshitz, Phys. Zs. Sowjet. **8**, 153 (1935).

[2] A. Akhiezer, V. Bar'yakhtar, and S. Peletminskii, *Spin Waves* (North Holland, Amsterdam, 1968).

[3] S. Vonsovsky, *Magnetism* (Wiley, New York, 1974).

[4] A. Aharoni, *Introduction to the Theory of Ferromagnetism* (Oxford University Press, Oxford, 2000).

[5] I. Žutić, J. Fabian, and S. Das Sarma, Rev. Mod. Phys. **76**, 323 (2004).

[6] T. Gerrits, H. van den Berg, J. Hohlfeld, L. Bär, and T. Rasing, Nature **418**, 509 (2002).

[7] A. Kimel, A. Kirilyuk, P. Usachev, R. Pisarev, A. Balbashov, and T. Rasing, Nature **435**, 655 (2005).

[8] B. Koopmans, J. Ruigrok, F. Dalla Longa, and W. de Jonge, Phys. Rev. Lett. **95**, 267207 (2005).

[9] A. Melnikov, A. Povolotskiy, and U. Bovensiepen, Phys. Rev. Lett. **100**, 247401 (2008).

[10] E. Beaurepaire, J.-C. Merle, A. Daunois, and J.-Y. Bigot, Phys. Rev. Lett. **76**, 4250 (1996).

[11] K. Novoselov, A. Geim, S. Dubonos, E. Hill, and I. Grigorieva, Nature **426**, 812 (2003).

[12] V. Dobrovitski, M. Katsnelson, and B. Harmon, Phys. Rev. Lett. **90**, 067201 (2003).

[13] V. Antropov, M. Katsnelson, M. van Schilfgaarde, and B. Harmon, Phys. Rev. Lett. **75**, 729 (1995).

[14] V. Antropov, M. Katsnelson, B. Harmon, M. van Schilfgaarde, and D. Kuznecov, Phys. Rev. B **54**, 1019 (1996).

[15] B. Skubic, J. Hellsvik, L. Nordström, and O. Eriksson, J. Phys.: Condens. Matter **20**, 315203 (2008).

[16] J. Hellsvik, B. Skubic, L. Nordström, B. Sanyal, O. Eriksson, P. Nordblad, and P. Svedlindh, Phys. Rev. B **78**, 144419 (2008).

[17] B. Skubic, O. Peil, J. Hellsvik, P. Nordblad, L. Nordström, and O. Eriksson, Phys. Rev. B **79**, 024411 (2009).

[18] U. Nowak, in *Annual Reviews of Computational Physics IX*, edited by D. Stauffer (World Scientific, Singapore, 2001), p. 105.

[19] N. Kazantseva, U. Nowak, R. Chantrell, J. Hohlfeld, and A. Rebei, Europhys. Lett. **81**, 27004 (2008).

[20] M. d'Aquino, C. Serpico, G. Coppola, I. Mayergoyz, and G. Bertotti, J. Appl. Phys. **99**, 08B905 (2006).

[21] E. Hairer, C. Lubich, and G. Wanner, *Geometric Numerical Integration: structure preserving algorithms for ordinary differential equations* (Springer, 2002).

[22] J. Frank, W. Huang, and B. Leimkuhler, J. Comp. Phys. **133**, 160 (1997).

[23] T. Arponen and B. Leimkuhler, BIT Num. Math. **44**, 403 (2004).

[24] G. Milstein, M. Repin Yu, and M. Tretyakov, SIAM J. Numer. Anal. **40**, 1583 (2002).

[25] G. Milstein and M. Tretyakov, *Stochastic Numerics for Mathematical Physics* (Springer, 2004).

[26] R. Davidchack, R. Handel, and M. Tretyakov, J. Chem. Phys. **130**, 234101 (2009).

[27] M. Krech, A. Bunker, and D. Landau, Comp. Phys. Comm. **111**, 1 (1998).

[28] R. Steinigeweg and H. Schmidt, Comp. Phys. Comm. **174**, 853 (2006).

[29] L. Banas, in *Lecture Notes in Computer Science: Numerical Analysis and its Applications*, edited by Z. L. et al (Springer, Berlin/Heidelberg, 2005), p. 158.

[30] R. Kubo and N. Hashitsume, Prog. Theor. Phys. Suppl. **46**, 210 (1970).

[31] W. Brown, Phys. Rev. **130**, 1677 (1963).

[32] C. Gardiner, *Handbook of Stochastic Methods* (Springer, 2004).

[33] R. Stratonovich, *Conditional Markov Processes and their Application to the Theory of Optimal Control* (Elsevier, 1968).

[34] R. Hasminskii, *Stochastic Stability of Differential Equations* (Sijthoff & Noordhoff, 1980).

[35] G. Milstein and M. Tretyakov, J. Stat. Phys. **77**, 691 (1994).

[36] G. Milstein and M. Tretyakov, SIAM J. Numer. Anal. **34**, 2142 (1997).

[37] S. Shubin and M. Zolotukhin, Zh. Eksp. Teor. Fiz. **6**, 105 (1936).

[38] M. Fisher, Am. J. Phys. **32**, 343 (1964).

CHAPTER 4

Onsager's relations for spin dynamics

In this chapter we present a general theoretical treatment of Onsager's relations and it's application to longitudinal spin dynamics in multisublattice magnets. The main aim is to demonstrate how the macroscopic nonequilibrium dynamics is linked to the microscopic properties of the system. Onsager's relations were first derived by studying the symmetry of the kinetic coefficients that describe the relaxation of a macroscopic system towards equilibrium. Such relaxation is by definition an irreversible process. Nevertheless, by comparison with the rate equations for chemical reactions, Onsager suggested to use the concept of *microscopic reversibility*, *i.e.* the existence and time-reversal symmetry of the microscopic equations of motion, to derive the symmetry of the kinetic coefficients. This theory was for example applied to thermoelectric phenomena, where it links the heat flow caused by electrical voltage gradients with the electrical current generated by temperature gradients. In this chapter we first show how to derive Onsager's relations directly from first-principles following the work of Zubarev [1]. Second, we present in detail the application of Onsager's relations to spin dynamics and generalize this approach for the study of longitudinal spin dynamics in multisublattice magnets. Thirdly, we show how to calculate the macroscopic free energy directly from a microscopic Heisenberg spin Hamiltonian and discuss how to link this model to the conventional phenomenological free energy.

4.1 Microscopic derivation of Onsager's relations

Onsager's relations were first derived on a purely phenomenological basis, only assuming the existence and symmetry of microscopic equations of motion [2]. Instead, here we present a more rigorous microscopic derivation following the work of Zubarev [1], starting from the full microscopic description of the system and using the explicit form of the microscopic equations of motion. This has the advantage that it not only yields the symmetry relations, but also provides (formal) expressions for the kinetic coefficients. We start by introducing general equations for the change of observables with time based on the Liouville equation and express their linearized form using two-time Greens' functions. Second, we use these equations to establish linear relations between fluxes and forces. Third, we indicate how the kinetic coefficients can be obtained from first principle calculations and show that their symmetry is determined by the symmetry of the Greens' functions.

Generally, the problem of relating macroscopic observables to the microscopic properties of a physical system belongs to the field of statistical physics. A central role is played by the density matrix or statistical operator ρ (distribution function for classical systems). Knowledge of the statistical operator enables us to calculate the average value $\langle A \rangle$ of any dynamical variable A

$$\langle A \rangle = \mathrm{Tr}(\rho A). \tag{4.1}$$

In equilibrium we have

$$\rho = \rho_0 = e^{-\beta \mathcal{H}}/Z, \tag{4.2}$$

with $Z = \mathrm{Tr}(e^{-\beta \mathcal{H}})$ the partition function, $\beta = (k_\mathrm{B} T)^{-1}$ the inverse temperature in units of energy and $\mathcal{H}$ the Hamiltonian of the system under study.

Nonequilibrium dynamical processes follow from the evolution of the statistical operator as is determined by the Liouville equation:

$$i\hbar \partial \rho / \partial t = [\mathcal{H} + H_t^1, \rho], \tag{4.3}$$

where H_t^1 describes the perturbation which brings the system out of equilibrium. The subscript t denotes the explicit time dependence due to the external force (see also Eq. (4.10)). Initially the system is assumed to be in equilibrium: $H_t^1|_{t \to -\infty} = 0$. When the perturbation H_t^1 is small, we can obtain the solution of Eq. (4.3) by iteration, using ρ_0 as zeroth order solution. The first order approximation reads:

$$\rho(t) = \rho_0 + \frac{1}{i\hbar} \int_{-\infty}^{t} dt' \, [H_{t'}^1(t' - t), \rho_0], \tag{4.4}$$

where

$$H_t^1(t) = e^{i\mathcal{H}t/\hbar} H_t^1 e^{-i\mathcal{H}t/\hbar}, \tag{4.5}$$

is the perturbation operator in the Heisenberg picture. In the remainder we will restrict ourselves to the regime of linear response. Substituting Eq. (4.4) in Eq. (4.1) and using the invariance of the trace under cyclic permutation of the operators we obtain:

$$\langle A\rangle = \langle A\rangle_0 + \frac{1}{i\hbar}\int_{-\infty}^{t} dt'\,\langle [A(t), H^1_{t'}(t')]\rangle_0, \tag{4.6}$$

where $\langle\cdots\rangle_0 = \mathrm{Tr}(\rho_0\cdots)$ and $A(t) = e^{i\mathcal{H}t/\hbar}Ae^{-i\mathcal{H}t/\hbar}$ the operator A in the Heisenberg picture. It is convenient to extend the time integration formally to $+\infty$ by introducing the step function $\theta(t-t')$:

$$\theta(t) = \begin{cases} 1, & \text{if } t > 0, \\ 0, & \text{if } t < 0. \end{cases} \tag{4.7}$$

Then

$$\langle A\rangle = \langle A\rangle_0 + \int_{-\infty}^{\infty} dt'\,\langle\langle A(t)H^1_{t'}(t')\rangle\rangle, \tag{4.8}$$

where

$$\langle\langle A(t)B(t')\rangle\rangle = \theta(t-t')\frac{1}{i\hbar}\langle [A(t), B(t')]\rangle_0 \tag{4.9}$$

is called the retarded two-time Greens' function [1]. It depends only on the difference $t-t'$ as follows from the invariance of the trace under cyclic permutation of the operators and expresses within the linear approximation how the average value of A changes due to the perturbation $H^1_{t'}$. We emphasize that the full Hamiltonian of the system is included in the Greens' function.

Now we have the general expressions to calculate how observables change due to a perturbation, we focus on a particular case of flux operators $\dot{x}_j = dx_j/dt$, which gives the rate of change of the operator x_j in response to the forces $F_k(t)$. To this end we write the perturbation H^1_t as:

$$H^1_t = -\sum_{j=1}^{n} x_j F_j(t), \quad F_j(t) \sim e^{\varepsilon t} \quad \text{for } t \to -\infty, \tag{4.10}$$

with $\varepsilon > 0$. In equilibrium there are no fluxes since

$$\langle \dot{x}_j\rangle_0 = \frac{d}{dt}\langle x_j\rangle_0 = 0. \tag{4.11}$$

Consequently, substitution of Eq. (4.10) in Eq. (4.8) yields

$$\langle \dot{x}_j\rangle = -\sum_{k=1}^{n}\int_{-\infty}^{t} dt'\,\langle\langle \dot{x}_j(t)x_k(t')\rangle\rangle F_k(t') \equiv \sum_{k=1}^{n}\int_{-\infty}^{t} dt'\,L_{jk}(t-t')F_k(t'). \tag{4.12}$$

These equations yield *linear relations between fluxes and forces* and $L_{jk}(t-t')$ denote the *kinetic coefficients*. We emphasize that this result is obtained entirely from first principles, we only made the assumption of linear response.

Next we study the kinetic coefficients in more detail. For this it is useful to use the Fourier representation

$$L_{jk}(\omega) = \int_{-\infty}^{\infty} L_{jk}(t) e^{i\omega t} dt \equiv -\langle\langle \dot{x}_j | x_k \rangle\rangle_\omega. \tag{4.13}$$

We can get rid of the dependence on $\dot{x}_j$ by performing integration by parts. Using the identity

$$i\hbar \frac{d}{dt} \langle\langle x_j(t-t') x_k \rangle\rangle = \delta(t-t') \langle [x_j(t), x_k(t')] \rangle + i\hbar \langle\langle \dot{x}_j(t) x_k(t') \rangle\rangle, \tag{4.14}$$

we obtain

$$L_{jk}(\omega) = \frac{1}{i\hbar} \langle [x_j(0), x_k(0)] \rangle + i\omega \langle\langle x_j | x_k \rangle\rangle_\omega. \tag{4.15}$$

This equation expresses that the kinetic coefficients depend only on the *equilibrium correlations* $\langle x_j(t) x_k(t') \rangle_0$ between the operators x_j and x_k. Such equilibrium properties can be well assessed by first-principle calculations.

We can also derive the symmetry properties of the kinetic coefficients from the equilibrium correlation functions. In the presence of a magnetic field $\mathbf{B}$ the equations of motion remain the same when both time and the sign of the magnetic field are reversed:

$$\langle x_j(-t) x_k(-t') \rangle_{-\mathbf{B}} = \epsilon_j \epsilon_k \langle x_j(t) x_k(t') \rangle_{\mathbf{B}}, \tag{4.16}$$

where $x_j \to \epsilon_j x_j$ under time reversal, with $\epsilon_j = +1$ or -1 according to wether the operator x_j is even or odd with respect to time reversal. We omitted the subscript $\langle \cdots \rangle_0$ for clarity. Furthermore, from the invariance of the trace under permutation of the operators we get

$$\begin{aligned} \langle x_j(-t) x_k(-t') \rangle_{-\mathbf{B}} &= \langle e^{-i\mathcal{H}t/\hbar} x_j e^{i\mathcal{H}t/\hbar} e^{-i\mathcal{H}t'/\hbar} x_k e^{i\mathcal{H}t'/\hbar} \rangle_{-\mathbf{B}} \\ &= \langle e^{i\mathcal{H}t'/\hbar} x_j e^{-i\mathcal{H}t'/\hbar} e^{i\mathcal{H}t/\hbar} x_k e^{-i\mathcal{H}t/\hbar} \rangle_{-\mathbf{B}} \\ &= \langle x_j(t') x_k(t) \rangle_{-\mathbf{B}} = \langle x_k(t) x_j(t') \rangle_{-\mathbf{B}}, \end{aligned} \tag{4.17}$$

where in the second step we interchanged both the inner and outer exponents. Combining Eq. (4.16) and Eq. (4.17) we obtain for the symmetry of the kinetic coefficients:

$$L_{jk}(\omega, \mathbf{B}) = L_{kj}(\omega, -\mathbf{B}) \epsilon_j \epsilon_k, \tag{4.18}$$

This result completes the first part of this section, where we have derived the linearized equations of motion Eq. 4.12. Their kinetic coefficients Eq. (4.15) are determined by equilibrium correlation functions and from this we have proven their symmetry Eq. 4.18. In the next section we use the symmetry relations to derive the equations of motion for the longitudinal dynamics of multisublattice magnets.

4.2 Longitudinal spin dynamics from Onsager's relations

In the previous section we have derived Onsager's relations in a general form. In this section we apply these general results for the derivation of the equations of motion for spin dynamics. First we introduce the appropriate perturbation operator. Second, we derive the general equation of motion for ferromagnets, including both transverse and longitudinal dynamics. Thirdly we focus on longitudinal dynamics only and generalize the equations of motion to multisublattice magnets and finally we draw conclusions.

For the application of Onsager's relations to spin dynamics we assume the perturbation operator in the form

$$H_t^1 = -\mathbf{S} \cdot \mathbf{H}(t), \tag{4.19}$$

where $\mathbf{S}$ is the operator of the total spin angular momentum per unit volume. The cartesian components S_j play the role of the operators x_j, $j = x, y, z$ and for their time-reversal symmetry we have $\epsilon_j = -1$ and $\epsilon_j \epsilon_k = 1$. Similarly, the components $H_j(\mathbf{x}, t)$ of the external magnetic field $\mathbf{H}(\mathbf{x}, t)$ determine the forces $F_j(t)$. In the following, the conservation of angular momentum will be very important. Therefore we use the units of angular momentum $\hbar$ rather than those of the magnetization $\mu_{\mathrm{B}} = \hbar q_e/(2m_e)$. Consequently, the magnetic field $\mathbf{H}$ is scaled as $q_e/(2m_e)\tilde{\mathbf{H}}$ and has as units s^{-1}.

To obtain the equations of motion we follow the derivation by Baryakhtar [3]. It is useful to introduce first the symmetric and antisymmetric components of the kinetic coefficients:

$$L_{jk}^s(\mathbf{B}) = (L_{jk}(\mathbf{B}) + L_{kj}(-\mathbf{B}))/2, \tag{4.20}$$

$$L_{jk}^a(\mathbf{B}) = (L_{jk}(\mathbf{B}) - L_{kj}(-\mathbf{B}))/2, \tag{4.21}$$

which we take only for the static case $\omega = 0$. From this definition it follows that the (anti)symmetric components of the kinetic coefficients contain only (odd) even powers of $\mathbf{B}$. For magnetically ordered media we can replace $\mathbf{B}$ with $\mathbf{S}$ in the kinetic coefficients. To lowest non-zero order, the commutation relations for angular momentum yield an antisymmetric tensor of the form:

$$L_{jk}^a = \epsilon_{jkl} S_l, \tag{4.22}$$

where ϵ_{jkl} is the totally antisymmetric Levi-Civita tensor. Using this form of L_{jk}^a and by keeping only the zeroth order terms in the expansion of the symmetric components we obtain an equation of motion of the form

$$d\mathbf{S}/dt = \mathbf{S} \times \mathbf{H} + \hat{L}^s \mathbf{H}, \tag{4.23}$$

where $\hat{L}^s$ is a tensor with components $L_{jk}^s(0)$. The first term on the right hand side describes the well-known homogenous precessional motion which conserves the

magnitude $S = |\mathbf{S}|$. In contrast, the second term describes longitudinal dynamics which changes $|\mathbf{S}|$ and has our main interest. This term must stem from relativistic interactions since it changes the length of $\mathbf{S}$ even in the case of uniform motion. Generally the crystal structure determines the tensor $\hat{L}^s$ [4]. Below we will take only the simplest form, $\lambda^s_{jk} = \delta_{jk}\lambda$. Furthermore, since longitudinal motion is in general much faster than precessional motion we restrict ourselves to longitudinal dynamics in the remainder.

For the generalization to multisublattice magnets we assume collinear sublattices and take the orientation of the angular momentum along the z-axis. The equation of motion for two sublattices $S_\nu = S^\nu_z$, $\nu = a, b$ can then be written as

$$\begin{pmatrix} \dot{S}_a \\ \dot{S}_b \end{pmatrix} = \begin{pmatrix} L^s_{aa} & L^s_{ab} \\ L^s_{ba} & L^s_{bb} \end{pmatrix} \begin{pmatrix} H_a \\ H_b \end{pmatrix} \tag{4.24}$$

The symmetry relation Eq. (4.18) dictates that $L^s_{ab} = L^s_{ba}$. Hence the matrix can contain at most 3 independent relaxation parameters. We can further decompose this matrix by considering two limits. First, in the limit of uncoupled sublattices we should recover the longitudinal term in Eq. (4.23), giving diagonal relativistic contributions $L_{\nu\nu} = \lambda_\nu$. Second, when only relaxation between the sublattices is taken into account, the total angular momentum is conserved, yielding a tensor of the form:

$$\begin{pmatrix} L^s_{aa} & L^s_{ab} \\ L^s_{ba} & L^s_{bb} \end{pmatrix} = \begin{pmatrix} \lambda_e & -\lambda_e \\ -\lambda_e & \lambda_e \end{pmatrix}. \tag{4.25}$$

This relaxation process is described by λ_e and is determined by exchange interactions, which are isotropic and hence conserve the total angular momentum. By taking into account both the relativistic and the exchange relaxation we obtain equations of motion of the form

$$dS_a/dt = \lambda_a H_a + \lambda_e(H_a - H_b), \tag{4.26}$$

$$dS_b/dt = \lambda_b H_b + \lambda_e(H_b - H_a). \tag{4.27}$$

This results finishes the microscopic derivation of longitudinal spin dynamics in multisublattice magnets. In addition to the phenomenological equations of motion, this derivation has lead to explicit expressions Eq. (4.15) for the calculation of the relaxation parameters in terms of equilibrium correlation functions. We emphasize that actual calculations of these parameters can be performed within the same first-principle approach as has recently been worked out for the calculation of the transverse Gilbert relaxation parameter [5–7]. In the next section we continue our microscopic treatment by also deriving the magnetic fields, so far considered as purely external, from a microscopic spin model.

4.3 Nonequilibrium Free Energy

The equations of motion presented above assume that the time-dependent perturbation is caused by an external magnetic field. In the phenomenological theory the external field is replaced by an *effective* magnetic field. The latter is derived from a free energy and takes into account internal interactions as well. Such an approach is very useful since it does not alter the structure of the equations of motion themselves. The goal of this section is to derive the free energy and effective fields directly from a microscopic Heisenberg spin Hamiltonian. We start by recalling the concept of effective magnetic field and the general definition of the free energy. Secondly, we introduce the Gibbs-Bogoliubov inequality for the actual calculation of the nonequilibrium free energy, which is subsequently worked out in the mean-field approximation. Thirdly we present the resulting effective fields, recover the equilibrium results and indicate how the results can be generalized to include anisotropy. Finally we relate the microscopic results with the phenomenological expressions for the free energy.

The concept of an effective magnetic field was first introduced by Landau and Lifshitz [8]. They define it as the functional derivative of the macroscopic free energy: $H_\nu = -\delta F/\delta S_\nu$, where F is the free energy and $S_\nu = \langle \sum_i s_i^\nu \rangle / V$ is the operator of the total angular momentum per unit volume V of sublattice ν. Instead of the purely phenomenological approach we want to derive the macroscopic free energy from a microscopic Hamiltonian $\mathcal{H}$. To illustrate this we chose the Heisenberg spin model, which for 2-sublattices ($\nu = a, b$) can be written as:

$$\mathcal{H} = -{\sum_{\substack{i\in a\\ i'\in a}}}' J_{ii'}^{aa} s_i^a s_{i'}^a - {\sum_{\substack{i\in b\\ i'\in b}}}' J_{ii'}^{bb} s_i^b s_{i'}^b - {\sum_{\substack{i\in a\\ i'\in b}}}' J_{ii'}^{ab} s_i^a s_{i'}^b - {\sum_{\substack{i\in b\\ i'\in a}}}' J_{ii'}^{ab} s_i^b s_{i'}^a \tag{4.28}$$

Here $J_{ii'}^{\nu\nu'}$ are exchange parameters and $\sum'_{i,i'} = \sum_i \sum_{i'\neq i}$ indicates a double sum where each sum runs over a whole sublattice. In the following, we treat the spins s_i^ν as classical, similar as is done in the atomistic spin dynamics approach. Calculations for quantum spins proceed in a similar way [9].

To calculate the relation between the Hamiltonian $\mathcal{H}$ and the free energy F, we could in principle use the fundamental relation

$$F(\mathcal{H}) = \langle \mathcal{H} \rangle - T\mathbb{S}, \tag{4.29}$$

where $\mathbb{S}$ is the entropy and T the temperature of the medium in which the spin system is embedded. This relation can be used both in equilibrium and out of equilibrium[1], but actual calculation is difficult. Therefore, to illustrate the approach, we limit

[1] For example, the distribution function ρ does not necessarily satisfy the equilibrium Boltzmann distribution.

ourselves in the remainder to the mean field approximation: $S_\nu = N_\nu \langle s_i^\nu \rangle$, where N_ν is the number of spins of sublattice ν per unit volume. In calculating the mean-field approximation of F, we need to ensure that it is valid also out of equilibrium. This can be achieved by performing statistical perturbation theory. Writing $\mathcal{H} = H_0 + (\mathcal{H} - H_0)$, we obtain to first order in $\mathcal{H} - H_0$:

$$F \leq F(H_0) + \langle \mathcal{H} - H_0 \rangle_0 \equiv \Phi, \tag{4.30}$$

where $\langle x \rangle_0 = \langle x \exp(-\beta H_0) \rangle / \langle \exp(-\beta H_0) \rangle$ indicates averaging over the equilibrium distribution function of the trial Hamiltonian H_0. This inequality bears the name of Gibbs and Bogoliubov for the classical and quantum case, respectively [10] and follows from the mathematical expression $\langle \exp(x) \rangle \geq \exp(\langle x \rangle)$.

To arrive at the mean-field approximation, we chose the simple form

$$H_0 = -\sum_{i \in a} h_a s_i^a - \sum_{i \in b} h_b s_i^b, \tag{4.31}$$

where h_ν are variational parameters. Direct calculation gives

$$F(H_0) = -\beta^{-1} \left[N_a \ln Z_a + N_b \ln Z_b \right], \tag{4.32}$$

$$\langle H_0 \rangle_0 = -\frac{\partial}{\partial \beta} (N_a \ln Z_a + N_b \ln Z_b) = -N_a h_a s_a - N_a h_b s_b, \tag{4.33}$$

and

$$\langle \mathcal{H} \rangle_0 = -N_a z_{aa} J_{aa} s_a^2 - N_b z_{bb} J_{bb} s_b^2 - 2 N_p J_{ab} s_a s_b \tag{4.34}$$

with

$$s_\nu = \langle s_i^\nu \rangle_0 = \frac{\partial \ln Z_\nu}{\partial \beta h_\nu} = \sigma_\nu \mathcal{L}(\beta h_\nu \sigma_\nu). \tag{4.35}$$

where we defined the Langevin function $\mathcal{L}(x) = \coth(x) - 1/x$ and the single-spin partition function $Z_\nu = 4\pi \sinh(\beta h_\nu \sigma_\nu)/(\beta h_\nu \sigma_\nu)$, with $\sigma_\nu = |s_i^\nu|$ the length of the local spin moment. $N_p = N_a z_{ab} = N_b z_{ba}$ denote the number of pairs and $z_{\nu\nu'}$ the number of neighbors in sublattice ν' of a spin in sublattice ν. Eq. (4.35) provides a one-to-one relation between the mean-field spin moment per site s_ν and the variational parameter h_ν. Hence we can regard h_ν as an explicit function of s_ν and this enables us to define the mean-field free energy both in equilibrium and out of equilibrium as

$$\Phi(s_a, s_b) = N_a f_a(s_a) + N_b f_b(s_b) - 2 N_p J_{ab} s_a s_b, \tag{4.36}$$

with

$$f_\nu(s_\nu) = -\left[\beta^{-1} (\ln Z_\nu - \eta_\nu s_\nu / \sigma_\nu) + z_{\nu\nu} J_{\nu\nu} s_\nu^2 \right], \tag{4.37}$$

where $\eta_\nu = \beta h_\nu \sigma_\nu = \mathcal{L}^{-1}(s_\nu/\sigma_\nu)$. These equation provide the desired connection between the microscopic spin Hamiltonian and the nonequilibrium free energy in the mean-field approximation.

Next we derive from the free energy the effective fields and indicate how we recover the equilibrium results. Taking into account Eq. (4.35) we find that

$$\frac{\partial}{\partial s_\nu}(\ln Z_\nu - \eta_\nu s_\nu/\sigma_\nu) = \frac{\partial \ln Z_\nu}{\partial \eta_\nu}\frac{\partial \eta_\nu}{\partial s_\nu} - \frac{\partial \eta_\nu}{\partial s_\nu}\frac{s_\nu}{\sigma_\nu} - \eta_\nu/\sigma_\nu = -\eta_\nu/\sigma_\nu, \tag{4.38}$$

such that the effective fields $H_\nu = -\frac{1}{N_\nu}\frac{\partial \Phi}{\partial s_\nu}$ become

$$\begin{aligned} H_a &= -\beta^{-1}\eta_a/\sigma_a + 2z_{aa}J_{aa}s_a + 2z_{ab}J_{ab}s_b, \\ H_b &= -\beta^{-1}\eta_b/\sigma_b + 2z_{bb}J_{bb}s_b + 2z_{ba}J_{ab}s_a, \end{aligned} \tag{4.39}$$

In equilibrium the effective fields vanish[2] yielding special values $\overline{h}_\nu = \beta^{-1}\overline{\eta}_\nu/\sigma_\nu$:

$$\begin{aligned} \overline{h}_a &= 2z_{aa}J_{aa}\overline{s}_a + 2z_{ab}J_{ab}\overline{s}_b, \\ \overline{h}_b &= 2z_{bb}J_{bb}\overline{s}_b + 2z_{ba}J_{ab}\overline{s}_a, \end{aligned} \tag{4.40}$$

where the equilibrium values $\overline{s}_\nu$ can be determined by the self-consistent solution of the coupled set of equations

$$\overline{s}_\nu = \sigma_\nu \mathcal{L}(\beta\sigma_\nu \overline{h}_\nu) \tag{4.41}$$

The same result is obtained in the usual equilibrium mean-field theory and the quantities $\overline{h}_\nu$ can be interpreted as Weiss fields. We emphasize that in general $h_\nu \neq \overline{h}_\nu$ and to obtain the correct relaxation to equilibrium it is crucial to use h_ν in the effective fields.

So far we have taken into account only exchange contributions in the microscopic Hamiltonian. The results can however easily be generalized to the case of uniaxial anisotropy. By adding the single-spin Hamiltonian

$$\mathcal{H}_d = -\sum_{i\in a} d_a (s_i^a)^2 - \sum_{i\in b} d_b (s_i^b)^2, \tag{4.42}$$

to both $\mathcal{H}$ and H_0, we find that all formulas remain the same, except for the mathematical form of Z_ν and $\mathcal{L}$. Direct calculations yield:

$$Z_{\nu,\delta_\nu}(\eta_\nu) = 4\pi\frac{\sqrt{\pi}}{2}e^{-\beta\eta_\nu^2/4\delta_\nu}\left[\mathrm{Erfi}\left(\frac{\eta_\nu}{\sqrt{2\delta_\nu}} + \sqrt{\delta_\nu}\right) - \mathrm{Erfi}\left(\frac{\eta_\nu}{\sqrt{2\delta_\nu}} - \sqrt{\delta_\nu}\right)\right], \tag{4.43}$$

$$\mathcal{L}_{\delta_\nu}(\eta_\nu) = \frac{\partial \ln Z_{\nu,\delta_\nu}(\eta_\nu)}{\partial \eta_\nu}, \tag{4.44}$$

where $\mathrm{Erfi}(x) = \frac{2}{\sqrt{\pi}}\int_0^x dt\ e^{t^2}$ is the imaginary error function. The mathematical expression for $\mathcal{L}_{\delta_\nu}$ is easily calculated but rather lengthy and therefore we do not

[2]Here we assume that also no external field is present.

write it out explicitly. Here $\delta_\nu = \beta d_\nu \sigma_\nu^2$ is the dimensionless anisotropy constant. In contrast to η_ν this is not a variational parameter. To indicate the different role of δ_ν and η_ν, we have labeled the generalized expressions with the parameter δ_ν.

As final part of this section we relate the nonequilibrium mean-field free energy with the usual phenomenological theory. The connection follows simply from the first order expansion of Φ around equilibrium. Above the Curie temperature we have $\overline{s}_\nu = 0$ and we can expand directly in s_ν. Keeping only the lowest nonzero powers and by writing explicitly the dependence on S_ν, we get

$$\Phi(S_a, S_b) - \Phi(0,0) = \frac{1}{2N_a\chi_a} S_a^2 + \frac{1}{2N_b\chi_b} S_b^2 - \frac{2N_p}{N_a N_b} J_{ab} S_a S_b \tag{4.45}$$

where

$$\chi_\nu^{-1} = \frac{3}{\sigma_\nu^2} k_\mathrm{B} T - 2 z_{\nu\nu} J_{\nu\nu} \tag{4.46}$$

Below the Curie temperature we expand around nonzero $\overline{s}_\nu$. Taking into account that $f_\nu(s_\nu)$ is an even function of s_ν we can write

$$f_\nu(S_\nu) - f_\nu(\overline{S}_\nu) = \frac{f''(\overline{s}_\nu)}{8N_\nu^2 \overline{S}_\nu^2} (S_\nu^2 - \overline{S}_\nu^2)^2, \tag{4.47}$$

recovering the phenomenological expression where

$$f''(\overline{s}_\nu) = \frac{k_\mathrm{B} T}{\sigma_\nu^2 \mathcal{L}'(\overline{\eta}_\nu)} - 2 z_{\nu\nu} J_{\nu\nu}, \tag{4.48}$$

with $\mathcal{L}'(x) = d\mathcal{L}(x)/dx$ and $f''(x) = d^2 f(x)/dx^2$. Eq. (4.46) and Eq. (4.48) contain the main result of this section, *i.e.* they provide a direct connection between the microscopic Hamiltonian (4.28) and the macroscopic free energy Eq. (4.36).

To summarize, the equations for the effective magnetic field Eq. (4.39) provide a microscopic description of the effective magnetic fields for macroscopically longitudinal spin dynamics in multisublattice magnets, based on the Heisenberg spin model. We emphasize that the parameters of the Heisenberg spin model, which are the spin moments and exchange interactions, can be calculated from first principles using the methods described in [11–13]. Further, since also the relaxation parameters can be calculated within a first-principle framework, the present theory provides a complete multiscale description of longitudinal spin dynamics, insofar as the approximations that have been made are valid. We emphasize that the approach is not restricted to the mean-field approximation employed here and the results can be systematically improved by taking different forms for the trial Hamiltonian H_0 and by using higher order expansions in $\langle \mathcal{H} - H_0 \rangle$. Nevertheless, in the present form the theory can already be quite useful to obtain a general understanding on the nonequilibrium longitudinal spin dynamics in magnets with multiple magnetic sublattices. Furthermore,

our present results can already be used as a fit model for experiments, by choosing the exchange parameters to match the equilibrium temperature dependencies of the sublattice magnetizations and using the relaxation parameters as fit parameters for the nonequilbrium spin dynamics.

In conclusion, in this chapter we have presented a microscopic theory of macroscopically longitudinal spin dynamics in multiple sublattice magnets. This not only establishes a rigorous physical basis of the theory, but also gives us a framework for calculating the hitherto purely phenomenological free energy and relaxation parameters from first principles. Hence, within the approximations made, the theory provides a complete multiscale description of longitudinal spin dynamics. In the next chapters we further work out the implications of the theory. First, in Chapter 5, we use the phenomenological equations and compare this with atomistic simulations. Subsequently, in Chapter 6 we use the microscopic theory to assess the role of the exchange interaction on the dynamics and to investigate further generalizations of the theory to include orbital degrees of freedom.

References

[1] D. Zubarev, *Nonequilibrium statistical thermodynamics* (Consultants Bureau, New York, 1974).

[2] L. Onsager, Phys. Rev. **37**, 405 (1931).

[3] V. Baryakhtar, Zh. Eksp. Teor. Fiz **87**, 1501 (1984).

[4] V. Baryakhtar, Zh. Eksp. Teor. Fiz. **94**, 196 (1988).

[5] A. Brataas, Y. Tserkovnyak, and G. Bauer, Phys. Rev. Lett. **101**, 037207 (2008).

[6] H. Ebert, S. Mankovsky, D. Ködderitzsch, and P. Kelly, Phys. Rev. Lett. **107**, 066603 (2011).

[7] Y. Liu, A. Starikov, Z. Yuan, and P. Kelly, Phys. Rev. B **84**, 014412 (2011).

[8] L. Landau and E. Lifshitz, Phyz. Z. Sowjetunion **8**, 153 (1935).

[9] O. Abubrig, D. Horvath, and A. Bobak, Phys. A **296**, 437 (2001).

[10] H. Falk, Am. J. Phys. **38**, 858 (1970).

[11] A. Liechtenstein, M. Katsnelson, and V. Gubanov, J. Phys. F: Met. Phys. **14**, L125 (1984).

[12] A. Liechtenstein, M. Katsnelson, V. Antropov, and V. Gubanov, J. Magn. Magn. Mater. **67**, 65 (1987).

[13] M. Katsnelson and A. Lichtenstein, Phys. Rev. B **61**, 8906 (2000).

CHAPTER 5

Ultrafast spin dynamics in multisublattice magnets [1]

5.1 Introduction

Intense femtosecond laser pulses are able to excite magnetic order of condensed matter systems on a timescale of the exchange interaction [1], *i.e.* on a the timescale pertinent the period of spin motion in the exchange field. Laser-induced demagnetization [2], magnetization reversal [3, 4], change of magnetic anisotropy [5, 6] or even a change of the exchange integral [7, 8] have been experimentally demonstrated. These observations have pushed spin dynamics to a new regime, where the observed dynamics appears to be dominantly longitudinal, which can thus not be described by the conventional transverse Landau-Lifshitz dynamics [9] which conserves the magnitude of the angular momentum for any sublattice. Although many experiments have been done in magnets with more than one magnetic sublattice, this fact has largely been ignored in the theoretical descriptions for longitudinal spin dynamics [10–13]. This suggests that the different sublattices would have the same dynamics. In striking contrast, femtosecond X-ray probes [14, 15] have elucidated recently that the sublattices in ferrimagnetic GdFe show distinct dynamics after femtosecond laser excitation [16], and this has been observed more recently also in permalloy [17].

In this chapter we present a general theoretical framework for ultrafast spin dynamics in multisublattice magnets which contains longitudinal relaxation of both

[1] Adapted from: J. Mentink, J. Hellsvik, D. Afansiev, B. Ivanov, A. Kirilyuk, A. Kimel, O. Eriksson, M. Katsnelson and T. Rasing, *Phys. Rev. Lett.* **108**, 057202 (2012).

relativistic and exchange origin. The latter is the key new ingredient of our theory and is only present in magnets with more than one sublattice. The reason is simply that the exchange interaction conserves the total angular momentum and therefore longitudinal exchange relaxation is not possible in magnets with only one sublattice. In the spirit of the models for one sublattice [11–13] we consider multisublattice magnets coupled to a heat bath with a (time dependent) temperature T. The heat bath represents the environment and can often be taken as the electron system, which rapidly heats upon laser excitation and subsequently cools down due to the coupling with the lattice, as can be modeled conveniently by a two-temperature model [18]. The magnetic system is considered to be neither in equilibrium with itself nor with the heat bath, as we are interested in the relaxation of the magnetic sublattices in approach to equilibrium. In order to illustrate our theory we classify the dynamics that occur in multisublattice magnets in three regimes, depending on whether the temperature of the heat bath is above, below, or in the vicinity of the critical temperature T_{C} of the multisublattice magnet. We demonstrate our theory further by showing explicit solutions in the regime $T < T_{\mathrm{C}}$. Finally, we substantiate our theory with recently reported experiments [16] and by performing atomistic spin dynamics simulations.

5.2 General theory

The basis of our theoretical framework is the description of spin dynamics using Onsager's relations. Such an approach was employed independently by Iwata [19, 20] and Baryakhtar [21–23], see also Sec. 4.2, who showed that using Onsager's relations and accounting for the symmetry of the exchange interaction naturally yields dynamics of the length of the macroscopic sublattice magnetizations, pertinent to the timescale of the exchange interaction. On this timescale the conventional transverse dynamics of the angular momentum is negligible and we can limit ourselves to longitudinal dynamics, such that the equations of motion for two non-equivalent collinear sublattices can be written as:

$$\dot{S}_a = \lambda_a H_a + \lambda_e (H_a - H_b), \tag{5.1}$$

$$\dot{S}_b = \lambda_b H_b + \lambda_e (H_b - H_a). \tag{5.2}$$

Here λ_ν is of relativistic origin and describes transfer of angular momentum between sublattice $\nu = a, b$ and the environment. λ_e is of exchange origin and stems from spin-spin interactions, conserving the total angular momentum but allowing for the transfer of angular momentum between the sublattices. S_ν, which can be both positive and negative, denotes the macroscopic angular momentum of sublattice ν and is related to the magnetization M_ν by the gyromagnetic ratio γ_ν: $S_\nu = M_\nu/\gamma_\nu$. Further $\dot{S}_\nu = dS_\nu/dt$ and the effective fields $H_\nu = -\delta F/\delta S_\nu$ are derived from the magnetic

energy F. As derived in Sec. 4.3, in the uniform exchange approximation F can be written as

$$F = \int d\mathbf{x} \left\{ f_a(S_a^2) + f_b(S_b^2) + f_{ab}(S_a \cdot S_b) \right\}. \tag{5.3}$$

Here $f_\nu(S_\nu^2)$ determines the exchange energy responsible for the formation of the macroscopic magnetic moment in sublattice ν. $f_{ab} = -J_{ab} S_a \cdot S_b$ is the exchange interaction between the sublattices, determining their mutual orientation, where $J_{ab} > 0$ for ferromagnetic (FM) coupling and $J_{ab} < 0$ for antiferromagnetic (AFM) coupling. Generally the exchange energies f_ν and J_{ab} in F are parametrically dependent on the temperature of the environment. We use this to classify the dynamics in three regimes.

5.3 Temperature Dominated Regime

The first regime, which we call the temperature dominated regime, is defined as $T \gg T_\mathrm{C}$. In this regime the system responds as if it was a paramagnet and we may write $f_\nu = S_\nu^2/(2\chi_\nu)$, where $\chi_\nu \sim 1/T$ denotes the longitudinal susceptibility of sublattice ν. Since in the paramagnetic regime $J_{ab} \ll k_B T$, the interaction between sublattices can be neglected, and the transfer of angular momentum with the environment dominates the dynamics. Consequently, the sublattices exhibit Bloch relaxation, with a relaxation time $\tau_\nu = \chi_\nu/\lambda_\nu$. Microscopic calculations [24–26] show that the longitudinal relaxation time can be written as

$$\tau_\nu = \sigma_\nu/(2\alpha_\nu k_B T), \tag{5.4}$$

where α_ν is a microscopic parameter of relativistic origin determining the coupling with the heat bath. Importantly, it follows that the longitudinal relaxation is determined by the atomic spin moment σ_ν, which is intuitively easy to understand. Reducing S_ν requires transfer of angular momentum, which is limited by the value of α_ν. Therefore, systems with small magnetic moments relax faster. Interestingly, this analysis shows that sublattices with different magnetic moments generally show distinct dynamics in the temperature dominated regime, despite their strong exchange coupling in the ground state. This regime can be accessed by suddenly heating the electron system using a fs laser pulse. Then, on the timescale of 10-100fs, the electron temperature will rise far above the Curie temperature, such that the spins feel a very hot environment. Such distinct dynamics has recently been observed using fs XMCD probes on fs laser excited ferrimagnetic GdFeCo [16].

5.4 Exchange Dominated Regime

The second regime, which we call the exchange dominated regime, is determined by $T < T_\mathrm{C}$. Since in the ordered regime generally exchange interactions are stronger than

relativistic interactions, this regime is characterized by $\lambda_\nu \ll \lambda_e$ and typically appears on the ps timescale. In this regime the transfer of angular momentum between the sublattices dominates the dynamics. For purely exchange driven dynamics the total angular momentum is conserved. As a consequence, for any form of the free energy F, the changes of the sublattice angular momentum sum up (approximately) to zero: $\dot{S}_a = -\dot{S}_b$. This yields highly counter-intuitive dynamics when the spin of one of the sublattices is close to zero. Contrasting the temperature dominated regime which would yield $\dot{S}_\nu \to 0$ when $S_\nu \to 0$, in the exchange dominated regime $\dot{S}_\nu$ remains finite even when $S_\nu = 0$. Therefore, the spin of the sublattices can reverse purely driven by the exchange relaxation. To illustrate this we consider $S_b < 0$ approaching zero while $S_a > 0$. We can express the requirement for sublattice reversal to occur with AFM coupling as

$$\dot{S}_b\Big|_{S_b=0} > 0 \Leftrightarrow 2\partial f_a/\partial S_a^2 > -J_{ab}(1+\lambda_b/\lambda_e) > 0. \tag{5.5}$$

Since $J_{ab} < 0$ it is required that $\partial f_a/\partial S_a^2 > 0$. As was derived in Sec. 4.3, to lowest order we have $f_\nu(S_\nu^2) \sim (S_\nu^2 - \overline{S}_\nu^2)^2$ and by definition $f_\nu(S_\nu^2)$ has a minimum at $S_\nu^2 = \overline{S}_\nu^2$, where $\overline{S}_\nu^2$ is the equilibrium value of the angular momentum at the specified temperature. Consequently, to fulfill requirement (5.5) we need $S_a^2 \gg \overline{S}_a^2$, which illustrates that sublattice reversal can only occur under strongly non-equilibrium conditions. This inequality can be satisfied when the temperature of the heat bath suddenly increases, as appears after fs laser excitation of the electron system, such that f_a dominates over f_{ab} and S_a lags behind the excitation.

In order to illustrate this novel exchange driven dynamics further we solve the Eqns. (5.1,5.2) at constant temperature of the heat bath. For a typical rare-earth ($\nu = a$) transition-metal ($\nu = b$) ferrimagnet we model the free energy in the Landau form as $f_a = AS_a^2/2$, $f_b = B(S_b^2 - \overline{S}_b^2)^2/4$, where we assume the usual FM form for sublattice b. For the rare-earth sublattice S_a we chose the paramagnetic form, since the exchange interactions between the rare-earth spins are usually weaker than the other exchange interactions in the system. For the present simulation we used the values $A/B = 0.4$, $B = 1 = \overline{S}_b$, $J_{ab}/B = -0.15$, $\lambda_a = \lambda_b = 0.15$ and $\lambda_e = 1$. We chose to present the results in a phaseplot, as is shown in Fig. 5.1. Such a plot shows the dynamics of S_a as function of S_b, which enables to visualize the solutions for various initial conditions in one graph. Stable equilibrium points are indicated with thick dots in the upper left and lower right quadrant, in accordance with the antiferromagnetic coupling between the sublattices. The lines with arrows show the relaxation of the system to these equilibria. The dynamics in which we are interested are the lines which transverse both the horizontal and vertical axis, and thereby connect the upper left and lower right quadrants, which corresponds to magnetization reversal. In this phase plane, a pure exchange relaxation appears as trajectories at 45 degrees from the vertical axis, fulfilling $\dot{S}_a/\dot{S}_b = -1$. Such trajectories occupy the majority of the

phase plane, bounded by lines of partial equilibrium along which slow dynamics owing to pure relativistic relaxation dominates. For our parameters the origin is a saddle point and the red and blue (dot)dashed lines indicate (un)stable manifolds. The blue shaded area, bounded by the stable manifold and the vertical axis defines a region of non-equilibrium conditions where $|S_b| < S_a$ and S_b is substantially demagnetized. The simulations show that when the system is brought into this regime, it will proceed to reverse the sublattices showing temporal ferromagnetic alignment. Substitution of f_a given above in Eq. (5.5) yields $\lambda_b < \lambda_e(A/|J_{ab}| - 1)$. Since by definition $\lambda_b \geq 0$, we find that reversal is only possible when exchange relaxation is included ($\lambda_e > 0$). We stress that this type of reversal, driven by a temperature increase and without any magnetic field has recently been discovered [27].

Similarly, we can express the requirement for sublattice reversal to occur for FM coupling as

$$\dot{S}_b\Big|_{S_b=0} < 0 \Leftrightarrow 2\partial f_a/\partial S_a^2 < -J_{ab}(1 + \lambda_b/\lambda_e) < 0. \tag{5.6}$$

Since $J_{ab} > 0$ it is required that $S_a^2 \ll \overline{S}_a^2$ for the reversal of S_b. Note that criterion (5.6) requires a specific form of the energy $f_a(S_a^2)$, *i.e.*, it cannot appear in a paramagnetic sublattice where $\overline{S}_a^2 = 0$, while it does not require a specific form for the energy $f_b(S_b^2)$. We predict that, contrary to the case with AFM coupling, sublattice reversal in FM coupled sublattices does not occur after a sudden increase of the electron temperature. Instead, requirement (5.6) typically occurs after a large and sudden *decrease* of the temperature. We anticipate this effect in materials exhibiting a strong magnetocalorimetric effect [28].

5.5 Critical Regime

The third regime, which we call the critical regime, is determined by a temperature close to the critical temperature $T \sim T_C$. Here both relativistic and exchange relaxation are of importance and this case is highly relevant for ultrafast demagnetization. To simplify the analysis we neglect the intersublattice contribution to the effective fields and write

$$\dot{S}_a = -\lambda_a S_a/\chi_a - \lambda_e(S_a/\chi_a - S_b/\chi_b), \tag{5.7}$$

with a similar equation for S_b, where we assumed $f_\nu = S_\nu^2/(2\chi_\nu)$ since in the vicinity of T_C $\overline{S}_\nu \approx 0$. From Eq. (5.7) it follows that the effect of exchange relaxation is quite different in AFM and FM coupled sublattices. When the sublattices are antiparallel, we have $S_a/\chi_a - S_b/\chi_b = S_a/\chi_a + |S_b|/\chi_b > 0$, and hence we predict that both sublattices demagnetize faster than in the uncoupled case $\lambda_e = 0$. With parallel sublattices either S_a or S_b is accelerated while the other is decelerated depending on whether $S_a/\chi_a \gtrless S_b/\chi_b$. Hence relativistic and exchange relaxation can have different

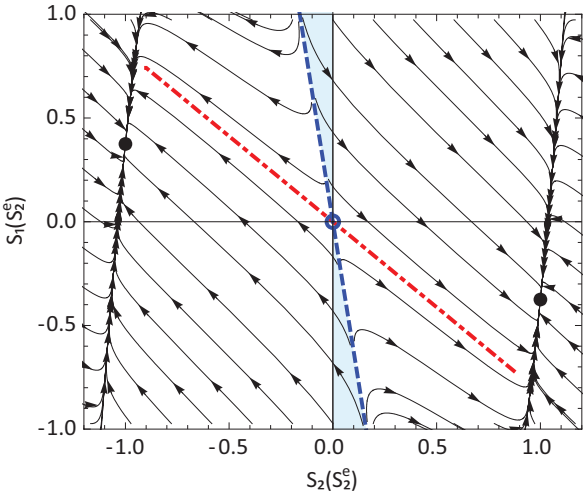

Figure 5.1: Numerical solution of the longitudinal equations of motion in the exchange dominated regime. The evolution of S_a is shown as function of S_b, where both are normalized to the final value S_b^e for various initial conditions. The arrows indicate the direction when time increases. The thick dots indicate stable equilibrium points. The origin is a saddle point with red and blue (dot)dashed lines indicating (un)stable manifolds. The blue shaded area encompasses the initial conditions from which the longitudinal relaxation will proceed to reversal showing temporal ferromagnetic alignment.

sign, which may have direct consequences for the demagnetization of ferromagnetic alloys like FeNi or FeCo. Similar conclusions are obtained when J_{ab} is included in the analysis, at least when $k_B T_C \gg |J_{ab}|$.

5.6 Comparison with Atomistic Spin Dynamics

To further substantiate the applicability of our theory we employ atomistic spin dynamics (ASD) simulations, using the UppASD method [29, 30]. Such simulations solve the dynamics of exchange coupled atomic spins coupled to a heat bath and hence goes beyond the conventional Landau-Lifshitz dynamics for macrospins. The heat bath ensures longitudinal dynamics of individual sublattices, while the coupling between atomic spins of different sublattices allows for exchange relaxation. We take a ferrimagnetic GdFe model system based on the cubic Laves phase structure characterized by the microscopic exchange parameters $J_{11} = 0.2\,\text{meV}$, $J_{12} = -2\,\text{meV}$, $J_{22} = 20\,\text{meV}$ for nearest neighbor interactions only. For the magnetic moments we take the bulk values $g\sigma_1 = 7.6\,\mu_B$ (Gd) and $g\sigma_2 = 2.1\,\mu_B$ (Fe). As system size we

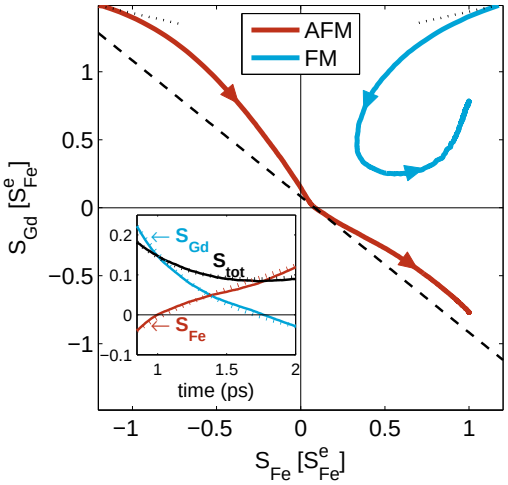

Figure 5.2: Atomistic spin dynamics simulation of laser-induced spin dynamics of a model GdFe system with either antiferromagnetic (AFM) or ferromagnetic (FM) sublattice coupling. The spin dynamics of Gd is shown as function of the spin dynamics of Fe, both scaled with the final value of Fe S^e_{Fe}. For both types of coupling the sublattices demagnetize at distinct timescales, where the dotted line indicates the expectation from Eq. 5.4. The dashed line shows a trajectory that would be obtained with purely exchange relaxation. Only with AFM coupling the sublattices do reverse, showing temporal FM alignment on the ps timescale, as highlighted in the inset, where dotted lines indicate a fit with the phenomenological model.

chose $D = 20^3$ unit cells and we averaged the simulations over $N = 10$ realizations of the heat bath. For these parameters we get $T_\mathrm{C} = 800\,\mathrm{K}$ and a compensation temperature of about $T_\mathrm{A} = 300\,\mathrm{K}$ (data not shown). The coupling to the thermal bath is fixed by $\alpha_a = \alpha_b = 0.02$, and we also used equal gyromagnetic ratios. Following [13], we model laser-induced spin dynamics by a time dependent temperature of the heat bath, which for simplicity is described by a rise time $\tau_a = 10\,\mathrm{fs}$ and a relaxation time $\tau_b = 1\,\mathrm{ps}$, capturing the essential physics of a two-temperature model [18]. The heat bath temperature is initially $T_0 = 200\,\mathrm{K}$, it peaks at about $T_\mathrm{P} = 1400\,\mathrm{K}$ and reaches finally $T_\mathrm{F} = 400\,\mathrm{K}$.

We visualize the results in Fig. 5.2 by showing the evolution of S_Gd as function of S_Fe, where both are normalized to the final value of Fe S^e_{Fe}. Initially (top left), when the temperature is high, S_Fe demagnetizes faster than S_Gd. The dotted line indicates the estimate determined by Eq. (5.4), showing reasonable agreement given that the peak temperature is only $T_\mathrm{P} \approx 2T_\mathrm{C}$. Subsequently, the spin of Fe reaches zero first and

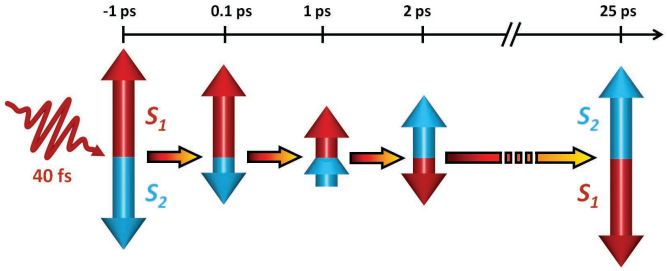

Figure 5.3: Visualization of the different stages of the laser-induced magnetization reversal in a GdFe ferrimagnet. In the temperature dominated regime on the sub-picosecond timescale, the sublattices show distinct dynamics owing to their different magnetic moment. Fe reaches zero first and subsequently, on the picosecond timescale the exchange relaxation dominates enabling temporal parallel alignment of Fe and Gd spins, until also the spin of Gd reverses. The final relaxation to full equilibrium proceeds at a lower rate according to small relativistic interactions which eventually bring the system in full equilibrium. Figure adapted from [16].

becomes temporarily parallel with the spin of Gd until also the spin of Gd reverses. This is further highlighted by the inset of Fig. 5.2, which presents the evolution of the sublattice angular momentum as a function of time. In this time interval we can fit the ASD results (solid lines) quite well with our model introduced above (dotted lines) for the parameters $A/B = 4$, $J_{ab}/B = -1$, $\overline{S}_b = 1$, $\lambda_a = \lambda_b = 0.5\lambda_e$ and the time scaled with $(B\lambda_e)^{-1} = 1.917$ ps. Note that the sign of $S_{\mathrm{Gd}} + S_{\mathrm{Fe}}$ remains positive on the picosecond timescale, where $T < T_{\mathrm{C}}$, indicating that exchange is dominating. This is also confirmed by the dashed line in the phaseplot, which shows the trajectory that would be obtained by only exchange relaxation. The relaxation to the new equilibrium values proceeds upon further cooling of both sublattices. Note that in principle also a fitting of the complete trajectory is possible when the temperature dependence of the parameters in the Landau expansion is known. To summarize, the whole reversal is illustrated in the time-domain as shown in Fig. 5.3.

By varying the laser intensity we found that the sublattice reversal only occurs above a critical fluence, as expected from Eq. (5.5). Further, by increasing the pulse length, it was found that For comparison, we also performed ASD simulations for the same model system but with FM coupling between the sublattices. For this case, the phase trajectory is located in one quadrant of the plane (top right of Fig. 5.2). Like in the AFM case, the sublattices show distinct dynamics but no reversal takes place, in accordance with Eq. (5.6) which only yields reversal for a temperature decrease. Hence, the simulations further confirm the predictive power of our phenomenological theory.

5.7 Conclusions

In summary, we propose a general theoretical framework for ultrafast spin dynamics in multisublattice magnets on the time scale of the exchange interaction. The dynamics can be classified in three regimes: Firstly, a temperature dominated regime, below 1 ps, where relativistic relaxation dominates which yields distinct dynamics for sublattices with different magnetic moments. Secondly, on the ps timescale exchange relaxation is dominant, transferring angular momentum between the sublattices. Thirdly, we predict that close to the critical temperature, where both relaxation parameters are of importance, exchange relaxation in sublattices with AFM coupling accelerates the demagnetization of both sublattices, while for FM coupled sublattices relativistic and exchange relaxation may counteract.

References

[1] A. Kirilyuk, A. Kimel, and T. Rasing, Rev. Mod. Phys. **82**, 2731 (2010).

[2] E. Beaurepaire, J.-C. Merle, A. Daunois, and J.-Y. Bigot, Phys. Rev. Lett. **76**, 4250 (1996).

[3] C. Stanciu, F. Hansteen, A. Kimel, A. Kirilyuk, A. Tsukamoto, A. Itoh, and T. Rasing, Phys. Rev. Lett. **99**, 047601 (2007).

[4] K. Vahaplar, A. Kalashnikova, A. Kimel, D. Hinzke, U. Nowak, R. Chantrell, A. Tsukamoto, A. Itoh, A. Kirilyuk, and T. Rasing, Phys. Rev. Lett. **103**, 117201 (2009).

[5] A. Kimel, A. Kirilyuk, A. Tsvetkov, R. Pisarev, and T. Rasing, Nature **429**, 850 (2004).

[6] F. Hansteen, A. Kimel, A. Kirilyuk, and T. Rasing, Phys. Rev. Lett. **95**, 047402 (2005).

[7] G. Ju, J. Hohlfeld, B. Bergman, R. van de Veerdonk, O. Mryasov, J.-Y. Kim, X. Wu, D. Weller, and B. Koopmans, Phys. Rev. Lett. **93**, 197403 (2004).

[8] J.-U. Thiele, M. Buess, and C. Back, Appl. Phys. Lett. **85**, 2857 (2004).

[9] L. Landau and E. Lifshitz, Phyz. Z. Sowjetunion **8**, 153 (1935).

[10] G. Zhang and W. Hübner, Phys. Rev. Lett. **85**, 3025 (2000).

[11] B. Koopmans, J. Ruigrok, F. Longa, and W. de Jonge, Phys. Rev. Lett. **95**, 267207 (2005).

[12] U. Atxitia, O. Chubykalo-Fesenko, N. Kazantseva, D. Hinzke, U. Nowak, and R. Chantrell, Appl. Phys. Lett. **91**, 232507 (2007).

[13] N. Kazantseva, U. Nowak, R. Chantrell, J. Hohlfeld, and A. Rebei, Europhys. Lett. **81**, 27004 (2008).

[14] C. Stamm, T. Kachel, N. Pontius, R. Mitzner, T. Quast, K. Holldack, S. Khan, C. Lupulescu, E. Aziz, M. Wietstruk, et al., Nature Mater. **6**, 740 (2007).

[15] C. La-O-Vorakiat, M. Siemens, M. M. Murnane, H. C. Kapteyn, P. Grychtol, R. Adam, C. M. Schneider, J. M. Shaw, H. Nembach, and T. J. Silva, Phys. Rev. Lett. **103**, 257402 (2009).

[16] I. Radu, K. Vahaplar, C. Stamm, T. Kachel, N. Pontius, H. Dürr, T. Ostler, J. Barker, R. Evans, R. Chantrell, et al., Nature **472**, 205 (2011).

[17] S. Mathias, C. La-O-Vorakiat, P. Grychtol, P. Granitzka, E. Turgut, J. M. Shaw, R. Adam, H. T. Nembach, M. E. Siemens, S. Eich, et al., PNAS **109**, 4792 (2012).

[18] S. Anisimov, B. Kapeliovich, and T. Perelman, Zh. Eksp. Teor. Fiz **66**, 776 (1974).

[19] T. Iwata, J. Magn. Magn. Mater. **31-34**, 1013 (1983).

[20] T. Iwata, J. Magn. Magn. Mater. **59**, 215 (1986).

[21] V. Baryakhtar, Zh. Eksp. Teor. Fiz **87**, 1501 (1984).

[22] V. Baryakhtar, Zh. Eksp. Teor. Fiz. **94**, 196 (1988).

[23] V. Baryakhtar, Fiz. Nizk. Temp. **11**, 1198 (1985).

[24] D. Garanin, Phys. Rev. B **55**, 3050 (1997).

[25] W. Brown, Phys. Rev. **130**, 1677 (1963).

[26] R. Kubo and N. Hashitsume, Prog. Theor. Phys. Suppl. **46**, 210 (1970).

[27] T. Ostler, J. Barker, R. Evans, R. Chantrell, U. Atxitia, O. Chubykalo-Fesenko, S. El Moussaoui, L. Le Guyader, E. Mengotti, L. Heyderman, et al., Nat. Commun. **3**, 666 (2012).

[28] O. Tegus, E. Brück, K. Buschow, and F. de Boer, Nature **415**, 150 (2002).

[29] B. Skubic, J. Hellsvik, L. Nordström, and O. Eriksson, J. Phys.: Condens. Matter **20**, 315203 (2008).

[30] J. Mentink, M. Tretyakov, A. Fasolino, M. Katsnelson, and T. Rasing, J. Phys.: Condens. Matter **22**, 176001 (2010).

CHAPTER 6

Microscopic modeling of longitudinal spin dynamics in multisublattice magnets[1]

6.1 Introduction

Ultrafast longitudinal spin dynamics has intrigued researchers since the pioneering work of Beaurepaire et al.[1]. They found that optical excitation of ferromagnetic Ni with a femtosecond laser pulse resulted in a quenching of the magnetization on a sub-picosecond time-scale, much faster than the conventional precessional spin dynamics which can be described by the Landau-Lifshitz equation [2], with a (Gilbert) damping term that only accounts for transverse relaxation of relativistic origin. Later it was demonstrated that a femtosecond laser pulse can even act as an equally short magnetic field pulse [3] leading to the discovery of complete reversal of magnetization by a laser pulse alone [4, 5]. These intriguing observations have triggered intense experimental and theoretical efforts to understand the fundamental processes lying behind such ultrafast laser-induced dynamics [6]. Many of these studies were performed with magnetic compounds containing at least two magnetic elements[2], whereas also the spin dynamics of other well-known multi-component materials like NiFe and yttrium-

[1] In part adapted from: I. Radu, C. Stamm, A. Eschenlohr, K. Vahaplar, T. Kachel, N. Pontius, R. Mitzner, K.Holldack, A. Föhlisch, F. Radu, R. Evans, T. Ostler, J. Mentink, R. Chantrell, A. Tsukamoto, A. Itoh, A. Kirilyuk, A. Kimel and T. Rasing, submitted (2012).

[2] This includes the discovery of the coupling between the magnon modes in an exchange coupled multilayer, which eventually lead to the Giant Magneto Resistance Effect, see for instance the Gruenberg Nobel lecture.

iron-garnet has demonstrated interesting observations such as Bose-Einstein condensation [7], magnetic vortices [8] and spin-Seebeck effects [9]. It is remarkable that most experiments were analyzed in a macrospin approximation, where several sublattices are represented with just one macroscopic magnetization vector. This suggests that on the timescale of these experiments the different sublattices have the same dynamics. However, recent experiments using fs X-ray probes [10, 11] have revealed that the sublattices in ferrimagnetic GdFe have distinct dynamics after femtosecond laser excitation. This element-specific demagnetization subsequently lead to a switching between two antiferromagnetically ordered states via a transient ferromagnetic state[12]. Furthermore, using similar experimental techniques indications were found that also the spin and orbital moments can have distinct dynamics [13]. As was discussed in the previous chapter, considerable understanding of such distinct longitudinal dynamics in multisublattice magnets can be gained by employing a purely phenomenological approach based on Onsager's relations. Nevertheless, despite it's generality and usefulness, the purely phenomenological theory inherently possesses a number of shortcomings. First of all, since the theory is purely macroscopic, it does not provide a link between the microscopic properties and the macroscopic dynamics. Secondly, owing to it's generality, it is difficult to predict how the dynamics will change by changing the strengths of the exchange interactions and by changing the temperature. Furthermore, the dynamics of the orbital degrees of freedom are entirely neglected. In this chapter we address these issues using the full microscopic free energy as derived in Sec. 4.3. This allows us to study the influence of the exchange interaction on the ultrafast timescale and distinct demagnetization in multi-component magnetic alloys. In addition, we study in detail how the conditions of exchange-driven reversal will depend on the strength and sign of the exchange interaction, finally leading to the prediction of a novel route for magnetization reversal. The last section of this chapter discusses how orbital degrees of freedom can be taken into account and we investigate how this influences the dynamics.

6.2 Ultrafast Demagnetization in Multisublattice Magnets

In this section we study the ultrafast laser-induced demagnetization in multisublattice magnets. In particular, we focus here on the role of the exchange interaction, for which we can use the microscopically derived free energy described in Sect. 4.3 is ideally suited. We start the discussion by explaining how we model the laser-induced spin dynamics and recover the results for the ferromagnetic case with one sublattice. Subsequently, we discuss multisublattice magnets and elucidate the differences between ferromagnetic and antiferromagnetic coupling between the sublattices. To further illustrate the method, we present an analysis of the demagnetization time as function of composition for the case of ferromagnetically coupled $Ni_{1-x}Fe_x$ compounds, and compare this with recent experimental results.

Ferromagnets with one sublattice

For the modeling of laser-induced spin dynamics we employ the same approach as in Ch 5, by assuming that the main effect of the laser pulse on the magnetic system stems from the rapid increase of the electron temperature. Here we focus on the short timescale and in order to extract solely the time scale of the spin dynamics, we assume that electrons thermalize instantaneously to a temperature T above the Curie temperature T_{C}. This assumption can be justified when the electrons thermalize much faster than the spins and when the electron-phonon relaxation time τ_{ep} is much longer than the spin demagnetization time $\tau_s \ll \tau_{\mathrm{ep}}$[3]. Since we assume $T > T_{\mathrm{C}}$, we can use the quadratic expansion of the free energy Eq. (4.45) in the remainder.

Before discussing multisublattice magnets, we discuss the role of the exchange interaction in the demagnetization of ferromagnets with one sublattice. Using Eq. (4.46) we can write

$$dS_a/dt = N_a ds_a/dt = -[\lambda_a(3k_{\mathrm{B}}T - 2z_{aa}\tilde{J}_{aa})/\sigma_a^2]s_a, \tag{6.1}$$

where we defined $\tilde{J}_{\nu\nu'} = J_{\nu\nu'}\sigma_\nu\sigma_{\nu'}$ as the exchange interaction in units of energy. This expression yields the natural interpretation that temperature and exchange interaction are two competing energy terms, where the temperature attempts to disorder the magnet (reduce s_a) while the exchange interaction attempts to keep it ordered. Assuming that initially the magnet was in equilibrium, $s_a|_{t=0} = \sigma_a\mathcal{L}(\overline{\eta}_a)$, we obtain for the rate of change after a step-like change of the electron temperature $ds_a/dt \sim \lambda_a(T - T_{\mathrm{C}})/\sigma_a$, where $3k_{\mathrm{B}}T_{\mathrm{C}} = 2z_{aa}\tilde{J}_{aa}$. Hence the demagnetization time scales with the atomic magnetic moment and in the strict high-temperature limit ($T \gg T_{\mathrm{C}}$) we recover the scaling of the demagnetization time $\tau_a \sim \sigma_a/T$ mentioned before in Sec. 5.3 for the temperature dominated regime[4].

Multisublattice magnets

Next we turn to the discussion of ultrafast demagnetization in multisublattice magnets. Similar as in the discussion of the critical regime in Sec. 5.5, we first discuss generically the difference between ferromagnetic ($J_{ab} > 0$) and antiferromagnetic ($J_{ab} < 0$) coupling. In particular, we elaborate more extensively on the differences

[3]When $\tau_s > \tau_{\mathrm{ep}}$, the demagnetization time is strongly influenced by the relaxation of the electron temperature. This can lead to a two-step like behavior, with an initial fast drop of the magnetization followed by a much slower demagnetization process. This phenomenon has been discussed recently for elementary ferromagnets [14].

[4]Note that the relaxation parameters λ_ν have the dimension of angular momentum ($\hbar$), whereas the effective fields have the dimension of frequency (s^{-1}). Hence to determine the scaling of the relaxation time with the magnetic parameters it is sufficient to evaluate the effective field. Alternatively, as has been done in Sec. 5.3, we could introduce dimensionless relaxation parameters $\alpha_\nu = \lambda_\nu/\sigma_\nu$, and we can write $\tau_\nu = \chi_\nu/\lambda_\nu \sim \sigma_\nu/(\alpha_\nu T)$.

between the relativistic and exchange relaxation. The relativistic relaxation is determined by the effective fields H_ν for each sublattice individually. Writing this out for $\nu = a$ we obtain:

$$H_a = -\frac{1}{\sigma_a^2}\left(3k_\mathrm{B}T - 2z_{aa}\tilde{J}_{aa}\right)s_a - \frac{1}{\sigma_a\sigma_b}2z_{ab}\tilde{J}_{ab}s_b. \tag{6.2}$$

This formula remains unchanged under changing the sign of both $\tilde{J}_{ab}$ and s_b. Consequently, for both ferromagnetic and antiferromagnetic coupling we find that the purely relativistic relaxation can be reduced by increasing $|J_{ab}|$.

In contrast, the contribution of exchange relaxation is quite different for antiferromagnetic and ferromagnetic coupling. This relaxation depends on the difference $H_a - H_b$:

$$\begin{aligned} H_a - H_b \;=\; & -\frac{1}{\sigma_a^2}\left(3k_\mathrm{B}T - 2z_{aa}\tilde{J}_{aa} + 2z_{ba}\tilde{J}_{ab}\sigma_a/\sigma_b\right)s_a + \\ & +\frac{1}{\sigma_b^2}\left(3k_\mathrm{B}T - 2z_{bb}\tilde{J}_{bb} + 2z_{ab}\tilde{J}_{ab}\sigma_b/\sigma_a\right)s_b. \end{aligned} \tag{6.3}$$

Depending on the sign of s_b, the two effective fields add up or partly cancel each other. The latter is the case for ferromagnetic coupling. Since initially the two sublattices are parallel, the exchange relaxation either accelerates one sublattice and decelerates the other, or vice versa. In contrast, with antiferromagnetic coupling, both terms add up, and because the sublattices are initially antiparallel the demagnetization of both sublattices is enhanced when the temperature exceeds the exchange contributions. The same prediction was obtained from the purely phenomenological theory (Sec. 5.5) and has recently been confirmed experimentally [15]. Similar effects were recently found in magnetic multilayers, where different layers can act as different sublattices [16]. It was shown by changing only the mutual alignment of the sublattices from parallel to antiparallel, that the fastest demagnetization speed was achieved in the antiparallel configuration, confirming our analysis. It might be interesting as well to use GdFe multilayers and use synthetic structures to tune the strength of the exchange interaction.

Material specific analysis of ferromagnetic NiFe alloys

In the last part of this section we turn to a material-specific study. As an example we chose the ferromagnetic $\mathrm{Ni}_{1-x}\mathrm{Fe}_x$ amorphous alloy (permalloy), a material that has been extensively studied in the literature and keeps leading to intriguing new phenomena and applications, including magnetic race-track memory [17], magnetic vortices [8] and spin-Seebeck effects [9]. In particular, we assess the demagnetization time as function of composition. To this end, we start with introducing composition

dependent effective magnetic fields $H_\nu(x)$ and assess the regime of small Fe concentration. Subsequently we discuss the regime where the concentration of Ni and Fe is comparable. Finally we draw conclusions.

For a binary amorphous alloy in the nearest-neighbor approximation we can write $z_{aa} = z_{ba} = (1-x)z$, $z_{bb} = z_{ab} = xz$, and define effective exchange parameters as $J_a^0(x) = (1-x)zJ_{aa} + xzJ_{ab}$, $J_b^0(x) = xzJ_{bb} + (1-x)zJ_{ab}$, where x is the concentration of element b (Fe) and z the average number of nearest neighbors in the alloy [18]. With these definitions we can write the composition dependence of the effective magnetic fields as $H_\nu(x) = -(3k_\mathrm{B}T/\sigma_\nu^2 - 2J_\nu^0(x))$. In the small doping limit, we may neglect the exchange relaxation term since for ferromagnetic coupling the contributions $H_a - H_b$ partly cancel each other and the coupling between the sublattices itself is also a relatively small effect. Taking only the relativistic relaxation we can write for the demagnetization rate after a step-like change of the temperature

$$\frac{dS_a}{dt}(x) = -\lambda_a(x)[3k_\mathrm{B}T - \tilde{J}_a^0(x)]/\sigma_a(x), \tag{6.4}$$

where we assumed that $s_\nu|_{t=0} = \sigma_\nu$. Importantly, this formula suggests that we can control the demagnetization speed by both the magnetic moment and the exchange interaction. For the case of NiFe we have $\tilde{J}_\mathrm{NiNi} < \tilde{J}_\mathrm{NiFe}$ [19] and hence $\tilde{J}_\mathrm{Ni}^0(x) > \tilde{J}_\mathrm{Ni}^0(0)$. Since also $\sigma_\mathrm{Ni}(x) > \sigma_\mathrm{Ni}(0)$ [20], it follows from our analysis that in the small concentration limit the demagnetization speed of Ni decreases upon alloying with Fe. The demagnetization time of Fe in the same alloy is expected to be slower than that of Ni since $\sigma_\mathrm{Fe} > \sigma_\mathrm{Ni}$ and also $\tilde{J}_\mathrm{Fe}^0(x) > \tilde{J}_\mathrm{Ni}^0(x)$ because $\tilde{J}_\mathrm{FeFe} > \tilde{J}_\mathrm{NiFe} > \tilde{J}_\mathrm{NiFe}$ [19].

Secondly, we focus on the regime where $x \approx 0.5$, which is special since it is close to the invar point. In this regime the Ni sublattice remains almost collinear with the average magnetization, but the Fe sublattice is essentially noncollinear and frustrated, due to long-range oscillating exchange interactions [21] and due to local environment effects yielding a huge dispersion of the nearest-neighbor exchange parameters [22]. This frustration results in a decrease of the Curie temperature despite the fact that the magnitude of the exchange interactions increases [23]. Although the assessment of such frustrated magnetism goes beyond the mean-field approximation employed here, it may be expected that the frustrated Fe environment yields an effective exchange relaxation channel for Ni, thereby accelerating the demagnetization of Ni compared to the pure case. This is further supported by considering only the temperature contribution to the effective fields. Since $\sigma_\mathrm{Ni} < \sigma_\mathrm{Fe}$, we find that $\lambda_e(H_\mathrm{Ni} - H_\mathrm{Fe}) \approx -\lambda_e 3k_\mathrm{B}T(\sigma_\mathrm{Ni}^{-1} - \sigma_\mathrm{Fe}^{-1}) < 0$, thus increasing the demagnetization speed of Ni. When the exchange relaxation accelerates Ni it will decelerate Fe since the coupling is ferromagnetic. Hence we expect that in this regime Fe demagnetizes both slower than Ni and also slower than pure Fe which is not limited by this exchange relaxation channel.

Recent experimental studies on the laser-induced demagnetization using femtosecond XMCD probe pulses (data not shown) show good qualitative agreement with the theoretical analysis presented before, showing an increase of the demagnetization time of Ni at low concentration of Fe ($x = 20\%$), and a decreased demagnetization time of Ni in the proximity of the invar region ($x = 50\%$), while the demagnetization time of Fe is always larger than that of Ni. We conclude that we can control the demagnetization time both with the magnetic moment and the exchange interaction. Moreover, our results suggest that we can enhance the demagnetization of collinear magnets by placing them in a magnetically frustrated environment, thus enhancing the exchange relaxation.

6.3 Exchange-driven Magnetization Reversal

Recently it has been discovered numerically and demonstrated experimentally that a short heat pulse alone is sufficient to achieve magnetization reversal in a ferrimagnetic alloy [24]. The actual reversal stems from the exchange relaxation between the sublattices as explained in Sec. 5.6 and hence can only be observed in multisublattice magnets. In this section we aim to assess the conditions that are required for exchange-driven magnetization reversal and discuss the role of the intersublattice exchange interaction in particular. First we explain how to simulate sublattice dynamics in the time-domain. Second, we introduce phase plots as a tool to analyze in one plot which type of dynamics is possible for a specified set of model parameters. Subsequently, we analyze how the dynamics changes as a function of the sign and strength of the intersublattice exchange interaction. Finally, we suggest a new route along which exchange-driven magnetization reversal can proceed.

To explain how we simulate sublattice dynamics we start with the observation that in mathematical terms the equations of motion Eqns. (4.26)-(4.27) form a first order 2x2 initial value problem. Using the quadratic expansion of the free energy Eq. (4.45) the problem is linear and can be solved analytically. In the general case, the effective fields Eq. (4.39) are nonlinear in $s_\nu(t)$ and we solve the problem numerically in Mathematica using standard numerical integration routines. Since the equations are linear in the relaxation parameters, the mathematical solution depends only on the ratios λ_ν/λ_e which we denote as dimensionless relaxation parameters. Then, with the exchange parameters and spin moments given from the static equilibrium case, the dynamical problem has three parameters: the two dimensionless relaxation parameters λ_ν/λ_e and the temperature T. In principle we could use these parameters to fit experiments and test the model with more microscopic models. An example of the latter has been shown in Sec. 5.6 using phenomenological expressions for the free energy. However, rather than further illustrating the potential as a fit model, in the following we analyze qualitatively which dynamics can be expected as a function of

the exchange interactions. For this our model is ideally suited since it is valid for all types of exchange interactions and the numerical efforts are very low.

With all model parameters fixed, the sublattice dynamics is completely determined by specifying the initial conditions $s_\nu(0)$. Independent of the initial conditions, the model possesses one or two possible ground states determined by Eq. (4.41). Hence, different nonequilibrium initial conditions specify different routes towards the ground state. We can visualize all possible routes to the ground state as a phase plot, *i.e.* a parametric plot showing $S_b(t)$ as function of $S_a(t)$. Such a plot visualizes in one graph all the solutions of the mathematical problem for a fixed set of model parameters. Therefore, a phase plot is ideally suited to analyze which initial conditions give rise to sublattice reversal and how this depends on the model parameters.

To get acquainted with the phase plots, we first show how the solutions depend on the temperature and the relaxation parameters. As a reference system we use a ferrimagnetic $GdFe_2$ model system, characterized by $\tilde{J}_{aa} = 20$ meV, $\tilde{J}_{ab} = -2.0$ meV, $\tilde{J}_{bb} = 0.20$ meV for nearest neighbor interactions in a cubic Laves phase structure [25]. For the spin moments we take the bulk values $\sigma_a = 2.1\,\mu_\mathrm{B}$ (Fe) and $\sigma_b = 7.6\,\mu_\mathrm{B}$ (Gd). In this system, similar atomistic simulations have shown exchange-driven reversal (Sec. 5.6), as was first demonstrated by the York-group [12, 24].

Fig. 6.1 illustrates how the dynamics depends on the temperature. Results are shown for low temperature (Fig. 6.1a, $T = 0.2T_\mathrm{C}$) and for a temperature below and above the Curie temperature (Fig. 6.1b, $T = 0.8T_\mathrm{C}$) and (Fig. 6.1c, $T = 1.2T_\mathrm{C}$), respectively. In the upper right and lower left quadrants the sublattices are parallel, while antiparallel alignment corresponds to the upper left and lower right quadrants. The horizontal and vertical axis show the possible values of angular momentum per formula unit for Fe and Gd, respectively, both scaled on the saturation moment of Fe: $S^0_\mathrm{Fe} = N_\mathrm{Fe}\bar{s}_\mathrm{Fe}(0\,\mathrm{K})$, with N_Fe the number of Fe atoms per formula unit. Below T_C there are two possible ground states indicated by solid discs, one in the upper left quadrant and the other in the lower right quadrant, in accordance with the antiferromagnetic coupling between the sublattices. By increasing the temperature the equilibrium values approach the origin and above T_C the ground state is not magnetic as indicated by one solid disc in the origin.

All dynamics is computed with $\lambda_a = \lambda_b = 0.2\lambda_e$. For these values the phase plane contains two distinct features. Since we are in the exchange dominated regime, the fastest relaxation is of exchange origin which consequently occupies the majority of the phase plane[5]. This relaxation appears at -45 degrees from the horizontal axis since it conserves the total angular momentum. With exchange relaxation alone the system can only achieve partial equilibrium, which is the minimum energy for a given

[5]Note that we are dealing with the dynamics after the laser excitation. In accordance with the discussion in Chapter 5, the initial relaxation in response to the laser pulse is dominated by relativistic relaxation and is therefore even faster than exchange relaxation in the temperature dominated regime. Only after this initial temperature dominated dynaics we will observe the behavior discussed here

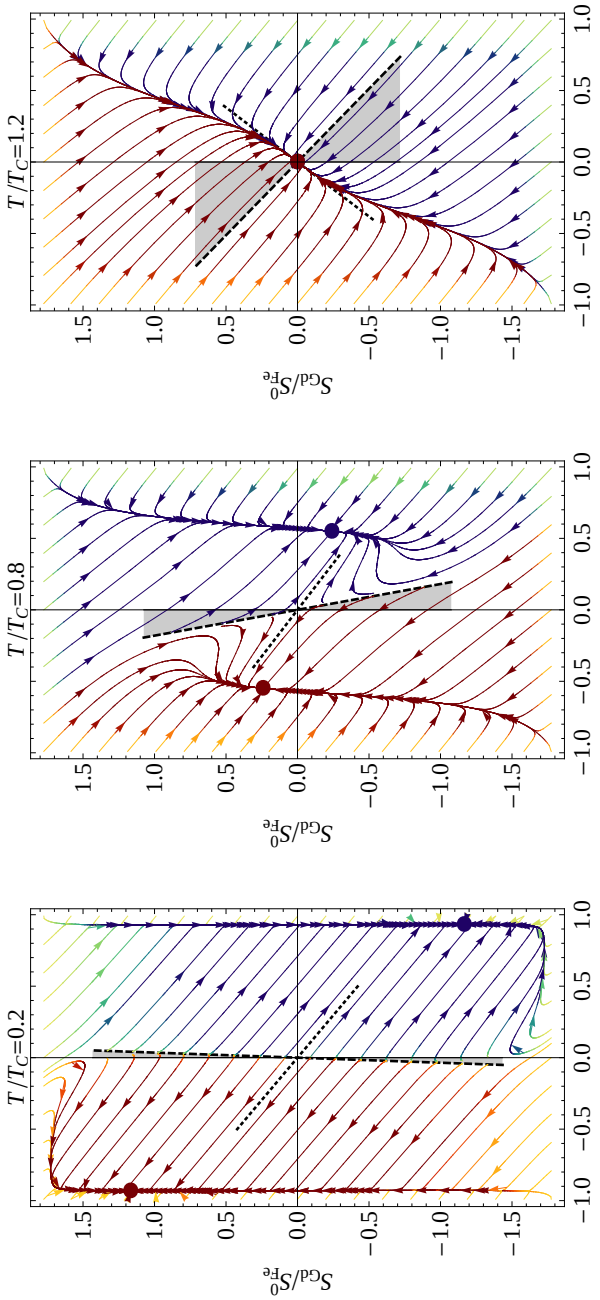

Figure 6.1: Phaseplot of the ferrimagnetic $GdFe_2$ model system introduced in the text for three different temperatures. Solid discs indicate stable equilibrium points and arrows indicate the direction of evolution. Trajectories that connect the upper left and lower right quadrant exhibit full exchange-driven reversal of the magnetization. The dashed (dotted) line indicate stable (unstable) manifolds that determine the structure of the phaseplot in the vicinity of the origin. They can serve as a fingerprint for the possibility of exchange-driven reversal. A sufficient condition for antiferromagnetically coupled sublattices is the alignment of both manifolds in the upper-left and the lower-right quadrants, as is exemplified in (b). Grey areas encompass initial conditions from which the longitudinal relaxation will proceed to reverse at least one sublattice. All phase plots are computed at $\lambda_a = \lambda_b = 0.2\lambda_e$.

value of total angular momentum. Slower dynamics of relativistic origin transfer angular momentum to or from the magnetic system allowing it to relax to complete equilibrium. The actual shape of these trajectories is determined by the equality $H_a = H_b$ and hence depends both on the temperature and the relative strengths of the exchange interactions.

We now focus on the possibility of exchange-driven reversal and consider the situation that the nonequilibrium initial condition is in the upper left quadrant. Full reversal is characterized by relaxation that brings the system in the lower right quadrant, where both sublattice are reversed. It is useful to examine the structure of the phase plane close to the origin. Below T_C the origin is a saddle point. Linearization of the problem (Eq. (4.45)) yields stable and unstable manifolds indicated by dashed and dotted lines, respectively. A crucial role is played by the stable manifold, which determines the possibility of crossing the vertical axis for small values of the sublattice angular momentum. When the stable manifold is close to the vertical axis or even in the upper right quadrant, exchange driven reversal is practically forbidden. This is the case at low temperature in Fig. 6.1a, where only for very large S_{Gd} a trajectory crosses the vertical axis and ends up with reversed sublattices, despite the fact that the majority of the phase plane is determined by exchange relaxation.

When the temperature increases, the stable manifolds rotate counterclockwise and open up a shaded region in the upper left quadrant. As illustrated in Fig. 6.1b, this region encompasses initial conditions that yield exchange driven reversal. For large values S_{Gd} outside the regime where the linearization is valid, even more trajectories yield reversal of sublattices. Note further that in this parameter range it is sufficient to cross the vertical axis. Subsequent relaxation always gives rise to reversal of both sublattices without the application of a magnetic field.

When the temperature is further increased, the stable manifold continues rotating thereby further increasing the possibility of crossing the vertical axis. This is even possible for $T > T_C$ as illustrated in Fig. 6.1c. However, at this temperature the origin is a stable minimum. Consequently, the dotted line has become a stable manifold as well and also rotated counterclockwise thereby passing the horizontal axis. The sublattices can reverse their orientation but full reversal is not possible since the relaxation proceeds to the nonmagnetic ground state at the origin. Nevertheless, this simulation clearly shows that S_{Fe} may reverse even for $T > T_C$. In the course of a slow decrease of the electron temperature to $T < T_C$ stemming from electron-lattice relaxation, the initial reversal of S_{Fe} might be sufficient to achieve full reversal of both sublattices.

From the above analysis we conclude that we have the best opportunity to observe exchange driven reversal when the temperature is in the vicinity but slightly below T_C. In addition, we conclude that the structure of the phase diagram close to the origin gives us the following sufficient condition for exchange-driven reversal: when both manifolds are in the upper left (and lower right) quadrant, reversal is possible.

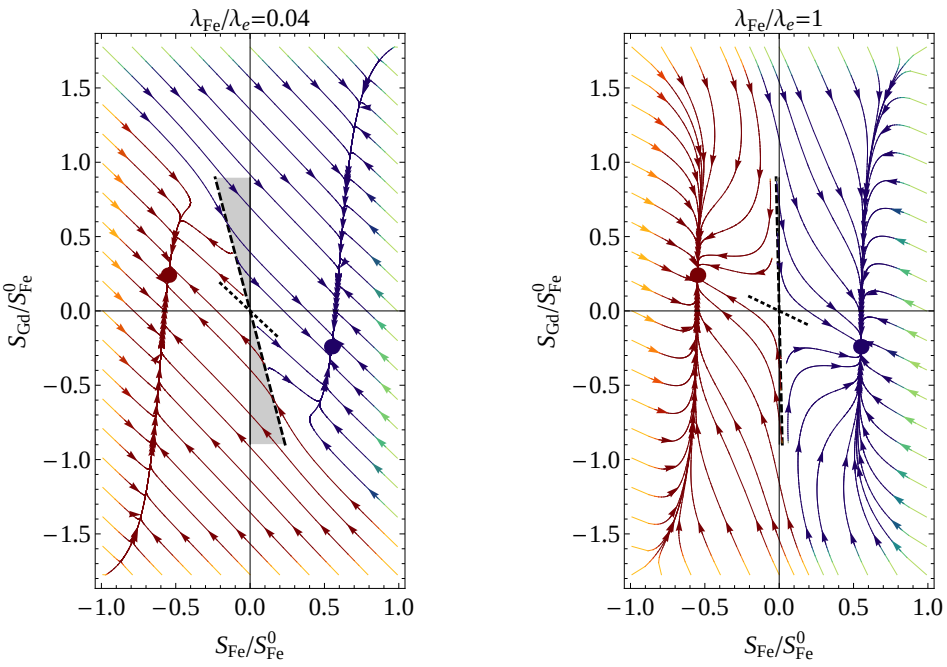

Figure 6.2: Same as in Fig. 6.1b, for stronger (a) and weaker (b) exchange relaxation. As expected the possibility of reversal is enhanced (reduced) when the exchange relaxation is increased (decreased).

Supplemented with criterion Eq. (5.5) this gives us a necessary and sufficient condition for reversal that in principle can be used for further optimization and design of synthetic materials. Moreover, for a given material the slope of the stable manifold can be used to estimate how the sublattices must be brought from equilibrium. For the model considered here, generally $|S_{\mathrm{Fe}}|$ should be small and $|S_{\mathrm{Gd}}|$ should be large. This situation can indeed be realized upon femtosecond laser excitation owing to the dependence of the relaxation time on the spin moment in the temperature dominated regime.

Role of the sign and strength of the intersublattice exchange interaction

Next we discuss briefly how the phase plot changes by changing the relaxation parameters. This is illustrated in Fig. 6.2a and Fig. 6.2b, both computed at $T = 0.8T_{\mathrm{C}}$. When exchange relaxation is made stronger ($\lambda_\nu/\lambda_e = 0.04$, Fig. 6.2a), the difference between the timescale of exchange and relativistic relaxation is more pronounced. This results in more trajectories that yield reversal, as expected since exchange relax-

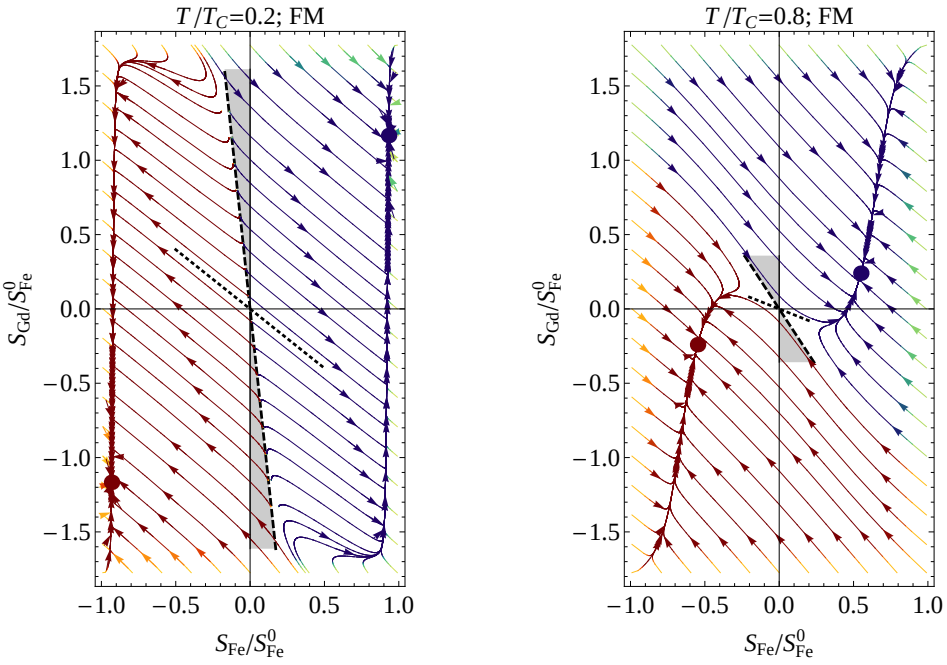

Figure 6.3: (a),(b) Same as in Fig. 6.1a,b, but for ferromagnetic coupling between the sublattices. Full reversal is not possible since there are no trajectories connecting the upper right and lower left quadrant. Nevertheless, transient antiferromagnetic alignment is possible and is best observable in (a) at low temperature.

ation is driving the reversal. This is visually also easily observed from the increased angle between the dashed stable manifold and the vertical axis. Conversely, when the relativistic relaxation is increased (Fig.6.2b, $\lambda_\nu/\lambda_e = 1$), reversal becomes less probable, as also observed from the stable manifold that is very close to the vertical axis. Note as well that in this case the distinction between exchange relaxation and relativistic relaxation is not visible anymore. Similar qualitative changes are obtained for the phase plots at lower and higher temperature.

Having introduced the phase plots and discussed how to analyze them we start using phase plots as a tool to study how the dynamics qualitatively changes as a function of the intersublattice exchange interaction. First, we study the possibility of reversal with ferromagnetic coupling between the sublattices. Secondly we will study how the strength of the intersublattice exchange interaction influences the dynamics and results in novel routes of exchange-driven reversal.

Fig. 6.3 shows the dynamics for the same model system as before but with the sign

of the exchange interaction changed to ferromagnetic coupling. Correspondingly, the groundstates below T_C are located in the upper right and lower left quadrants. It follows directly from the plots that full reversal is not possible. This can be understood from the fact that also for ferromagnetic coupling exchange relaxation corresponds to trajectories at -45 degrees from the horizontal axis. Consequently, the exchange driven dynamics cannot connect the upper right and lower left diagrams. Indeed, for parallel alignment exchange relaxation can only increase one sublattice and decrease the other, or vice versa, but not decrease the angular momentum of both sublattices. This arguments holds generally and is independent of the strength of the exchange interactions. Nevertheless, transient antiferromagnetic alignment is possible. Contrasting the case of antiferromagnetic coupling Fe remains along the same direction while Gd changes sign and becomes temporarily antiparallel and finally back parallel with Fe. From the comparison of Fig. 6.3a at low temperature and Fig. 6.3b slightly below T_C, we conclude that the best possibility to observe transient antiferromagnetic alignment is at low temperatures, similar as has been anticipated in Sec. 5.4.

Since full exchange-driven reversal is not possible with ferromagnetic coupling, in the remainder we turn back to the case of antiferromagnetic coupling and study how the dynamics depends on the strength of intersublattice exchange interaction. We use again the same model system and keep all parameters fixed, except for the relative strength of the intersublattice exchange $J_{aa}^{\text{eff}}/J_{ab}^{\text{eff}} = z_{aa}J_{aa}/(z_{ab}J_{ab})$. For the original model we have $J_{aa}^{\text{eff}}/J_{ab}^{\text{eff}} = -10$ and we decrease this to $J_{aa}^{\text{eff}}/J_{ab}^{\text{eff}} = -2.5$ (Fig. 6.4a) and $J_{aa}^{\text{eff}}/J_{ab}^{\text{eff}} = -0.5$ (Fig. 6.4b). Remarkably, although the exchange interactions are not changed dramatically, qualitatively the dynamics is very different. In particular, for large initial values of Gd and small values of Fe, trajectories exist that show first transient ferromagnetic alignment but owing to the increased intersublattice exchange subsequently relax back to the original orientation. The stable and unstable manifolds have the same structure as in Fig. 6.1a and full reversal is not possible. Interestingly, upon further increasing the exchange interaction a new reversal path opens up. Contrary to the original model, Gd reverses direction first and becomes temporarily parallel with Fe and subsequently also Fe reverses orientation. Consistently, the stable manifold is oriented below the unstable manifold and the shaded region encompassing initial conditions that yield reversal is located below the stable manifold and the horizontal axis. To our knowledge, this type of exchange driven reversal has not yet been observed experimentally. Experimental observation is in principle possible when we have an element specific excitation pulse, which demagnetizes Gd but not Fe. This can for example be achieved in magnetic multilayers where the spacing layer is insulating.

In conclusion, we have analyzed exchange-driven magnetization reversal in antiferromagnetically and ferromagnetically coupled sublattices. Full reversal is possible only with antiferromagnetic coupling and the best possibility to observe reversal is in the vicinity but below T_C. In addition, we have discovered that the path along

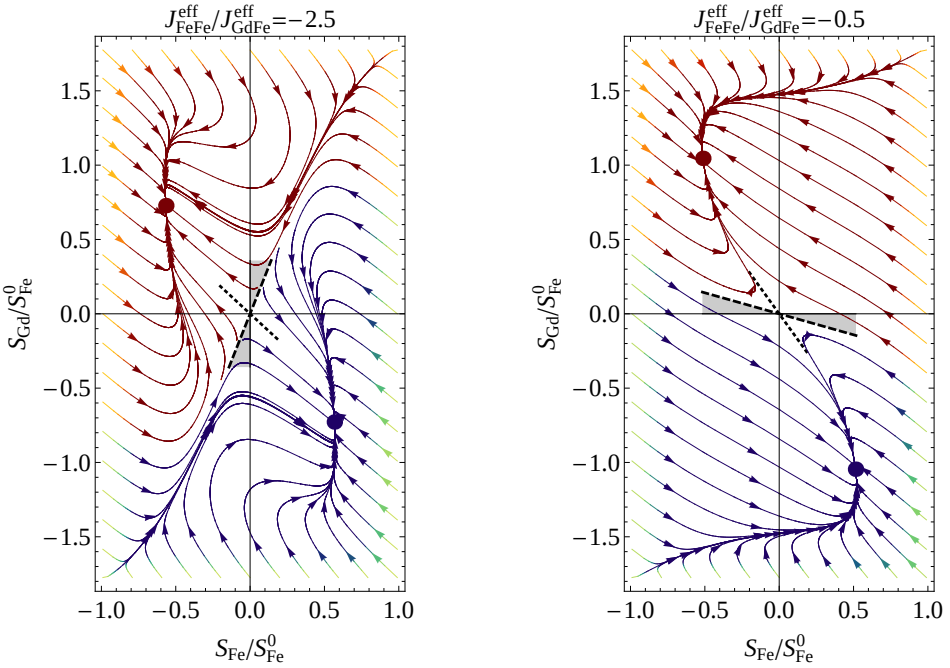

Figure 6.4: Same as in Fig. 6.1b, for an increased strength of the antiferromagnetic coupling between the sublattices. The structure of the phase plot changes significantly. (a) Contrasting Fig. 6.1b, it is not sufficient to cross the vertical axis. Instead the increased sublattice coupling seems to prevent complete reversal. Interestingly, at even larger coupling between the sublattices (b), a novel full reversal route opens up where first the horizontal axis is crossed and subsequently the vertical axis.

which exchange driven reversal is possible can be controlled with the relative strength of the intersublattice exchange interaction. This shows the potential of our model to further explore and assess the nonequilibrium dynamics of multisublattice magnets. We emphasize that our framework also enables the possibility to study how the dynamics changes with changing ratio of the spin moments and the influence of unequal relativistic relaxation parameters. While the latter are generally determined by orbital degrees of freedom, so far we have not taken into account their influence explicitly. This will be the topic of the next section.

6.4 The role of orbital degrees of freedom

Recent advances in experimental techniques open the possibility to study spin dynamics with an unprecedented level of detail. For example, while with femtosecond optical pulses usually only the spin polarization of the d electrons is probed, femtosecond X-ray pulses can distinguish between the 4f spins and 3d spins in an element-specific way [12], and moreover can disentangle the spin and orbital contributions [13]. By combining optical and X-ray probes, even spins in different bands of the same element can be distinguished [26, 27]. While we have shown in the preceding sections how to model theoretically element-specific spin dynamics, so far such additional spin and orbital degrees of freedom have not been taken into account explicitly. Here we aim to assess exactly which effects may arise when considering explicitly the spins in different orbits as well as the orbital degrees of freedom itself. To this end, we start by discussing on a general level how spin and orbital degrees of freedom can be included in our effectively macroscopic treatment of spin dynamics. Subsequently, we single out different contributions of the additional spin and orbital degrees for ferromagnets with only one magnetic elements. Subsequently, we discuss their effects in compounds with several magnetic elements. In particular, we focus on the effect of anisotropy on the exchange-driven magnetization reversal. Finally we draw conclusions.

6.4.1 Modeling additional spin and orbital degrees of freedom

On a fundamental level it is always possible to distinguish spins of different orbital levels, as well as to separate the spin angular momentum from the orbital angular momentum. It is only that sometimes the quantities cannot easily be calculated and/or do not have a clear physical meaning. In contrast, here we are interested in the development of an effective macroscopic theory. The essential problem then is to select the additional degrees of freedom that can be modeled as an additional magnetic sublattice. First, we discuss how to treat the spins in different orbital levels as different sublattices, leading to orbital-resolved spin dynamics. Second, we discuss to what extend the orbital motion itself can be taken as an additional magnetic sublattice, which we treat separately for rare-earth metals and transition metals.

We start with the treatment of spins in different orbital levels. This generalization is relatively straightforward, as becomes clear by referring back to the introduction of effective exchange interactions within the adiabatic approximation in Sec. 2.3.2. In particular, Eq. (2.10) shows that it is possible to define effective exchange interactions $J_{iL,i'L'}$ between spins at different sites i, as well as between spins in different orbits L. Hence it follows that we can model the spins in different orbital levels as being part of different magnetic sublattices, which forms the basis for *orbit-resolved* spin dynamics within the macroscopic theory. Unlike the exchange interaction between

different elements, which can be both ferromagnetic and antiferromagnetic, the exchange interaction $J_{iL,iL'}$ between spins in different orbital levels of the same element is always ferromagnetic. Note further that when the spins are in different orbits of the same band, the on-site interaction can be quite large ($\sim 1\,\mathrm{eV}$) and the definition of exchange parameters itself becomes questionable, as a consequence of the breakdown of the adiabatic approximation. Nevertheless, for spins in different bands this approach seems quite reasonable.

Next we discuss the possibility to consider the orbital degrees of freedom itself as an additional sublattice. First of all, it is important to realize that in principle the orbital dynamics is the dynamics of the electrons itself. Consequently, it is in general not straightforward to treat the orbital dynamics as an effective magnetic sublattice. Furthermore, the orbital angular momentum is very sensitive to the electric field of the local crystal environment. On the one hand this tends to (partly) quench the orbital angular momentum. On the other hand, the crystal field also can give rise to orbital ordering, such as for example in magnetic insulators with Jahn-Teller distortions [28]. Consequently, it is not possible to derive a general macroscopic theory of orbital dynamics in magnetic materials. In this section we therefore limit ourselves to metallic rare-earth and transition-metal magnets, briefly reviewing the more extensive treatment in [29].

Orbital degrees of freedom in rare-earth metals

In rare-earth metals, the 4f electrons are strongly shielded by the s-, p- and d-shells and consequently only weakly disturbed by the crystal field. Hence, the 4f system retains largely it's atomic character with spin and orbital moments in good agreement with Hund's first and second rule. This generally leads to large orbital moments, except for Gd which has a spherical half-filled shell. The spin and orbital moment are coupled by the spin-orbit interaction (Hund's third rule). As a result of the large nuclear charge, this interaction is rather strong, in the order of 100 meV, much stronger than the energy of the crystal field (1-10 meV). Therefore, like in the atomic case, the total quantum number $j_i = l_i + s_i$ is conserved but not l_i and s_i individually. Hence the rotations of the local moments are governed by the total on-site angular momentum j_i. This means that also the macroscopic theory should be based on the dynamics of j_i, otherwise it would not be possible to correctly recover the low-frequency limit. The possible distinct dynamics of the local s_i and l_i will then appear as changes of the magnitude $|j_i|$, which we can safely neglect since the collective excitations of j_i are much easier to excite. The orbital angular momentum l_i can thus not be considered as an individual sublattice for the 4f system of the rare earth metals. Nevertheless, there is an obvious difference between the transverse dynamics of j_i with different l_i. Although small, the crystal field does couple the local spins to the lattice and this coupling is evidently much stronger for $l_i \neq 0$ than for $l_i = 0$. As a result, in rare-earth metals, the effect of the orbital degrees of freedom on the macroscopic dynamics

is mainly apparent in the anisotropy experienced by the local j_i.

Orbital moments in transition metals

For transition metals, the situation is reversed in comparison with the rare earths. Here the crystal field is much stronger than the spin-orbit interaction and destroys the atomic structure of the d electrons, in particular the multiplet structure of the total angular momentum j_i. As compared to the atomic case, Hund's first and second rule have a somewhat different origin in itinerant systems. For the spin moment we have the Stoner-splitting owing to spin-dependent on-site exchange correlations (see Sec. 2.3.1). It was realized only recently [30, 31] that in a similar fashion the orbital-dependent on-site exchange correlations are responsible for the formation of orbital moments. Hence, similar as in atoms, orbital moments are formed due to non-relativistic interactions between the electrons. Their values are usually rather small ($\sim 10\%$ of the spin moments). Owing to the weak spin-orbit coupling ($< 1\,\mathrm{meV}$), the spin and orbital moments can be treated as independent. Orbital moments couple strongly to the lattice and therefore experience a rather strong on-site anisotropy. Nevertheless, the orbits are not ordered by themselves since the different alignments with the crystal axis (or axes) have the same energy. Hence, the orbital moments are aligned only in the presence of macroscopic spin-order, due to their coupling via the spin-orbit interaction. As a result, we can study the transverse dynamics of the orbital moments in the crystal field and spin-orbit field with the length of the orbital moments approximately constant[6]. Therefore, for the magnetic transition metals we can take the transverse degrees of freedom of the local orbital moments as an additional magnetic sublattice.

Having discussed how orbital degrees of freedom can be taken into account, we will discuss in the following how it influences the longitudinal dynamics in single-element ferromagnets of transition metals and rare-earth metals and their compounds.

6.4.2 Orbit-resolved spin and orbital dynamics

In the previous section we have discussed how to take into account additional spin and orbital degrees of freedom in our macroscopic theory. In this section we discuss the influence on the longitudinal dynamics for ferromagnetic metals with only one type of atom. First we discuss the case of orbit-resolved spin dynamics. Subsequently, we treat the spin and orbital dynamics in transition metals. Finally, we assess the role of the anisotropy in rare-earth metals.

For the assessment of orbit-resolved spin dynamics it is important to emphasize that the coupling between spins in different orbital levels is always ferromagnetic.

[6] Note that in thin films the orbital moments themselves are also anisotropic due to symmetry lowering at the surface [32].

Therefore, with regard to the application of laser-induced spin dynamics, we generally do not expect sublattice reversal (see also Sec. 6.3). The application of orbit-resolved spin dynamics seems not very useful for transition metals, since all their magnetic properties are determined by one band, and the intra-band exchange is very strong (in the order of the Stoner splitting). The situation is better for rare-earth metals, where both 4f and 5d band are magnetically active. Still, the dynamics will be dominated by the 4f moments, since the moments in the 5d band are only induced and much smaller than the 4f spin moments. Since still on-site interaction is relatively strong, it is expected that already in the ps regime the two sublattices have very similar dynamics. We expect only for the very short timescales ($< 1\,\mathrm{ps}$) distinct dynamics in the different bands. In this regime (high temperatures) it is expected that the 5d spins have faster dynamics owing to their smaller magnetic moments.

Next we discuss the role of the orbital moment itself. In transition metals the orbital moment is much smaller than the spin moment and the coupling is parallel. Contrasting the situation of orbit-resolved spin dynamics, the coupling between the orbit and spin sublattices is rather weak. As a consequence, upon femtosecond laser excitation the sublattices of spin and orbital moments will generally show distinct dynamics. In accordance with Eq. (5.7), the orbital sublattice is expected to be faster than the spin sublattice owing to it's strong coupling to the environment ($\lambda_\mathrm{o} \gg \lambda_\mathrm{s}$) and smaller moment ($\sigma_\mathrm{o} \ll \sigma_\mathrm{s}$). In addition, since the orbital sublattice generally depends stronger on the temperature, the ratio $\langle l_i \rangle / \langle s_i \rangle$ will be decreased after the excitation. Both findings were recently reported in experiments on $Co_{0.5}Pd_{0.5}$ [13] and we expect that this might be a general phenomenon. Nevertheless, it should be mentioned that the differences between the reported demagnetization times of spin and orbit were rather small (280 fs and 220 fs, respectively [13]) and fall essentially within the time resolution of the experiment ($\sim 100\,\mathrm{fs}$). Similar studies were reported on Ni [33]. However, in this study the demagnetization times were reported to be equal and much shorter (120 fs), which makes it even more difficult to draw conclusions on the differences between spin and orbital motion. In both experiments it was found that the direct influence of the dynamics of the orbital sublattice on the dynamics in the spin sublattice is relatively small, as expected from our analysis, owing to the weak coupling and small contribution to the total angular momentum.

For rare-earth metals, the effect of the orbital moment is apparent in the anisotropy, which is largest in the 4f system. To gain insight in the effect of the anisotropy on the demagnetization, we explicitly write the quadratic expansion of the free energy (Eq. (4.45)) with anisotropy included. The quantity χ_ν^{-1} then becomes to first order in d_ν:

$$\chi_\nu^{-1}(d_\nu) = \frac{k_\mathrm{B}T}{\sigma_\nu^2}\left(\frac{1}{3} + \frac{4}{45}\frac{d_\nu \sigma_\nu^2}{k_\mathrm{B}T}\right)^{-1} - 2z_{\nu\nu}J_{\nu\nu}. \tag{6.5}$$

Therefore, $\chi_\nu^{-1}(d_\nu) < \chi_\nu^{-1}(0)$ and the temperature fluctuations are less effective in the presence of anisotropy. The physical reason is simply that the anisotropy tends to sta-

bilize the orientation of the local moments. Hence, purely the inclusion of anisotropy reduces the speed of demagnetization. However, an increased orbital moment also increases the coupling to the environment, which might enhance the demagnetization speed. Hence both effects counteract and it is difficult to make general predictions. The situation is actually reversed in the process of magnetization recovery. Here the increased relativistic relaxation parameter and the presence of anisotropy cooperate. Hence it is expected that rare-earth magnets with large orbital moments show faster recovery, and this has indeed recently been reported by comparing Gd and Tb [26].

Having discussed the effects of additional spin and orbital degrees of freedom for pure rare-earth and transition metals, we focus our attention on magnets composed of several of such magnetic elements.

6.4.3 The role of anisotropy in exchange-driven reversal

In this section we discuss the influence of additional spin and orbital degrees of freedom in compounds. As was discussed in Sec. 6.3, the most special effects occur in multi-component magnets with antiferromagnetic coupling between the sublattices. These compounds therefore have our main interest.

From the above analysis we have found that the explicit modeling of spins in different bands, as well as the modeling of the orbital degrees of freedom as separate sublattices, does not largely influence the dynamics, since the additional sublattices contribute only weakly to the total angular momentum and the coupling is always ferromagnetic. Therefore, we also do not expect qualitatively new phenomena when modeling compounds. On the other hand, the influence of the anisotropy on the timescale of the dynamics of the rare-earth metals was found to be appreciable. This was particular true for the relaxation back to equilibrium, and it is especially during this relaxation where the exchange-driven magnetization reversal appears. Hence it is of interest to investigate the role of the anisotropy on the possibility of reversal. Experimentally this can be done, for example, by changing the rare-earth element Gd ($l_i = 0$) to Tb ($l_i = 3$).

We have modeled the exchange-driven reversal for the same system as in Sec. 6.3, for the same parameter values, in particular the system in Fig. 6.1. For a clean comparison, we have only included the anisotropy of the rare-earth sublattice but did not change the relaxation parameters. To illustrate the effect of the anisotropy Fig. 6.5 shows one solution at constant temperature $T = 0.8\,T_{\mathrm{C}}$ where reversal is found without anisotropy. Interestingly, when anisotropy is included reversal does not occur anymore. Here we have used a value $d_{\mathrm{RE}} = 10\,\mathrm{meV}$, corresponding to $d_{\mathrm{RE}}/J^{\mathrm{eff}}_{\mathrm{FeFe}} = 0.04$. Additional calculations (data not shown) indicate that reversal is still possible when the system is brought further from equilibrium, but it generally takes longer. Hence, as a result we find the rare-earth anisotropy tends to reduce the possibility of

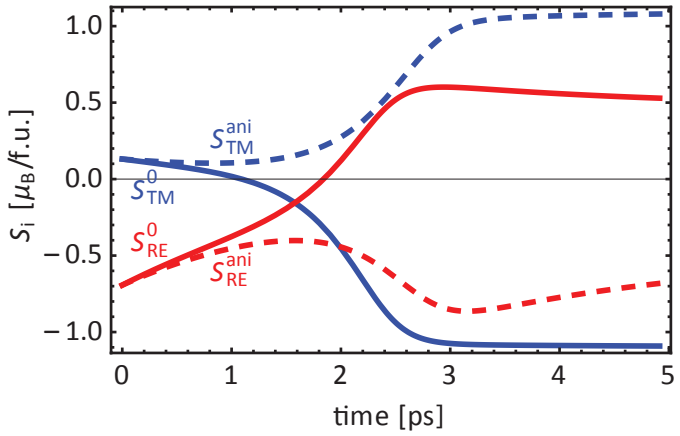

Figure 6.5: Influence of rare-earth anisotropy on the exchange-driven reversal. Solid and dashed lines show the evolution of the sublattice angular momentum with and without anisotropy. For the latter no reversal takes place, indicating that the possibility of reversal is reduced when anisotropy is included. The value of the anisotropy used is $d_{\mathrm{RE}} = 10\,\mathrm{meV}$. All other parameters were kept constant and the same as in Fig. 6.1b. Time is scaled by setting $\lambda_e/\hbar = 0.1$.

reversal, which can be understood as follows. The anisotropy of the rare-earth spin tends to keep it along the original direction and therefore stronger exchange forces are required for the exchange-driven reversal compared to the case without anisotropy. Note that the inclusion of anisotropy generally also increases the relativistic relaxation parameter. This will also contribute to a reduction of the possibility of reversal since it makes the relativistic relaxation of the rare-earth sublattice more effective compared to the exchange relaxation. In conclusion, we find that the main effect of the additional spin and orbital degrees of freedom on the exchange-driven reversal in multi-component magnets is due to the anisotropy. While this is generally weak for transition metals, for rare-earth elements it can be strong enough to reduce the possibility of exchange-driven reversal, which is consistent with recent experimental studies on TbFe systems [34].

In summary, we have discussed on a general level the effect of the inclusion of additional spin and orbital degrees of freedom on the spin dynamics. It was found that qualitatively the dynamics does not change much. The reason is that insofar as the additional degrees of freedom could be treated as additional sublattices, their contribution is much smaller than the sublattices that were taken into account already. Nevertheless, some interesting findings were obtained. In particular, it was found that in transition metals the spin and orbital sublattice are generally expected to have

different dynamics, with the orbits being fastest. For rare-earth metals, the most pronounced effect of the orbital moments is the enhanced recovery speed owing to the increase of the anisotropy. It was shown that this can even prevent exchange-driven reversal, since the anisotropy of rare-earth magnets can be quite large. While the present discussion was mostly qualitative, the presented development can also be very useful for a more quantitative study. For such a study the calculation of the relaxation parameters themselves, and in particular their temperature dependence, is needed. To further investigate the effects of orbital magnetism, it is also interesting to study systems that show orbital ordering by themselves, such as for example d-compounds with Jahn-Teller distortions that were recently also studied experimentally [35].

6.5 Conclusions

In this chapter we have used microscopic models to assess ultrafast demagnetization of multicomponent magnetic alloys and exchange-driven magnetization reversal. In addition, we have generalized the microscopic theory to take into account orbital degrees of freedom. From this we conclude that it is possible to tune the demagnetization time both by the magnetic moment and the sign and strength of the exchange interaction. In addition, we have found that full heat-driven reversal of magnetization is only possible with antiferromagnetic coupling between the sublattices and is most probable to occur slightly below the Curie temperature. Moreover, we predict that the path along which exchange-driven reversal is possible can be controlled by the relative strength of the inter-sublattice exchange interaction. Furthermore, we have found that an important effect of orbital degrees of freedom is to reduce the possibility of exchange-driven of reversal by increasing the anisotropy. These findings are of high relevance for future design and optimization of magnetic materials for magnetic storage technology.

References

[1] E. Beaurepaire, J.-C. Merle, A. Daunois, and J.-Y. Bigot, Phys. Rev. Lett. **76**, 4250 (1996).

[2] L. Landau and E. Lifshitz, Phyz. Z. Sowjetunion **8**, 153 (1935).

[3] A. Kimel, A. Kirilyuk, P. Usachev, R. Pisarev, A. Balbashov, and T. Rasing, Nature **435**, 655 (2005).

[4] C. Stanciu, F. Hansteen, A. Kimel, A. Kirilyuk, A. Tsukamoto, A. Itoh, and T. Rasing, Phys. Rev. Lett. **99**, 047601 (2007).

[5] K. Vahaplar, A. Kalashnikova, A. Kimel, D. Hinzke, U. Nowak, R. Chantrell, A. Tsukamoto, A. Itoh, A. Kirilyuk, and T. Rasing, Phys. Rev. Lett. **103**, 117201 (2009).

[6] A. Kirilyuk, A. Kimel, and T. Rasing, Rev. Mod. Phys. **82**, 2731 (2010).

[7] S. Demokritov, V. Demidov, O. Dzyapko, G. Melkov, A. Serga, and A. Hillebrands, B.and Slavin, Nature **443**, 430 (2006).

[8] B. Van Waeyenberge, A. Puzic, H. Stoll, K. Chou, T. Tyliszczak, R. Hertel, M. Fähnle, H. Brückl, K. Rott, G. Reiss, et al., Nature **444**, 461 (2006).

[9] K. Uchida, S. Takahashi, K. Harii, J. Ieda, W. Koshibae, K. Ando, S. Maekawa, and E. Saitoh, Nature **455**, 778 (2008).

[10] C. Stamm, T. Kachel, N. Pontius, R. Mitzner, T. Quast, K. Holldack, S. Khan, C. Lupulescu, E. Aziz, M. Wietstruk, et al., Nature Mater. **6**, 740 (2007).

[11] C. La-O-Vorakiat, M. Siemens, M. M. Murnane, H. C. Kapteyn, P. Grychtol, R. Adam, C. M. Schneider, J. M. Shaw, H. Nembach, and T. J. Silva, Phys. Rev. Lett. **103**, 257402 (2009).

[12] I. Radu, K. Vahaplar, C. Stamm, T. Kachel, N. Pontius, H. Dürr, T. Ostler, J. Barker, R. Evans, R. Chantrell, et al., Nature **472**, 205 (2011).

[13] C. Boeglin, E. Beaurepaire, V. Halte, V. Lopez-Flores, C. Stamm, N. Pontius, D. H.A., and J.-Y. Bigot, Nature **465**, 458 (2010).

[14] B. Koopmans, G. Malinowski, F. D. Longa, D. Steiauf, M. Fähnle, T. Roth, M. Cinchetti, and M. Aeschlimann, Nature Mater. **9**, 259 (2010).

[15] I. Radu, C. Stamm, A. Eschenlohr, K. Vahaplar, T. Kachel, N. Pontius, R. Mitzner, K.Holldack, A. Föhlisch, F. Radu, et al., submitted (2012).

[16] G. Malinowski, F. Dalla Longa, J. Rietjens, P. Paluskar, R. Huijink, H. Swagten, and B. Koopmans, Nat. Phys. **4**, 855 (2008).

[17] S. Parkin and M. Hayashi, Science **320**, 190 (2008).

[18] T. Ostler, R. Evans, R. Chantrell, U. Atxitia, O. Chubykalo-Fesenko, I. Radu, R. Abrudan, F. Radu, A. Tsukamoto, A. Itoh, et al., Phys. Rev. B **84**, 024407 (2011).

[19] P. Yu, X. Jin, J. Kudrnovský, D. Wang, and P. Bruno, Phys. Rev. B **77**, 054431 (2008).

[20] B. Glaubitz, S. Buschhorn, F. Brüssing, R. Abrudan, and H. Zabel, J. Phys.: Condens. Matter **23**, 254210 (2011).

[21] M. van Schifgaarde, I. Abrikosov, and B. Johansson, Nature **400**, 46 (1999).

[22] A. Ruban, M. Katsnelson, W. Olovsson, S. Simak, and I. Abrikosov, Phys. Rev. B **71**, 054402 (2005).

[23] J. Kudrnovský, V. Drchal, and P. Bruno, Phys. Rev. B **77**, 224422 (2008).

[24] T. Ostler, J. Barker, R. Evans, R. Chantrell, U. Atxitia, O. Chubykalo-Fesenko, S. El Moussaoui, L. Le Guyader, E. Mengotti, L. Heyderman, et al., Nat. Commun. **3**, 666 (2012).

[25] R. Wyckoff, *Crystal Structures*, vol. 1 (John Wiley & Sons, New York, London, 1963).

[26] M. Wietstruk, A. Melnikov, C. Stamm, T. Kachel, N. Pontius, M. Sultan, C. Gahl, M. Weinelt, H. Dürr, and U. Bovensiepen, Phys. Rev. Lett. **106**, 127401 (2011).

[27] M. Sultan, U. Atxitia, A. Melnikov, O. Chubykalo-Fesenko, and U. Bovensiepen, Phys. Rev. B **85**, 184407 (2012).

[28] K. Kugel and D. Khomskii, Ups. Fiz. Nauk **136**, 621 (1982).

[29] V. Irkhin and I. Yu.P., *Electronic structure, correlation effects and physical properties of d- and f-metals and their compounds* (Cambridge International Science Publishing, Cambridge, 2007), URL `http://arxiv.org/abs/cond-mat/9812072v2`.

[30] I. Solovyev, A. Liechtenstein, and K. Terakura, Phys. Rev. Lett. **80**, 5758 (1998).

[31] I. Solovyev, Phys. Rev. Lett. **95**, 267205 (2005).

[32] P. Bruno, Phys. Rev. B **39**, 865 (1989).

[33] C. Stamm, N. Pontius, T. Kachel, M. Wietstruk, and H. Dürr, Phys. Rev. B **81**, 104425 (2010).

[34] S. Khorsand et al. (2012), submitted.

[35] M. Först, R. Tobey, S. Wall, H. Bromberger, V. Khanna, A. Cavalieri, Y.-D. Chuang, W. Lee, R. Moore, W. Schlotter, et al., Phys. Rev. B **84**, 241104 (2011).

APPENDIX A

Stochastic Numerics

A.1 Weak order convergence and statistical errors

In this Appendix we recall some generic facts from stochastic numerics [1]. In particular, we define the weak order of convergence of numerical methods for stochastic differential equations (SDEs) and discuss errors arising in computing ergodic limits.

Let us introduce a system of SDEs of a general form

$$dX = \alpha(X)dt + \sum_{l=1}^{r} \beta_l(X)dW_l(t),\ X(0) = x, \tag{A.1}$$

where X, α, β_l are d-dimensional column-vectors and $W_l(t)$, $l = 1, \ldots, r$, are independent standard Wiener processes. Consider a numerical method for Eq. (A.1) based on the one-step approximation:

$$X_{t,x}(t+h) \simeq \bar{X}_{t,x}(t+h) = x + A(t, x, h; \xi),\ 0 \le t < t+h \le t_\star, \tag{A.2}$$

where ξ is a random vector with moments of a sufficiently high order and A is a d-dimensional vector function. Introduce (for simplicity) the equidistant partition of the time interval $[0, t_\star]$ into N parts with the step $h = t_\star/N$: $0 = t_0 < t_1 < \cdots < t_N = t_\star$, $t_{k+1} - t_k = h$. According to Eq. (A.2), we construct the sequence

$$X_0 = x,\ X_{k+1} = X_k + A(t_k, X_k, h; \xi_{k+1}),\ k = 0, \ldots, N-1, \tag{A.3}$$

where ξ_1 is independent of X_0 and ξ_{k+1} for $k > 0$ is independent of $X_0, \ldots, X_k$, $\xi_1, \ldots, \xi_k$. We note that Eq. (A.3) contains both explicit and implicit one-step schemes. In explicit integration schemes the approximate solution at the next time-step, X_{k+1}, can be computed explicitly from the previous time-step value X_k. For implicit methods, $A(t, x, h; \xi)$ is a solution of an implicit relation with respect to x, i.e., implicit schemes in general require additional work.

We usually distinguish two types of convergence of numerical methods for SDEs: mean-square (also called strong) and weak [1]. Mean-square methods are used for direct simulation of SDEs' trajectories which, e.g., can give information on general behavior of a stochastic model. Weak methods are sufficient for evaluation of mean values and are simpler than mean-square ones. We say that the method Eq. (A.3) is weakly convergent with order $p > 0$ if

$$| \langle \varphi(X_N) \rangle - \langle \varphi(X(t_\star)) \rangle | \leq Ch^p \tag{A.4}$$

for functions φ which, together with their derivatives of a sufficiently high order, have growth at infinity not faster than polynomial. If a method converges with an order p in the mean-square sense, it also converges in the weak sense with order equal to or larger than p. The opposite is not true. Since weak methods suffice for computing averages, they are appropriate for the purposes of this thesis.

To evaluate the expectation $\langle \varphi(X_N) \rangle$ on a computer, one can apply the Monte Carlo technique:

$$u \equiv \langle \varphi(X(t_\star)) \rangle \simeq \bar{u} \equiv \langle \varphi(X_N) \rangle \simeq \hat{u} \equiv \frac{1}{M} \sum_{m=1}^{M} \varphi(X_N^{(m)}) \ , \tag{A.5}$$

where $X_N^{(m)}$, $m = 1, \ldots, M$, are independent realizations of the random variable X_N. In Eq. (A.5) the first approximate equality involves the numerical integration error (cf. Eq. (A.4)) and the error in the second approximate equality (the statistical error) comes from the Monte Carlo technique.

The error of the Monte Carlo method in Eq. (A.5) is evaluated by

$$\bar{\Delta} = c \, \frac{\left[\mathrm{Var} \left\{ \varphi(\mathrm{X_N}) \right\} \right]^{1/2}}{M^{1/2}} \ ,$$

where, e.g., the values $c = 1, 2, 3$ correspond to the fiducial probabilities 0.68, 0.95, 0.997, respectively, with the practical implication that

$$\begin{aligned} \bar{u} \quad &\in (\hat{u} - \tfrac{c}{\sqrt{M}} \sqrt{\hat{v}}, \hat{u} + \tfrac{c}{\sqrt{M}} \sqrt{\hat{v}}) \ , \\ \hat{v} \quad &\equiv \tfrac{1}{M} \textstyle\sum_{m=1}^{M} \left[\varphi({}_m X_N) \right]^2 - \hat{u}^2 \ , \end{aligned} \tag{A.6}$$

with probability 0.68 for $c = 1$, 0.95 for $c = 2$, and 0.997 for $c = 3$.

Now we assume that the solution of Eq. (A.1) is ergodic (see also Appendix A.2). In computing ergodic limits an additional error arises. We note that ergodic limits can be computed using the ensemble averaging or time averaging. In the former case it follows from a relation of the form Eq. (A.10) (see below) for the solution $X(t)$ of Eq. (A.1), that for any $\varepsilon > 0$ there exists $t_a > 0$ such that for all $t_\star \geq t_a$

$$|\langle \varphi(X_x(t_\star)) \rangle - \varphi^{erg}| \leq \varepsilon. \tag{A.7}$$

Then we can use the following estimator for the ergodic limit φ^{erg}:

$$\varphi^{erg} \approx \langle \varphi(X_x(t_\star)) \rangle \approx \langle \varphi(X_N) \rangle \approx \hat{\varphi}^{erg} \equiv \frac{1}{M} \sum_{m=1}^{M} \varphi\left(X_N^{(m)}\right) \ , \tag{A.8}$$

where the first approximate equality corresponds to the time cut-off while the second one relates to the numerical integration error, and the third to the statistical error as before. In this ensemble-averaging approach each of the errors is controlled by its own parameter (see [2]).

The time-averaging approach to computing ergodic limits is based on a relation of the form Eq. (A.11). By approximating a single trajectory, one gets for a sufficiently large $\tilde{t}_\star$:

$$\varphi^{erg} \sim \frac{1}{\tilde{t}_\star} \int_0^{\tilde{t}_\star} \varphi(X_x(s)) ds \sim \check{\varphi}^{erg} \equiv \frac{1}{L} \sum_{k=1}^{L} \varphi(X_k), \tag{A.9}$$

where $Lh = \tilde{t}_\star$. Let us emphasize that $\tilde{t}_\star$ in Eq. (A.9) is much larger than $t_\star$ in Eq. (A.8) because $\tilde{t}_\star$ should be such that it not just ensures the distribution of $X(t)$ to be close to the invariant distribution (like it is required from $t_\star$) but it should also guarantee smallness of the variance of $\check{\varphi}^{erg}$. See further details about computing ergodic limits in, e.g. [2–4] and the references therein.

A.2 Ergodicity of the stochastic Landau-Lifshitz equation

In this Appendix we discuss the ergodicity of the solution $\mathbf{X}(t)$ to Eqns. (3.7)-(3.9). For the solution $\mathbf{X}(t)$ of Eqns. (3.7)-(3.9), we will also use the notation $\mathbf{X}_\mathbf{x}(t)$ to reflect the dependence on the initial condition $\mathbf{X}_\mathbf{x}(0) = \mathbf{x}$. Taking into account Eq. (3.2) and Eq. (3.3), we observe that the coefficients of Eqns. (3.7)-(3.9) are smooth functions and due to Eq. (3.10) they remain bounded for all $t \geq 0$.

One can show [5, 6] that for $D > 0$ and $\alpha > 0$ the process $\mathbf{X}(t)$ is ergodic, i.e., there exists a unique invariant measure μ of $\mathbf{X}$ and independently of $\mathbf{x} \in \mathbb{R}^{3n}$ there exists the limit

$$\lim_{t \to \infty} \langle \varphi(\mathbf{X}_\mathbf{x}(t)) \rangle = \int \varphi(\mathbf{x}) \, d\mu(\mathbf{x}) \equiv \varphi^{erg} \tag{A.10}$$

for any function $\varphi(x)$ with polynomial growth at infinity. Indeed, the solution $\mathbf{X}(t)$ of Eqns. (3.7)-(3.9) lives on the compact due to Eq. (3.10). Then to prove ergodicity, it is enough to show that there is sufficient mixing. When $\alpha = 0$, the stochastic perturbation is only precessional and, in general (e.g., for constant B) the process $\mathbf{X}(t)$ is not ergodic. When $\alpha > 0$, the stochastic perturbation acts in all the directions on the spheres $|x^i| = 1$ and so ensures a mixing sufficient for the ergodicity.

We also recall the ergodic theorem, which gives the equivalence between the ensemble and time averaging:

$$\lim_{t\to\infty} \frac{1}{t} \int_0^t \varphi(\mathbf{X}_{\mathbf{x}}(s))ds = \varphi^{erg} \quad \textit{almost surely}, \tag{A.11}$$

where the limit does not depend on $\mathbf{x}$. Here the meaning of *almost surely* is that the equality holds with probability one.

Further, the invariant measure associated with the solution $\mathbf{X}(t)$ of Eqns. (3.7)-(3.9) is Gibbsian with the density

$$\rho(\mathbf{x}) \propto \exp(-\beta H(\mathbf{x})) \ , \tag{A.12}$$

where $\beta = \hat{X}\hat{B}/(k_B T) > 0$ is the inverse temperature if we choose the noise intensity D as in Eq. (3.6). To check that Eq. (A.12) is the density of the invariant measure for Eqns. (3.7)-(3.9) and Eq. (3.6), one needs to verify that this $\rho(\mathbf{x})$ is the solution of the stationary Fokker-Planck equation for Eqns. (3.7)-(3.9),(3.6). Such calculations are available, e.g. in [7].

References

[1] G. Milstein and M. Tretyakov, *Stochastic Numerics for Mathematical Physics* (Springer, 2004).

[2] G. Milstein and M. Tretyakov, Physica D **229**, 81 (2007).

[3] J. Mattingly, A. Stuart, and M. Tretyakov (2009), arXiv:0908.4450v2.

[4] D. Talay, Stochastics and Stochastics Reports **29**, 13 (1990).

[5] R. Hasminskii, *Stochastic Stability of Differential Equations* (Sijthoff & Noordhoff, 1980).

[6] C. Soize, *The Fokker-Planck Equation for Stochastic Dynamical Systems and its Explicit Steady State Solutions* (World Scientific, 1994).

[7] J. García-Palacios and F. Lázaro, Phys. Rev. B **58**, 14937 (1998).

Summary

Magnetism has been fascinating mankind since the ancient Chinese and Greek civilizations. The origin of magnetism could only be understood after the development of electro-magnetism and quantum mechanics. Magnetism originates from the intrinsic angular momentum of the electrons, called spin, which is very similar to the spinning motion of for example spinning tops and gyroscopes. Spins in magnetic materials are ordered owing to their coupling, which is called exchange interaction. Following to the deeper understanding of magnetism also new applications became possible. Nowadays magnetism is widely used for storing and processing of information in, for example, magnetic hard disc drives. Here the sense of rotation of the spins (clockwise or counter-clockwise) is being used as information carrier. The speed at which the sense of rotation can be switched determines the speed at which information can be recorded. This forms an important driving force for the scientific research on spin dynamics, which is the topic of this thesis.

Chapter 1 starts with a general introduction to spin dynamics. The limits of the spin dynamics based on precession, or rotation, of the magnetization around a magnetic field are explained. Recent experimental developments with femtosecond (a femtosecond is one quadrillionth of a second (10^{-15} of a second)) laser pulses have elucidated a new regime of spin dynamics. Interestingly, this dynamics is much faster than the precessional dynamics. The short and intense perturbation of the laser pulse can bring the magnetic material far out of equilibrium and may lead to *longitudinal* dynamics. The latter deals with a change of the magnitude of the total magnetization. Recent experimental progress has shown that in certain magnetic materials even a femtosecond laser pulse alone can be sufficient for complete reversal of the spins. This switching is seen in a special type of magnets which internally consists of two or more different magnets. In such magnets the spins order in different sublattices and are therefore called multisublattice magnets. However, the actual mechanism of the reversal in these materials remained unclear. This reveals a fundamental gap in our understanding of spin dynamics, *i.e.* it is generally unknown what kind of

spin dynamics can be expected when the spins in different sublattices are not in equilibrium with each other. At the same time, this problem is highly relevant for technology, since the laser-induced reversal is roughly 1000 times faster than with the current methods. Therefore, the main goal of this thesis is the theoretical study of the strongly nonequilibrium and longitudinal spin dynamics in multisublattice magnets.

Chapter 2 provides an overview of the available concepts for the theoretical description of spin dynamics. This eventually leads to two complementary approaches that are further developed in this thesis to address the longitudinal spin dynamics in multisublattice magnets.

The first method deals with numerical simulations on the individual dynamics of coupled atomistic spins. Chapter 3 describes numerical integration methods that are developed for this goal. A new integration scheme is introduced that preserves the symmetry and corresponding constant of motion of the exchange interaction. This makes the method more stable and therefore enables the use of much larger step sizes, eventually yielding much faster simulations than possible with existing methods.

The second approach is introduced in Chapter 4, which presents the derivation of a phenomenological theory for the description of longitudinal spin dynamics in multisublattice magnets. This includes a derivation of the corresponding non-equilibrium free energy for the description of the exchange interactions. This theory distinguishes between relaxation of relativistic and exchange origin. The latter is only present in multisublattice magnets.

Chapter 5 presents the results of the phenomenological theory for the application to laser-induced spin dynamics in three different regimes. First, the theory shows that the spins in different sublattices have different dynamics when the relativistic relaxation dominates. Second and even more interesting, in the exchange dominated regime sublattices can show highly counterintuitive transitions between parallel and antiparallel alignment. Only with antiparallel coupling between the sublattices this results in reversal of the spins of both sublattices and eventually reversal of the total magnetization. These results are quantitatively supported by atomistic simulations. Third, when both the relativistic and the exchange relaxation are important, it is found that only with anti-parallel coupled sublattices the spins in both sublattices can demagnetize faster compared to the situation of uncoupled, independent, sublattices.

Subsequently, Chapter 6 deals with a microscopic analysis of the laser-induced demagnetization and exchange driven magnetization reversal. It follows that the demagnetization time can be controlled with both the spin moment and the exchange interaction. In addition, it is found that the exchange-driven reversal is most probable to occur slightly below the Curie temperature. Moreover, it is shown that the route along which exchange-driven magnetization reversal is possible can be controlled with the strength of the coupling between the sublattices. Furthermore, it is found that the reversal possibility can be reduced by increasing the magnetic anisotropy.

In summary, the theoretical methods presented in Chapter 3 and 4 of this thesis

describe the spin dynamics that is governed by the coupling between the spins itself. In other words, they deal with *magnetism on the timescale of the exchange interaction.* In the chapters 5 and 6 it is shown that this can *explain* and *predict* the spin dynamics that is possible when the sublattices are not in equilibrium with each other. In particular, the theory explains why and under which conditions laser-induced magnetization reversal is possible in multisublattice magnets. This reversal is driven by the exchange interaction and can therefore proceed roughly 1000 times faster than with the current methods. Furthermore, this thesis presents predictions for novel ways to control magnetism out of equilibrium. These predictions are already partly confirmed experimentally for the laser-induced demagnetization of multisublattice magnets.

Future research may focus on the further development of the theory by calculations of the exchange relaxation parameter, for example using atomistic simulations or based on more fundamental parameter-free theory. It is particular interesting to further confront such calculations with experimental results on laser-induced experiments on multisublattice magnets. Moreover, it is interesting to further develop the theory by including the effects of the nonequilibrium conditions on the coupling between the spins itself. This has the potential to provide direct insight in the most powerful and most fundamental force in magnetism: the exchange interaction.

Samenvatting

Magnetisme heeft de mensheid gefascineerd sinds de vroege Chinese en Griekse beschavingen. Pas met de ontwikkeling van elektromagnetisme en kwantummechanica kon ook de oorsprong van magnetisme worden begrepen. Magnetisme vindt zijn oorsprong in het intrinsieke draai-impulsmoment van de elektronen, kortweg spin, dat grote overeenkomsten vertoont met de spinnende beweging van bijvoorbeeld speelgoedtollen en gyroscopen. Spins in magnetische materialen zijn geordend door de koppeling tussen de spins, die exchange-interactie wordt genoemd. Als gevolg van dit diepere inzicht in de oorsprong van magnetisme zijn ook nieuwe toepassingen mogelijk geworden. Tegenwoordig wordt magnetisme veel gebruikt als middel om informatie op te slaan en te verwerken, zoals bijvoorbeeld in magnetische harde schijven. De draairichting van de spins (links of rechtsom) wordt hierbij gebruikt als informatiedrager. De snelheid waarmee kan worden geschakeld tussen beide toestanden bepaalt de snelheid waarmee informatie kan worden weggeschreven en vormt daarmee een belangrijke drijfveer achter het wetenschappelijk onderzoek van spindynamica, het onderwerp van dit proefschrift.

Hoofdstuk 1 begint met een algemene inleiding in de spindynamica. Hier wordt uitgelegd wat de limieten zijn van de spindynamica die is gebaseerd op de precessie, ofwel draaiing, van de magnetisatie in een magneetveld. Recente experimentele ontwikkelingen met femtoseconde (een femtoseconde is 1 biljardste van een seconde (10^{-15} van een seconde)) laserpulsen hebben een heel nieuw type spindynamica blootgelegd die interessant genoeg veel sneller is dan de precessie. Door de korte en intense verstoring kan een laserpuls het magnetische materiaal sterk uit evenwicht brengen en aanleiding geven tot *longitudinale* dynamica. Hierbij verandert de grootte van de totale magnetisatie. De recente experimentele vooruitgang op dit gebied laat zien dat, in sommige magnetische materialen, een femtoseconde laserpuls alleen voldoende is om te zorgen voor volledige omkering van de spins. Dit schakelen is gezien in een speciaal type magneet die intern bestaat uit twee of meer verschillende magneten. In dit type magneten ordenen de spins in verschillende subroosters en ze worden daarom multisubrooster

magneten genoemd. Het mechanisme dat zorgt voor de omkering van de spins in deze materialen was tot nu toe echter onbekend. Dit duidt op een fundamenteel gebrek aan begrip van spindynamica. In het bijzonder is het onbekend wat voor dynamica kan worden verwacht wanneer de spins in verschillende subroosters niet met elkaar in evenwicht zijn. Tegelijkertijd is het een zeer relevant probleem voor de technologie, omdat de tijdschaal waarop de laser-geïnduceerde omkering plaatsvindt ruwweg 1000 keer korter is dan haalbaar met de huidige methodes. Het hoofddoel van dit proefschrift is daarom de theoretische studie van sterk niet-evenwichts en longitudinale spindynamica in multi-subrooster magneten.

Hoofdstuk 2 geeft een overzicht van de beschikbare concepten voor de theoretische beschrijving van spindynamica. Dit mondt uit in twee complementaire aanpakken van longitudinale spindynamica in multisubrooster magneten die verder worden uitgewerkt in dit proefschrift.

De eerste methode betreft numerieke simulaties van de individuele dynamica van gekoppelde atomistische spins. Hoofdstuk 3 beschrijft numerieke integratiemethodes speciaal ontworpen voor dit doel. Er wordt een nieuwe integratiemethode geïntroduceerd die de symmetrie en de bijbehorende bewegingsconstante van de exchange-interactie behoudt. Dit maakt de methode veel stabieler waardoor veel grotere tijdstappen en dus veel snellere simulaties mogelijk zijn dan met de tot nu toe gangbare methodes.

De tweede aanpak wordt geïntroduceerd in hoofdstuk 4. Hier wordt een phenomenologische theorie afgeleid voor de beschrijving van longitudinale spindynamica in multisubrooster magneten, inclusief de bijbehorende niet-evenwichts vrije energie waarmee de exchange-interacties worden beschreven. Deze theorie maakt onderscheidt tussen relaxatie van relativistische oorsprong en de relaxatie van exchange oorsprong. De laatste is uniek voor multisubrooster magneten.

In hoofdstuk 5 worden de resultaten van de fenomenologische theorie voor de toepassing op laser-geïnduceerde spindynamica gepresenteerd in drie verschillende regimes. In het eerste regime laat de theorie zien dat de spins in verschillende subroosters verschillende dynamica hebben wanneer de relativistische relaxatie domineert. In het tweede regime, als de exchange relaxatie dominant is kunnen verrassende tegenintuïtieve overgangen tussen parallelle en anti-parallelle oplijning van de subroosters optreden. Alleen voor anti-parallelle koppeling tussen de subroosters resulteert dit in een omkering van de spins in beide subroosters en uiteindelijk in een omkering van de totale magnetisatie, wat kwantitatief wordt ondersteund met atomistische simulaties. In het derde regime, waar zowel relativistische als exchange relaxatie van belang zijn, volgt dat de exchange relaxatie de demagnetisatiesnelheid van de spins in beide subroosters kan vergroten alleen als ze antiparallel gekoppeld zijn.

Vervolgens wordt in hoofdstuk 6 een microscopische analyse gepresenteerd van laser-geïnduceerde demagnetisatie en exchange-gedreven magnetisatie-omkering. Hier-

uit volgt dat het mogelijk is om de demagnetisatietijd te controleren met zowel de grootte van het spinmoment als met de exchange-interactie. Eveneens wordt gevonden dat de mogelijkheid tot exchange-gedreven omkering het grootste is wanneer de temperatuur dichtbij, maar beneden, de Curie temperatuur ligt. Daarnaast wordt voorspeld dat de weg waarlangs de spins in de subroosters omkeren, kan worden gecontroleerd door het veranderen van de sterkte van de koppeling tussen de subroosters. Bovendien wordt gevonden dat de mogelijkheid op exchange-gedreven omkering kan worden verkleind door het vergroten van de magnetische anisotropie.

Samengevat beschrijven de theoretische methodes uit hoofdstuk 3 en 4 van dit proefschrift de spindynamica die het gevolg is van de koppeling tussen de spins zelf. Met andere woorden, dit proefschrift behandelt *magnetisme op de tijdschaal van de exchange-interactie*. In hoofdstuk 5 en 6 laten we zien dat we hiermee kunnen *verklaren* en *voorspellen* welke dynamica optreedt als de magnetische subroosters niet met elkaar in evenwicht zijn. In het bijzonder verklaart de theorie waarom, en onder welke condities, laser-geïnduceerde omkering van de magnetisatie mogelijk is in multisubrooster magneten. Omdat deze omkering is gedreven door de exchange-interactie, gaat het schakelen ruwweg 1000 keer sneller dan met de huidige methodes. Bovendien biedt dit proefschrift voorspellingen voor nieuwe manieren om magnetisme te controleren onder niet-evenwichts condities. Voor de laser-geïnduceerde demagnetisatie van multisubrooster magneten zijn deze voorspellingen reeds deels experimenteel geverifieerd.

Toekomstig onderzoek kan zich richten op het verder uitwerken van de theorie door middel van het berekenen van de exchange relaxatie parameter, bijvoorbeeld met atomistische simulaties of met behulp van meer fundamentele parametervrije theorie. Dit is in het bijzonder interessant voor verdere confrontatie met experimentele resultaten van laser-geïnduceerde dynamica in multisubrooster magneten. Bovendien is het interessant om de theorie verder uit te breiden naar de effecten van de niet-evenwichts condities op de koppeling tussen de spins zelf. Dit heeft de potentie om direct inzicht te verschaffen in de meest krachtige en meest fundamentele kracht van magnetisme: de exchange-interactie.

List of Publications

[1] **J. Mentink**, J. Hellsvik, D. Afansiev, B. Ivanov, A. Kirilyuk, A. Kimel, O. Eriksson, M. Katsnelson, and T. Rasing, "Ultrafast spin dynamics in multisublattice magnets," *Physical Review Letters*, vol. **108**, p. 057202, 2012.

[2] T. Ostler, J. Barker, R. Evans, R. Chantrell, U. Atxitia, O. Chubykalo-Fesenko, S. El Moussaoui, L. Le Guyader, E. Mengotti, L. Heyderman, F. Nolting, A. Tsukamoto, A. Itoh, D. Afanasiev, B. Ivanov, A. Kalashnikova, K. Vahaplar, **J. Mentink**, A. Kirilyuk, T. Rasing, and A. Kimel, "Ultrafast heating as a sufficient stimulus for magnetization reversal in a ferrimagnet," *Nature Commununications*, vol. **3**, p. 666, 2012.

[3] **J. Mentink**, M. Tretyakov, A. Fasolino, M. Katsnelson, and T. Rasing, "Stable and fast semi-implicit integration of the stochastic Landau-Lifshitz equation.," *Journal of Physics: Condensed Matter*, vol. **22**, p. 176001, 2010. This article has been selected for the "Highlights of the Journal of Physics: Condensed Matter 2010".

[4] I. Radu, C. Stamm, A. Eschenlohr, K. Vahaplar, T. Kachel, N. Pontius, R. Mitzner, K.Holldack, A. Föhlisch, F. Radu, R. Evans, T. Ostler, **J. Mentink**, R. Chantrell, A. Tsukamoto, A. Itoh, A. Kirilyuk, A. Kimel, and T. Rasing, "Ultrafast and distinct spin dynamics in magnetic alloys and heterostructures," *submitted*, 2012.

[5] **J. Mentink**, D. Afansiev, B. Ivanov, A. Kirilyuk, A. Kimel, M. Katsnelson, and T. Rasing, "Microscopic modeling of longitudinal spin dynamics in multisublattice magnets," (in preparation).

[6] "Magnetization reversal," 2011. Patent Pending.

[7] **J. Mentink** and L. Evers, "Frequency response and design parameters for differential microbarometers," *The Journal of the Acoustical Society of America*, vol. **130**, p. 33, 2011.

[8] **J. Mentink** and S. Kokkelmans, "Two interacting atoms in an optical lattice site with anharmonic terms," *Physical Review A*, vol. **79**, p. 032709, 2009.

[9] **J. Mentink**, J. Bergmans, L. Kamp, and T. Schep, "Dynamics of plasma vortices: The role of the electron skin depth," *Physics of Plasmas*, vol. **12**, p. 052311, 2005.

Curriculum Vitae

Name:
Johan Hendrik Mentink
Date of birth:
July 8, 1979
Place of birth:
Winterswijk, The Netherlands

1991 - 1995	Christelijk College Schaersvoorde, Aalten: Junior Technical School Electrical Engineering.
1995 - 1999	Graafschap College, Doetinchem: Intermediate Technical School Electrical Engineering.
1999 - 2000	Fontys University of Applied Sciences, Eindhoven: Engineering Physics, foundation course.
2000 - 2006	Eindhoven University of Technology: B.Sc. (cum laude) and M.Sc. studies in Applied Physics.
2007 - 2008	Royal Netherlands Meteorological Institute, De Bilt: Research as part of the LOFAR project.
2008 - 2012	Radboud University Nijmegen: Ph.D. studies in the groups of prof. dr. Th. Rasing. and prof. dr. M.I. Katsnelson.
2012 -	Max-Planck Department for Structural Dynamics at the University of Hamburg: postdoc in the group of prof. dr. M. Eckstein funded by a Rubicon grant.

Magnetism on the timescale of the exchange interaction:
explanations and predictions

The exchange interaction determines the ordering of microscopic spins in magnetic materials. Understanding the spin dynamics in magnetic materials is an issue of crucial importance for progress in information processing and recording technology. However, little is known about the behavior of spins directly after they are excited on a timescale equivalent to, or faster than, that corresponding to the exchange interaction (10–100 femtosecond). This thesis describes novel theoretical methods to describe exactly this regime. The results *explain* why magnetization reversal can be driven by the exchange interaction, enabling roughly 1000 times faster magnetic recording than demonstrated with current methods. Furthermore, this thesis presents *predictions* to further explore the control of magnetic order out of equilibrium.